④

Applied Research Laboratory

AD-A220 442

Technical Report

PREDICTION OF GEAR TOOTH SEPARATION
IN SINGLE-STAGE GEAR SYSTEMS, USING
NUMERICAL TECHNIQUES

by

Warren G. Greczyn
Martin J. Pechersky

DTIC
S ELECTE D
APR 1 0 1990
E

PENNSTATE

4

The Pennsylvania State University
APPLIED RESEARCH LABORATORY
P.O. Box 30
State College, PA 16804

PREDICTION OF GEAR TOOTH SEPARATION
IN SINGLE-STAGE GEAR SYSTEMS, USING
NUMERICAL TECHNIQUES

by

Warren G. Greczyn
Martin J. Pechersky

Technical Report No. TR 90-005
April 1990

Supported by:
Space and Naval Warfare Systems Command

L.R. Hettche, Director
Applied Research Laboratory

Approved for public release; distribution unlimited

APR 1 6 1990

90
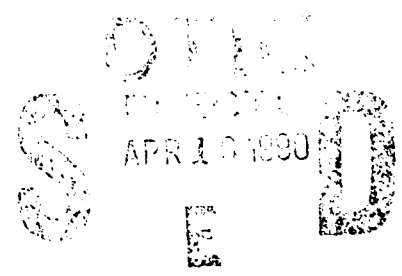
REPORT DOCUMENTATION PAGE

1a. REPORT SECURITY CLASSIFICATION	1b. RESTRICTIVE MARKINGS
Unclassified	

2a. SECURITY CLASSIFICATION AUTHORITY	3. DISTRIBUTION / AVAILABILITY OF REPORT
2b. DECLASSIFICATION / DOWNGRADING SCHEDULE	Unlimited

4. PERFORMING ORGANIZATION REPORT NUMBER(S)	5. MONITORING ORGANIZATION REPORT NUMBER(S)
TR-90-005	

6a. NAME OF PERFORMING ORGANIZATION	6b. OFFICE SYMBOL (If applicable)	7a. NAME OF MONITORING ORGANIZATION
Applied Research Laboratory Penn State University	ARL	

6c. ADDRESS (City, State, and ZIP Code)	7b. ADDRESS (City, State, and ZIP Code)
P. O. Box 30 State College, PA 16804	

8a. NAME OF FUNDING / SPONSORING ORGANIZATION	8b. OFFICE SYMBOL (If applicable)	9. PROCUREMENT INSTRUMENT IDENTIFICATION NUMBER
Space & Naval Warfare Systems Command	SPAWAR	N-00024-85-C-6041

8c. ADDRESS (City, State, and ZIP Code)	10. SOURCE OF FUNDING NUMBERS			
Department of the Navy Washington, DC 20363	PROGRAM ELEMENT NO.	PROJECT NO.	TASK NO.	WORK UNIT ACCESSION NO.

11. TITLE (Include Security Classification)

Prediction of Gear Tooth Separation in Single-State Gear Systems, Using Numerical Techniques

12. PERSONAL AUTHOR(S)

W. G. Greczyn, M. J. Pechersky

13a. TYPE OF REPORT	13b. TIME COVERED	14. DATE OF REPORT (Year, Month, Day)	15. PAGE COUNT
Technical	FROM _____ TO _____		155

16. SUPPLEMENTARY NOTATION

17.	COSATI CODES		18. SUBJECT TERMS (Continue on reverse if necessary and identify by block number)
FIELD	GROUP	SUB-GROUP	gears, modeling, tooth separation

19. ABSTRACT (Continue on reverse if necessary and identify by block number)

The following report describes a comprehensive numerical procedure for predicting tooth separation in a single-stage gear system, and provides information on its programming and use. This programmed procedure, named *Gearsep*, allows any segment of a spur gear train to be analyzed for the critical operating conditions under which tooth separation can occur.

20. DISTRIBUTION / AVAILABILITY OF ABSTRACT	21. ABSTRACT SECURITY CLASSIFICATION
☒ UNCLASSIFIED/UNLIMITED ☐ SAME AS RPT. ☐ DTIC USERS	Unclassified

22a. NAME OF RESPONSIBLE INDIVIDUAL	22b. TELEPHONE (Include Area Code)	22c. OFFICE SYMBOL
	814/865-6344	

Gear tooth separation, as evaluated in this report, occurs when the varying compliances (or, conversely, the "stiffnesses ") of the meshing teeth cause the contacting tooth pair to react against the system's shafts to such an extent that tooth surfaces loose contact with one another. When the teeth regain contact, they do so with an impact, causing high tooth stresses and unwanted noise.

The numerical procedure takes readily available gear tooth data and creates an analytical compliance model for a pair of mating teeth moving through different contact positions. This model is then passed to a numerical integration scheme which determines relative gear motion, and thus predicts separation. The particular tooth compliance model choosen is based on straightforward strength of materials concepts.

This report also presents a sample gear train investigation and confirms the accuracy and stability of the numerical integration algorithm by comparing it with an analytical solution of a simplified gear system.

ABSTRACT

The following report describes a comprehensive numerical procedure for predicting tooth separation in a single-stage gear system, and provides information on its programming and use. This programmed procedure, named *Gearsep*, allows any segment of a spur gear train to be analyzed for the critical operating conditions under which tooth separation can occur.

Gear tooth separation, as evaluated in this report, occurs when the varying compliances (or, conversely, the "stiffnesses ") of the meshing teeth cause the contacting tooth pair to react against the system's shafts to such an extent that tooth surfaces loose contact with one another. When the teeth regain contact, they do so with an impact, causing high tooth stresses and unwanted noise.

The numerical procedure takes readily available gear tooth data and creates an analytical compliance model for a pair of mating teeth moving through different contact positions. This model is then passed to a numerical integration scheme which determines relative gear motion, and thus predicts separation. The particular tooth compliance model choosen is based on straightforward strength of materials concepts.

This report also presents a sample gear train investigation and confirms the accuracy and stability of the numerical integration algorithm by comparing it with an analytical solution of a simplified gear system.

CONTENTS

LIST OF FIGURES

Chapter 1

INTRODUCTION

1.1. Gear Noise Background

The long history of gear noise studies stems from two major
concerns: the effect of noise on the immediate environment and the
effect of noise-producing processes on machinery. Issues in the
work environment center around employee health and safety due to
the potential for physically damaging noise levels emanating from
poorly designed machinery. Other environmental noise concerns are
more common, such as cabin noise in turboprop aircraft and
helicopters [1], and even household appliances [2]. Detrimental
effects on the machinery itself arise from the characteristics of
noise generation, such as abnormally high bearing, shaft, and tooth
loadings which may reach into the billions of cycles. If such
loadings are not anticipated and avoided, machine life could be
drastically reduced, most often from premature fatigue failure [3].

The early efforts in gear dynamics analysis of the 1920's and
30's were mostly concerned with the prediction of tooth stresses.
In the late 1940's, Buckingham described the "separation of elastic
bodies" and their subsequent impact [4]. Mass-spring models of the
1950's were at first employed in the usual search for tooth

stresses, but were then expanded to more detailed dynamics investigations. The modeling efforts of the 1970's and early 80's began to include more complicated effects such as three-dimensional effects, damping, and other nonlinearities. Current models may apply plate theory and also furnish transient responses [5]. A comprehensive treatment of the history of gear noise investigation is available through the referenced work of Ozguven and Houser [5].

1.2. Gear Noise Definition

Gear noise may be precisely defined as that *directly* produced by gear teeth or indirectly by other neighboring elements in a gear train (bearings, etc.). In a broader sense, however, it may be defined as the *transmitted* noise produced by a machine as a result of the vibrations at a gear pair. Mechanical vibrations are transferred along shafts and through bearings to structural mountings, while similar acoustic waves propagate through internal spaces, both finding their way to machinery housings [6]. The housings amplify and re-emit the vibrations and waves into the working environment as high amplitude airborne noise at the gear mesh frequency and its multiples, which may easily mask the actual noise of a gear pair [7].

1.3. Separation as a Source of Gear Noise

Gear noise is a direct product of the unsteady component of the *relative* angular motion of pairs of meshing gears [8]. If this unsteady component is large enough to create a relative angular gear displacement greater than the tooth deflection caused by the load on the system, then the contacting surfaces of the meshing teeth will separate. When the teeth regain contact, they do so with an impact, causing high tooth stresses and unwanted noise [9].

1.3.1. Definition of Separation

Gear tooth separation may be described by a linear system analogous to the true rotational system. In Figure 1, the series of frames show a segment of the free oscillation of two forced masses under the influence of a constant force F. These masses represent the bodies of the gears in question, and the two springs correspond to the flexible gear teeth, and are depicted as ending in flat, massless plates to represent the contacting tooth profiles. The two masses can therefore be held in a single, mutual system (spring plates in *forced* contact) only by maintaining a relative distance between the masses that is smaller than the combined unstressed lengths of their springs. If the linear system rebounds against its springs such that it reaches this unstressed position

(middle frame of Figure 1), it will then correspond to a rotational system with its tooth profiles touching, but with no transferred force (*unforced* contact). This condition may be thought of as *impending separation*.

SINGLE SYSTEM
(SPRING PLATES IN CONTACT)

APPLIED
FORCE

DIRECTION
OF MOTION

APPLIED
FORCE

F→ ←F

+

UNSTRESSED POSITION
(SPRING PLATES TOUCHING WITH NO
TRANSFERRED FORCE)

F→ ←F

F→ ←F
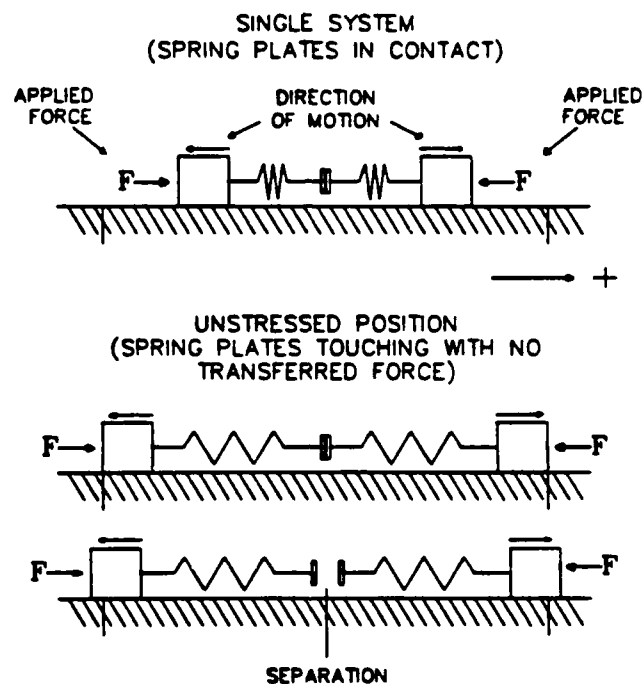
SEPARATION

Figure 1: Linear Separation System

The gears' relative displacement with respect to each other (*not* with respect to their initial positions) can be thought of as an oscillation around a quasi-equilibrium position, albeit in a complicated fashion. The corresponding block and spring behavior is a *lateral* oscillation about the system's center of mass. This is represented at the top of Figure 2 as the motion of the quasi-equilibrium or "relative" frame within the "global" frame.

By defining the datum of each block (and also each gear) in the relative frame at its respective unstressed, initial positon, and continuing to ignore rigid body motion, a straightforward definition of separation may be established based on the previous discussion. Specifically, if no separation is to take place, the motion of the right-hand block must not exceed that of the left-hand block as viewed from the global frame. The blocks or gears in question must remain within the confines of their quasi-equilibrium datums as viewed in Figure 1. Again, if the system elements return to their datums, any continued outward movement will result in a separation of the contacting surfaces. From Figure 2, which shows both forced contact and separation in the relative frame, it is possible to define a actual quantity called *separation* as the value of the relative displacement of the elements. This is depicted explicitly in the bottom frame of Figure 2. To further quantify "separation," consider the area of Figure 2 labeled with a " + " and note that the elements are located at their respective datums, implying that the plates are in contact, but the springs are not compressed. If element 1 were to move in the positive direction a distance of, say, five units, while element 2 were to move in the same direction, but only three units, the plates would remain in contact, held there because of a total spring compression of two units. By defining *separation* as that measure found by subtracting the distance moved by element 2
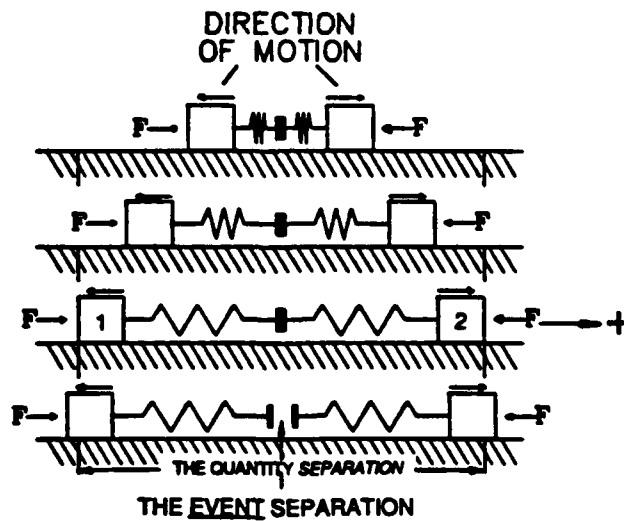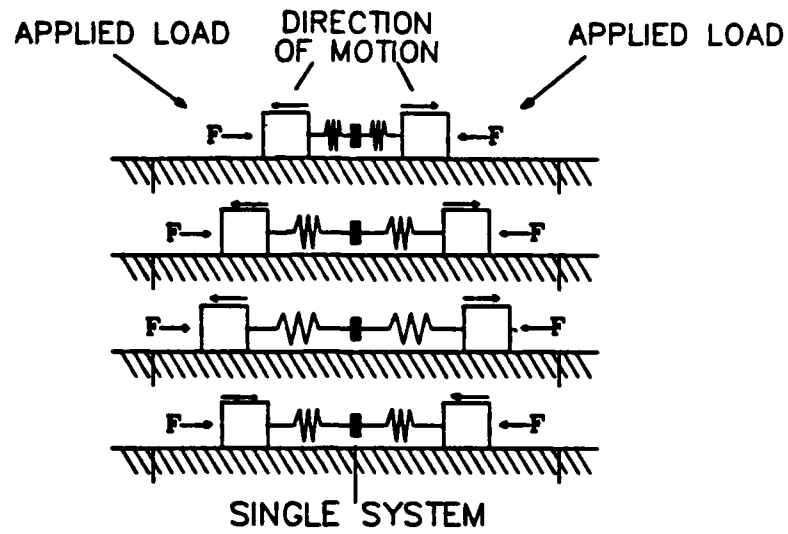
Figure 2: Separation in the Linear System

from that moved by element 1, the scenario just described would produce a separation value of *positive* 2. Thus defined, positive *separation* values of elements in the linear displacement system imply that the plate surfaces have remained in contact. Conversely, a negative separation implies that plate surfaces have lost contact, as shown in the last frame of Figure 2. In an analogous angular system, positive *separation* values imply that the tooth surfaces of a pair of meshing gears have remained in contact. Conversely, a negative separation implies that tooth surfaces have lost contact due to the relative angular displacement of their associated gear bodies.

1.3.2. Details of Separation

As previously stated, separation is caused by the unsteady component of relative angular gear motion. Mark [8] goes on to say:

> This unsteady component is caused by the periodic variation in the stiffness of the gear mesh that is attributed to the periodic variation in the numbers of teeth in contact, and the variation in the stiffness of individual tooth pairs as the location of their mutual line of contact changes during rotation. The intentional tooth-face modifications, machining errors and wear, and tooth deformations all provide non-negligible contributions to the deviation from exactly uniform relative angular motion of pairs of meshing rotating gears. (p. 1409)

These deviations are collectively known as *static transmission errors* (STE's) after the technique used to find them in which measurements are taken of the relative rotational displacements of statically loaded gears [10]. These errors are most often defined along the line of action (the locus of all contacting points for a gear pair: see Figure 46a) and in displacement units [10]. Despite their collective label, STE's should be considered to lie in two separate groups as indicated by Mark; *deformation* oriented errors, and those errors caused by *physical* imperfections of the gear teeth, either intentional or accidental.

Separation brought about solely by deformations of the tooth profile occurs because of the variation in tooth stiffness. This variation is in turn caused by the changing tooth thickness and load position that occurs as the teeth move through different positions in mesh. Figure 3 shows a single tooth pair entering mesh and leaving mesh, which are the two extremes of its range of contact. As tooth 1 moves through mesh, the point of mutual contact moves from its thick section and travels up the tooth profile to the tooth's narrow section at the tip, with the converse variation occurring to tooth 2. Unfortunately, the resulting opposite changes in stiffness do not cancel each other to produce a constant deflection. Rather, their sum creates the aforementioned unsteady component of rotational motion, causing the teeth to push against the system's shafts with a varying strength, possibly to such an
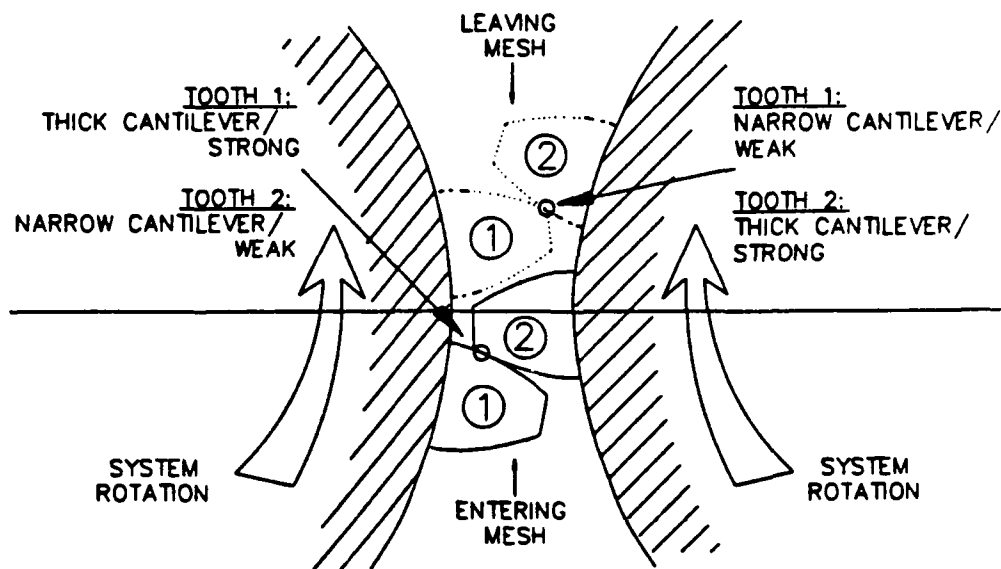
Figure 3: Variation of Tooth Thickness and Load Position with Mesh Position

extent that tooth surfaces lose contact with one another. This can be visualized by considering the action between a diving board and a diver. Imagine the diver standing on the board and causing it to oscillate up and down while keeping his feet in constant contact with the board surface. Such motion can continue indefinitely, until he correctly varies the "stiffness" of his legs, causing feet and board to separate.

Relative gear motion is further complicated by the fact that most gears are designed to have more than one pair of teeth in contact at one time in certain regions of mesh. As a result, a pair of meshing gears that alternate between one and two contacting tooth pairs will experience both the continuous, unsteady motion

from the previously described stiffness variations, and the sudden and repetitious rising and falling of the overall stiffness level owing to transitions to and from dual tooth pair contact.

Physical errors incur separation by introducing either true or effective raised areas to the tooth profile. Upon contact with the mating tooth surface, these raised areas produce rigid body rotations of the gears as a whole, which may be great enough to cause separation. This occurs in much the same way an unexpected bump may "separate" a bicycle, along with its rider, from a previously smooth road surface. Origins of *true* raised areas have already been considered (modifications of the tooth profile, etc. as discussed by Mark [8]), and *effective* errors may originate in the mispositioning on the gear body of entire teeth or in the misforming of the gear body itself during manufacture [11]. It should be noted again that while provisions have been made to include separation due to such physical errors, the bulk of this investigation will be aimed at separation caused by the changes in stiffness inherit in the relative positional changes of meshing gear teeth (as shown in Figure 3).

1.3.3. Post-Separation Behavior

After tooth surfaces loose contact, two related chains of events may occur, depending on the system's physical characteristics.

Common to each event is a degeneration of the single-stage system into two momentarily independent single shaft systems, with the division occurring at the separated teeth (just as a diver and a board separate into two dynamically independent systems). Figures 1 and 2 presented the linear analogy to this degeneration, while that of the rotational system is depicted in Figure 4: The insert shows the teeth of a gear pair still moving apart just after tooth separation, where the large arrows give the rotational direction of the system as a whole, and the smaller arrows indicate the relative tooth motion.

GEAR
PAIR

MOTOR
MASS

LOAD MASS

GEAR TEETH OUT OF
CONTACT:
SINGLE-STAGE SYSTEM
HAS BECOME TWO
DYNAMICALLY SEPARATE
SYSTEMS
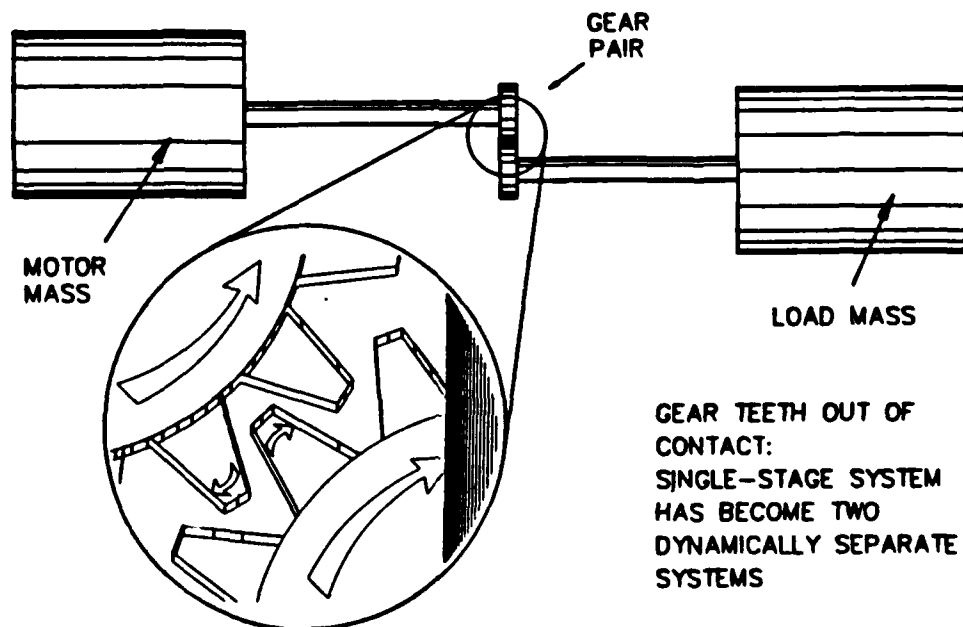
Figure 4: Degeneration of One System into Two Isolated Systems

1.3.3.1. Contacting Surface Impact

The first post-separation event that will be considered requires that the energy partially dissipated in the separation of the two tooth surfaces be completely expelled in twisting the system's shafts. At that point, the gears involved will stop their relative *forward* rotation and begin a relative *backward* motion, opposite to the directions of the smaller arrows in the inset of Figure 4. This is similar to the diver falling back towards the surface of the diving board.

When the teeth have moved back through the distance that had separated them, their contacting surfaces will meet with an impact, as described in reference [4]. The ensuing *dynamic separation load* can cause, in addition to the large vibrations which propagate through the system as previously described, tooth wear and general loss of performance [12] and may produce the largest load value encountered in the mesh cycle. This will cause obvious problems if only static loads are considered when designing tooth strength. It should also be noted that a dynamic load will occur even if there is no separation [4]: The unsteady relative gear motion produces a dynamic *acceleration load* even if the teeth retain contact, as indicated by the spring deformations in the oscillations of the linear system shown in the top of Figure 2. This is the oscillating load caused by a bouncing diver that deflects the

diving board past the point of static deflection from the divers weight alone. The key point is that this oscillating load will occur even if the diver's feet never leave the board.

1.3.3.2. Double Impact

The second possible event after the teeth have separated requires that the energy of separation be greater than that required to simply counter-rotate the system's shafts. This will produce a relative gear rotation equal to the gears' backlash (the clearance or play between adjacent pairs of teeth). When this occurs, there will be a second dynamic loading *in addition* to that previously described: Because shaft stiffnesses are no longer large enough to stop the gears' motion in "mid air," the *back sides* of adjacent teeth will impact [13]: This is analogous to an unfortunate diver hitting the underside of the board one level above him before returning to land on his own. Although much of the separation energy may be expelled by the time the tooth flanks meet, resulting in a less severe impact than that which will occur to the front sides a moment later (completing the "double" impact), the teeth will still be stressed in the direction opposite to that which occurs during normal operation, and due to the nature of bi-directional loadings, the chances of fatigue failure will increase. While this type of impact will not be included in this analysis, it nevertheless gives

support for the usage of a separation analysis program to predict and avoid gear tooth separation.

1.4. Program Description

This report presents a programmed numerical procedure which employs an established gear tooth compliance model for the prediction of the critical operating conditions under which gear tooth separation can occur in single-stage segments of spur gear systems. This task is accomplished with a set of programs collectively titled *Gearsep*, for "gear separation." There are two autonomous Gearsep program parts, the first using the aforementioned model to evaluate the varying compliances of the meshing tooth pairs (Gearsep1), and the second using this compliance information in a dynamic model of the single-stage system (Gearsep2).

Gearsep's focus will be on deflection induced separation, although provisions have been made to include the effects of the physical errors previously discussed. The reasoning for exclusion of these topics from the main flow of the program development is that such physical imperfections change from gear to gear and from system to system, so the selection of any one of these criteria would be completely arbitrary, and might only apply in limited circumstances. The requirements for deflection induced

separation, however, exist in all spur gear systems, and as such, this may be thought of as a global trial case for the Gearsep procedure.

1.5. Program Constraints

For a complete system analysis, a spur gear pair with involute tooth profiles and a contact ratio range between one and two is assumed. Such an analysis begins with common, elementary gear data, and implies no foreknowledge of the tooth compliance. However, experimental data or external analytical compliance data may be input directly into Gearsep2 (the dynamics section of Gearsep), which again is constructed to operate autonomously from the section which calculates the varying tooth compliance. Other constraints are discussed throughout Chapter 6.

The overall Gearsep program is designed to analyze a single-stage system, a component found in many common gear mechanisms. The single- stage system is composed of a driving mass and shaft, two gears in mesh, and a driven shaft and mass, where shaft bending is assumed to be negligible, eliminating the need for treatment of Coriolis and gyroscopic gear effects [14]. A single-stage system was used in Figure 4, and as is now presented in detail in Figure 5, where the driving mass is an

electric motor, and the driven mass. or load. is a compressor.
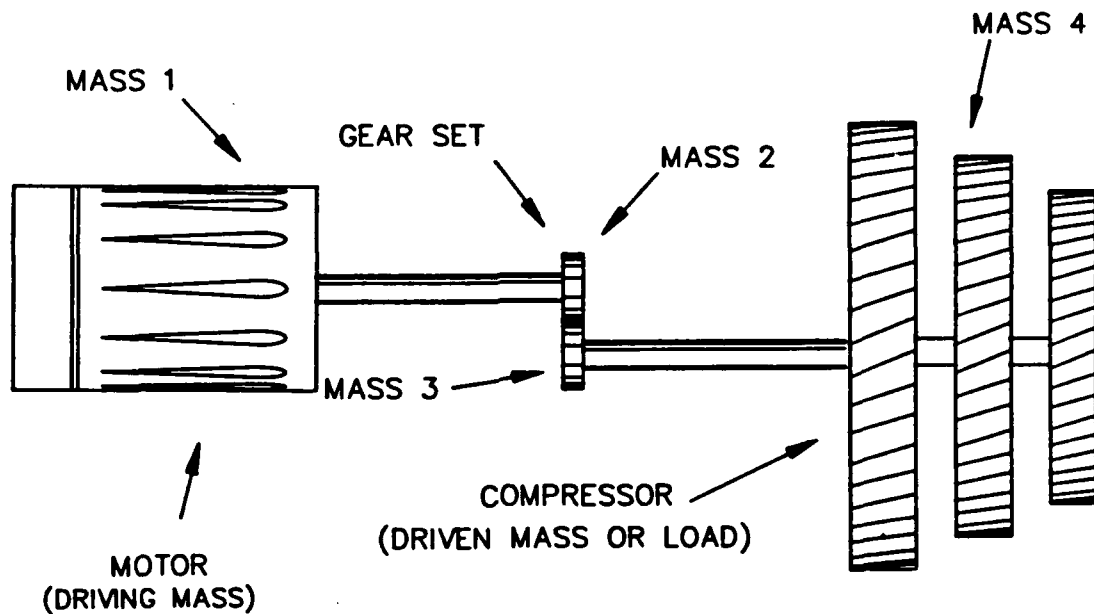
Figure 5: Typical Single-Stage Gear System

For a more complicated system where a discrete mass value for one or more of the end masses does not exist, *effective inertias* may be used to assemble a corresponding single-stage system [15]. This would be a necessary pre-Gearsep analysis for a dual system such as that shown in Figure 6, where a small power generator is being driven by a third gear mounted in tandem with the original two. This type of system would require two separate applications of the Gearsep analysis, one for each of the system's two gear meshes.

17
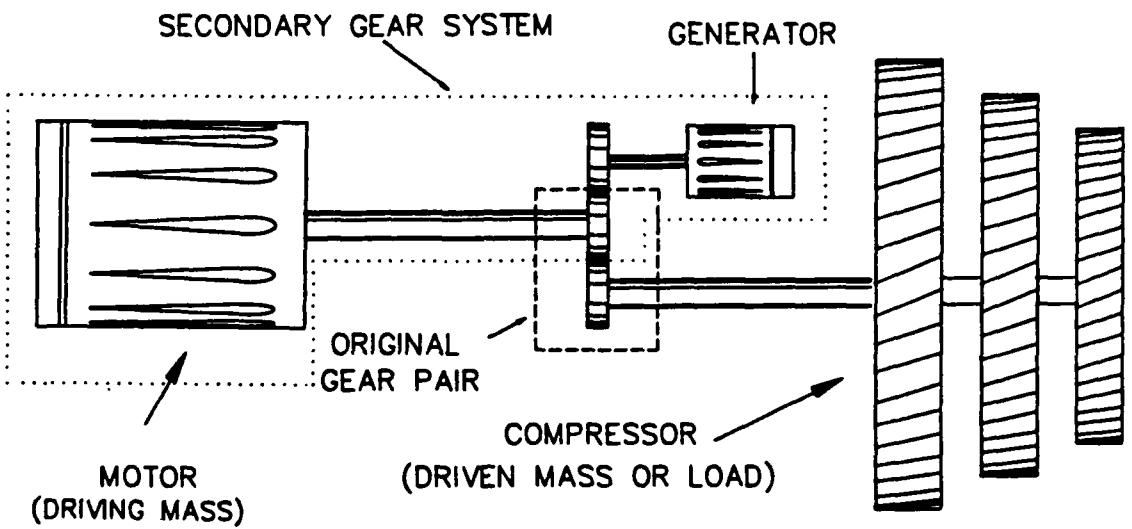
Figure 6: Dual Single-Stage Gear System

Chapter 2

ANALYTICAL SOLUTION OF THE GEAR SYSTEM

2.1. Chapter Overview

The following is a summary of the precursory analysis necessary to confirm the analytical model of the single-stage spur gear system shown in Figure 1. Details may be found in Appendix C.

The true gear system is first idealized and simplified by assuming that the gears are perfect rolling elements, which transfer uniform rotary motion with no unsteady components from tooth dynamics. This allows the single-stage system's four equations of motion to be rewritten as three representative equations of motion, a form that is solvable using standard techniques: For this analysis, generalized coordinates are used to create the analytical model [16].

2.2. Equations of Motion

For the analytical solution of a single-stage gear system, shown in lumped mass form in Figure 7, the gears are assumed to be, as stated, perfect rotational elements.
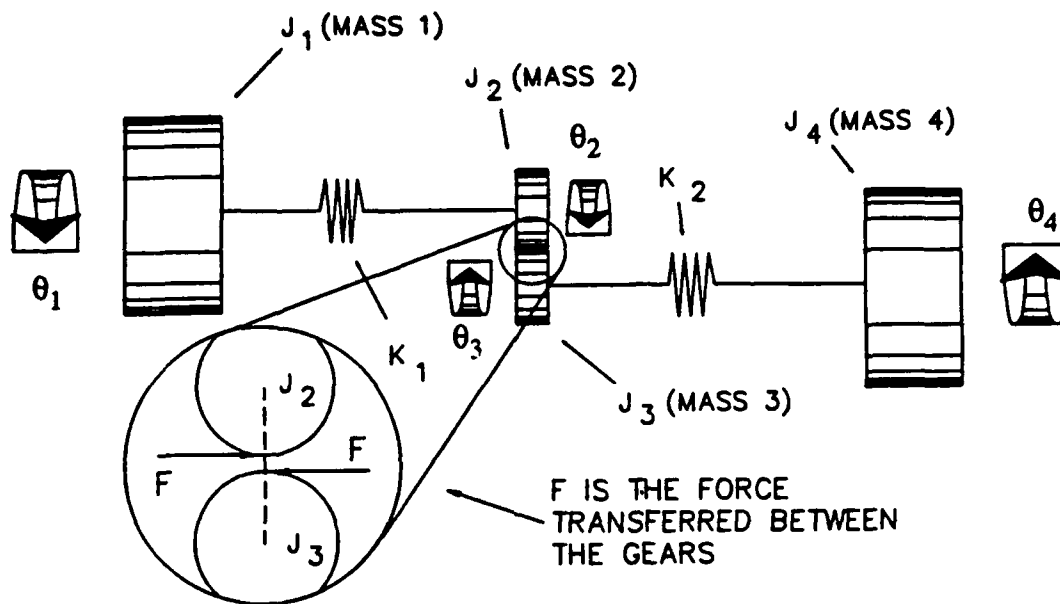
Figure 7: Lumped Parameter Gear System Model

The system is described by the following equations of motion:

$$J_1\ddot{\theta}_1 = k_1(\theta_2 - \theta_1) + c(\dot{\theta}_2 - \dot{\theta}_1) \qquad \text{Equation 1a}$$

$$J_2\ddot{\theta}_2 = k_1(\theta_1 - \theta_2) + c(\dot{\theta}_1 - \dot{\theta}_2) - Fr_2 \qquad \text{Equation 2a}$$

$$J_3\ddot{\theta}_3 = k_2(\theta_4 - \theta_3) + c(\dot{\theta}_4 - \dot{\theta}_3) - Fr_3 \qquad \text{Equation 3a}$$

$$J_4\ddot{\theta}_4 = k_2(\theta_3 - \theta_4) + c(\dot{\theta}_3 - \dot{\theta}_4) \qquad \text{Equation 4a}$$

where k is the shaft stiffness, c is a generalized damping (not considered directly in this analysis), and F is the transferred force shown in Figure 7. However, for the *real* single-stage system, this

transferred force is nothing more that the instantaneous tooth pair stiffness tooth pair stiffness as a function of position in mesh ($K_{TOOTH\ PAIR}$: see Chapter 3) multiplied by the relative displacements of the two gears (θ_2 and θ_3). Substituting this for F in Equations 1a through 4a, the equations of motion become:

$$J_1\ddot{\theta}_1 = k_1(\theta_2 - \theta_1) + c\,(\dot{\theta}_2 - \dot{\theta}_1) \qquad \text{Equation 1b}$$

$$J_2\ddot{\theta}_2 = k_2(\theta_1 - \theta_2) + c\,(\dot{\theta}_1 - \dot{\theta}_2) - K_{TOOTH\ PAIR}\,(\theta_2 - \theta_3) \qquad \text{Equation 2b}$$

$$J_3\ddot{\theta}_3 = k_2(\theta_4 - \theta_3) + c\,(\dot{\theta}_4 - \dot{\theta}_3) - K_{TOOTH\ PAIR}\,(\theta_3 - \theta_2) \qquad \text{Equation 3b}$$

$$J_4\ddot{\theta}_4 = k_2(\theta_3 - \theta_4) + c\,(\dot{\theta}_3 - \dot{\theta}_4) \qquad \text{Equation 4b}$$

Note that it is this set of equations that is actually solved by the numerical integrator (see Chapter 4) to predict separation.

Equations 1b through 4b must be altered slightly to allow an analytical solution benchmark. For the analytical solution, all damping is assumed negligible ($c = 0$) and mass moments of inertia are established in an arbitrary manner as described in Appendix D. The solution is found for a set of arbitrary initial displacements of the lumped mass system shown in Figure 7, where mass 1 and mass 4 correspond to the motor and load masses, respectively.

Because mass 2 and mass 3 in Figure 7 are assumed to be perfect in their transfer of rotary motion for the *analytical*

system, the transferred force F is constant for the benchmark solution. Through the algebraic elimination of F, Equations 1 through 4 may be combined to produce a reduced set of equations as follows:

$$J_1\ddot{\theta}_1 + k_1(\theta_1 - \frac{r_3}{r_2}\dot{\theta}_2) = 0 \qquad \text{Equation 5}$$

$$\left[J_3 + \left(\frac{r_3}{r_2}\right)^2 J_2\right]\ddot{\theta}_3 - \frac{r_3}{r_2}k_1\theta_1 + \left[\left(\frac{r_3}{r_2}\right)^2 k_1 + k_2\right]\theta_3 - k_2\theta_4 = 0 \qquad \text{Equation 6}$$

$$J_4\ddot{\theta}_4 + k_2(\theta_4 - \theta_3) = 0 \qquad \text{Equation 7}$$

At first, Equation 6 appears to be fairly obscure in its origin. However, its appearance simplifies by noting the placement of the gears' radii ratio r_3/r_2 when the four equations of motion reduce to three: Equation 6 must describe a single fictitious rotational body comprising the characteristics of the two original gears. Thus, mass and stiffness terms in Equation 6 may be regarded as *effective* quantities, numerically weighted by the radii ratio.

Having removed all reference to θ_2 from the equations of motion, the mass numbering system will now be redefined as shown in Figure 8. Notice that the positive direction of the load mass has been reversed from that of Figure 7.
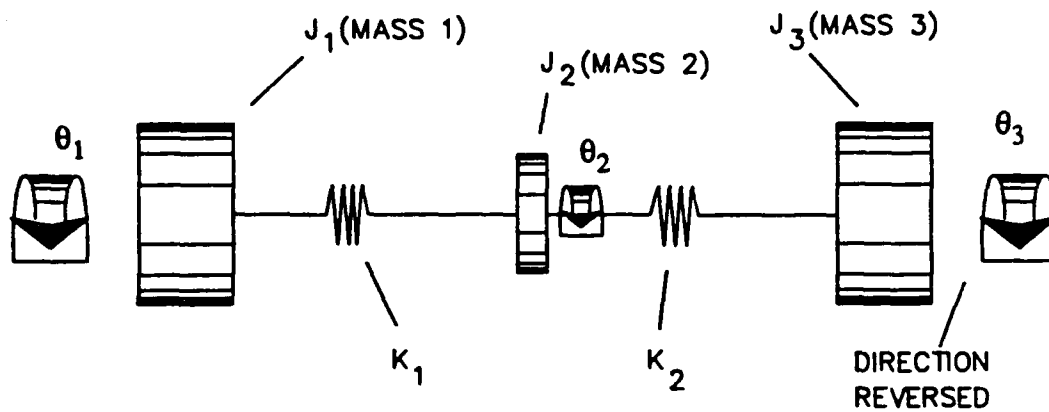
Figure 8:   Reduced Lumped Parameter Gear System Model

2.3.   Homogeneous Solution Components

The two homogeneous solution components necessary for
obtaining the particular solution are the natural frequencies and
the mode shapes, both of which are obtained by solving the
eigenvalue problem with standard techniques as discussed in
Appendix C. The natural frequencies in quadratic form become:

$$\omega^2 = \frac{-b \pm \sqrt{b^2 - 4ac}}{2a} \qquad \text{Equation 8}$$

with:

$$a = J_1 J_4 \left(J_3 + J_2 R^2 \right) \qquad \text{Equation 9}$$

$$b = -R^2 \left[J_1 J_2 k_2 + k_1 J_4 \left(J_1 + J_2 \right) \right] - k_2 J_1 \left(J_3 + J_4 \right) - J_3 J_4 k_1 \qquad \text{Equation 10}$$

$$c = k_1 k_2 \left[R^2 \left(J_1 + J_2 \right) + J_3 + J_4 \right] \qquad \text{Equation 11}$$

The modal matrix lists the naturally occurring mode shapes by column, and is normalized by defining the first row with unit displacements. All other elements are functions of the system's inertias, natural frequencies, shaft stiffnesses, and the gear radii ratio r_3/r_2 as contained in the set of variables $A_{i,j}$, where the subscripts represent row and column positions. For an unrestrained (free rolling) single-stage system, the modal matrix will take on the following form:

$$[\phi] \equiv \begin{bmatrix} 1 & 1 & 1 \\ 1 & A_{22} & A_{23} \\ 1 & A_{32} & A_{33} \end{bmatrix} \qquad \text{Equation 12}$$

where the entries of row 1 (what would more generically be A_{11}, A_{12}, and A_{13}) are unit displacements. Notice that the first column (entries A_{11}, A_{21}, and A_{31}) of Equation 12 indicates that the first

mode shape is made up of unit displacements of all of the elements. This is indicative of an unrestrained, or *semi-definite* system where the first displacement mode is a simple rigid body rotation [17], and the first natural frequency is zero (see Appendix C).

2.4. Particular Solution

Solving for the particular solution using generalized coordinates, the modal equations of motion are obtained:

$$M_1\ddot{q}_1 + M_1\omega_1^2 q_1 = 0 \qquad \text{Equation 13}$$

$$M_2\ddot{q}_2 + M_2\omega_2^2 q_2 = 0 \qquad \text{Equation 14}$$

$$M_3\ddot{q}_3 + M_3\omega_3^2 q_3 = 0 \qquad \text{Equation 15}$$

where the generalized coordinate q is defined by:

$$\{\theta(t)\} = [\phi]\{q(t)\} \qquad \text{Equation 16}$$

The modal equations are then solved by assuming a solution of the following form:

$$q_n(t) = E_n \, Sin(\omega_n t) + G_n \, Cos(\omega_n t), \quad n = 1,2,3 \qquad \text{Equation 17}$$

Finally, by assigning initial conditions and solving for the E's and G's in Equation 17, and substituting the resulting $q_n(t)$'s into Equation 12, the analytical solution of the system is obtained in the form (shown here for the displacement of the first mass only):

$$\theta_1(t) = A_{11}q_1(t) + A_{12}q_2(t) + A_{13}q_3(t)$$
$$= (A_{1n})(G_1)\cos\omega_1 t + (A_{2n})(G_2)\cos\omega_2 t + (A_{3n})(G_3)\cos\omega_3 t$$

$$n = 1,2,3 \qquad \text{Equation 18}$$

$\theta_2(t)$ and $\theta_3(t)$ are solved for in a similar manner.

Notice that no E_n's from the assumed generalized solution (Equation 17) appear in the final system solution: With initial conditions taken at time $t = 0$, the E_n's can only survive if there is a non-zero initial velocity. In foresight of the types of initial conditions which will be chosen for the analytical benchmark (see Chapter 5), the initial velocities for all masses are assumed to be zero, thus simplifying the analysis.

Chapter 3

TOOTH COMPLIANCE MODEL

3.1. Chapter Overview

This chapter presents the model used for the compliance of a pair of meshing gear teeth. Again, the principle source of gear excitation is assumed to be the deflection of the teeth from their unstressed positons, and that excitation is most naturally described in terms of displacements [18]. In this light, the model selected is that of Cornell [19], which predicts *linear* tooth deflection both at and in the direction of the tooth loading for any given tooth load. The tooth pair *compliance* is calculated (rather than the stiffness) in order to maintain continuity with Cornell and the majority of works in this area, both past and present. Furthermore, all work in this section, unless otherwise specified, is attributed to Cornell.

The total tooth pair deflection is calculated as a summation of tooth and fillet area cantilever beam deflection (bending and shear), foundation deformations, and Hertzian and localized tooth body deformations. In the discussion to follow, variables directly involved in the deformation equations are followed by qualitative descriptions, with a comprehensive treatment of all variables,

direct and indirect, available in reference [19].

It should be noted that the model chosen is not the most sophisticated available. Modeling techniques which relied on Fourier series or Legendre polynomial representations are avoided in favor of confirmed and straightforward relations based on strength of materials and common gear geometries. This is done to produce an analysis technique that is aimed less at pure gear dynamics research and more at an engineering application, with mathematics that may be readily understood and, more importantly, readily altered.

3.2. Beam Compliance

The tooth beam compliance Y_B is comprised of both cantilever and shear deflection, with all deflections defined at the load point and in the loading direction. The deflection equation itself comes from strength of materials, and is an integral over the length of the tooth cantilever. In numerical terms, this translates to a summation of a series of discrete elements. From Cornell [19] (p. 449):

$$Y_B = \frac{L\cos^2(\phi_L')}{E} \sum_{i=1}^{n} \delta_i \left\{ \frac{l_i^2 - l_i \delta_i + \frac{1}{3}\delta_i^2}{\bar{I}_i} + \frac{(2.4(1+\mu) + \tan^2(\phi_L'))}{\bar{A}_i} \right\} \qquad \text{Equation 19}$$

where:

n : the number of summation element increments into which the tooth cantilever is divided.

L : the load on the tooth: This is taken to be unity.

ϕ_L' : a localized pressure angle at the loading point: This results from using tooth centered coordinates where the tooth is horizontal to the viewer, as opposed to gear centered coordinates where the position of the tooth depends on its location in mesh (compare Figure 9 with Figure 3).

E : Young's modulus

δ_i : the summation element increment: This is the width of the interval of summation which takes the place of a continuous integral.

l_i : the location of δ_i at each summation step

μ : the material's Poisson's ratio

$(1-\mu^2)$: anticlastic term as applied to a "wide" tooth: Cornell defines such a tooth as one whose ratio of its width to it thickness (measured at pitch) is greater than five [19]. Anticlastic

terms take into account the possibility of
anticlastic curvature in the teeth, where usual
lateral bending gives rise to a longitudinal
bending of opposite sign.

$\overline{A}$: anticlastic tooth cross section area term at
each summation point

$\overline{I}$: anticlastic section modulus term at each
summation point

Note that the "barred" quantities ($\overline{A}, \overline{I}$, etc.) have a direct
geometric relation to the base of the tooth cantilever. The tooth
cantilever geometries are shown in Figure 9, with $\overline{h}$ defined as the
height or thickness of the base of the tooth cantilever:
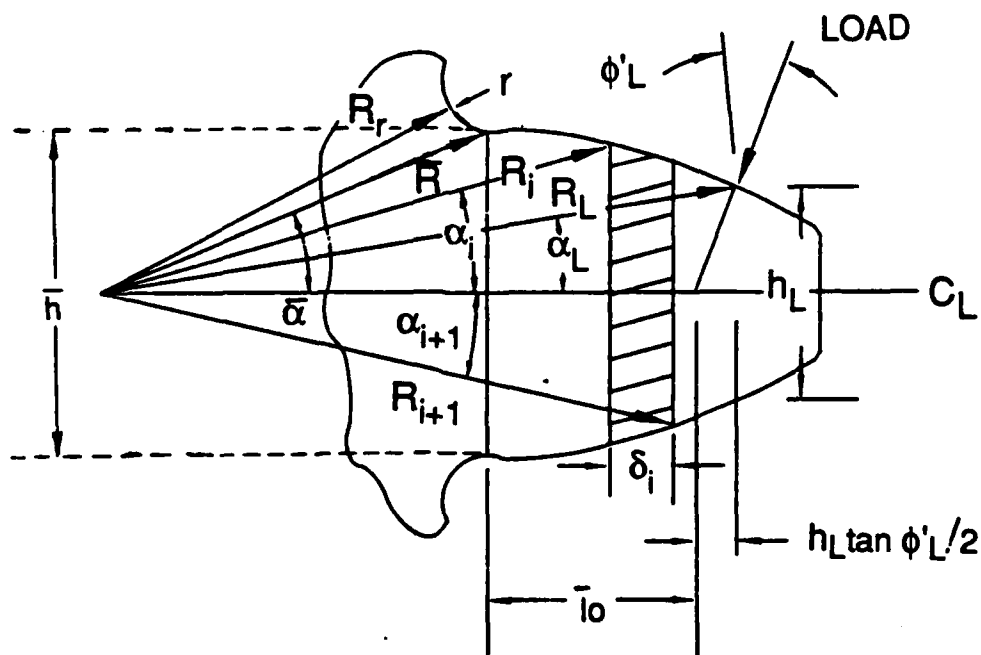
Figure 9: Geometry for Tooth Cantilever Beam Deflection

As a side note, anticlastic curvature is easily demonstrated with the aid of a "Pink Pearl" bar-type eraser. By holding the eraser with fingers and slowly bending it in half, the normally flat sides can be seen to curve in the opposite directing of, and at a right angle to the principal curvature.

3.3. Fillet and Foundation Compliance

The total fillet and foundation deflection Y_F is divided into fillet beam and shear bending Y_{FB}, and foundation flexibility Y_{FF}. Fillet deflection is based on the assumption that the fillet region may be considered to be a stout cantilever beam, thus allowing Equation 19 to be reused. The equation for the foundation deformation from Cornell [19] (p. 449) is:

$$Y_{FF} = \frac{L\cos^2(\phi_L)}{WE}\, \Omega_1 \left[\frac{16.67}{\pi}\left(\frac{l_f}{h_f}\right)^2 + 2(\Omega_2)\left(\frac{l_f}{h_f}\right) + 1.534\left(1 + \frac{\tan^2(\phi_L)}{2.4(1+\mu)}\right) \right] \qquad \text{Equation 20}$$

where: W :   the tooth's facewidth and also the gear thickness

Ω_1, Ω_2 :   the terms carrying the anticlastic properties of the tooth (see Appendix B, Section 11)

l_f: the location of the inboard boundary of the fillet region

h_f: the fillet thickness at l_f

All other variables are as described for Equation 19.

Foundation and fillet geometries are shown in Figure 10.
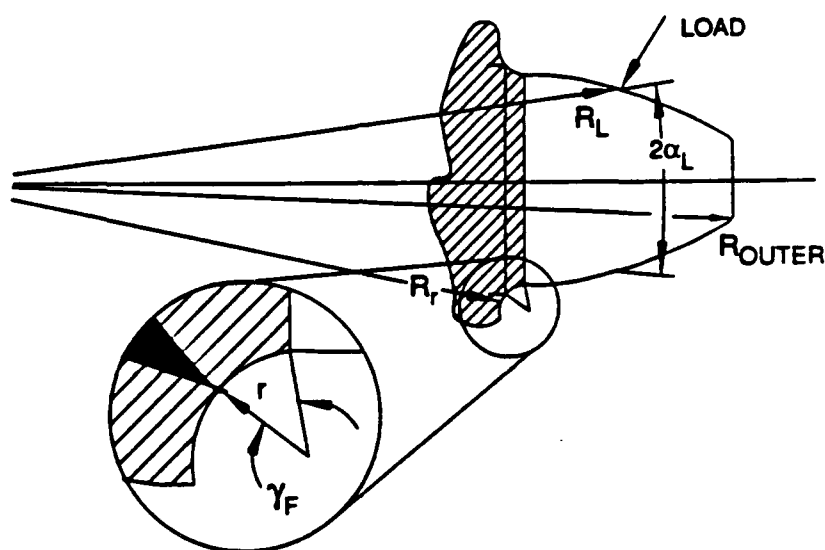
Figure 10:   Geometry for Fillet Cantilever and Foundation Deflection

Although the bulk of Equation 20 is based on simple gear tooth and body geometry, there exists no expression for the actual size of the fillet cantilever, which is described by the angle γ_F in Figure 10. Cornell contends that this should be the angle which produces the maximum deflection at the load point and in the direction of loading. It is therefore also the angle which causes Y_F to be a maximum in the following:

$$Y_F = Y_{FF} + Y_{FB} \qquad \text{Equation 21}$$

where both Y_{FF} and Y_{FB} are dependent on γ_F.

Although Cornell presents a variety of computed γ_F values for various gear forms that may be directly used in the analysis, Gearsep will calculate the actual value of the angle, the details of which are in Appendix A.

3.4. Localized and Hertzian Deformations

This final deformation type includes both the Hertzian surface deformation and the tooth body compression between the point of contact and the tooth centerline. Cornell offers three choices for the expression of these localized deformations. After presenting a comparsion of each choice with experimental results, a closed form solution was suggested, in part because of its handling of nonlinear effects. From Cornell [19] (p. 450):

$$Y_{hertz_i} = \frac{2L}{\pi W} \left(\frac{1 - \mu_p^2}{E_p} \right) \left\{ \ln \frac{2\bar{h}_p}{b} - \left(\frac{\mu_p}{2(1 - \mu_p)} \right) \right\} + \left(\frac{1 - \mu_g^2}{E_g} \right) \left\{ \ln \frac{2\bar{h}_g}{b} - \left(\frac{\mu_g}{2(1 - \mu_g)} \right) \right\}$$

Equation 22

In Equation 22:

p & g: subscripts indicating varibles for the pinion and gear, respectively: By convention, the "pinion" is the *driving* gear, while the "gear" is the *driven* gear.

ln: the natural logarithm function

$\overline{h}$: thickness at the base of the tooth cantilever

b: Hertzian half-contact width: This is defined by Cornell as:

$$b = \left\{ \frac{\frac{4L}{\pi W}\left[\left(\frac{1-\mu_p^2}{E_p}\right)+\left(\frac{1-\mu_g^2}{E_g}\right)\right]}{\left[\frac{1}{r_p}+\frac{1}{r_g}\right]} \right\}^{\frac{1}{2}} \qquad \text{Equation 23}$$

In Equation 23, r is the local radius of curvature of the involute profile, and all other variables are as previously described.

Figure 11 shows the geometries for these local deformations.

3.5. Assembled Compliance Model

Because the described deflections are for unit loads, the total compliance of a pair of meshing teeth may be obtained by simply inverting the sum of all individual deflection types for that pair.

This, however, provides a compliance value at only one point in mesh. As the process of calculating the unit load deflection for every iteration point would be too time consuming (Chapter 6 will show that there may easily be thousands of points *per tooth mesh*) the deflection will be calculated at five specific *compliance points* along the line of action. A five-term power series will then be used to represent the changing tooth pair compliance and will thus supply an easily solvable analytic compliance expression. A compliance function plot is shown in Figure 12; this particular plot is associated with the sample analysis system of Chapter 6.
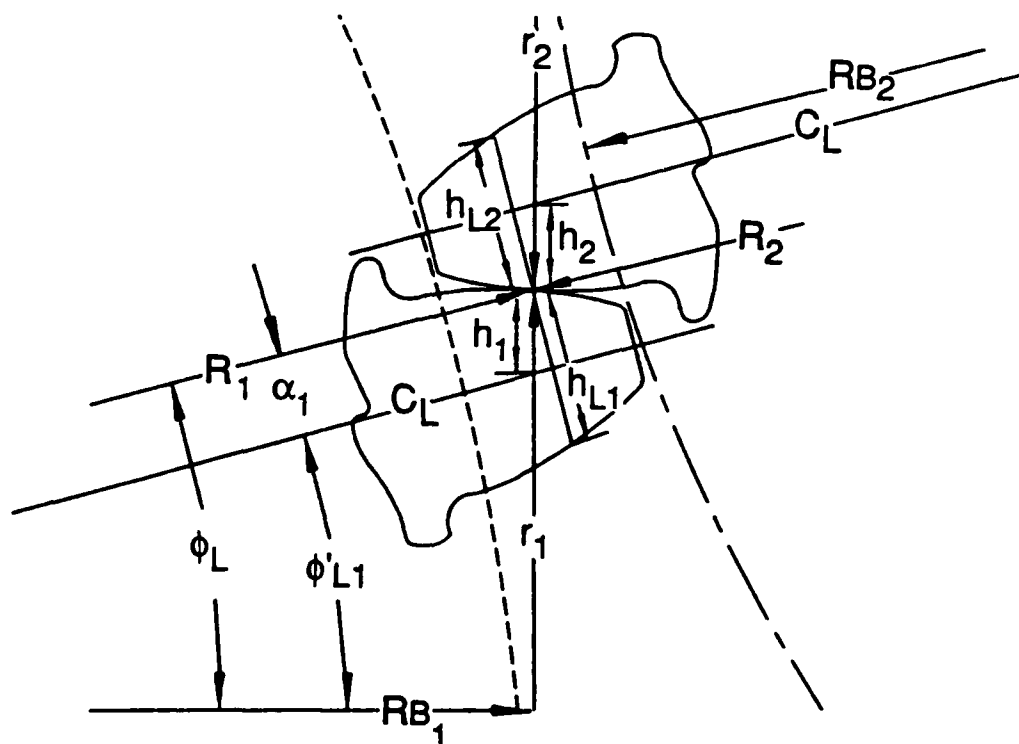
Figure 11: Geometry for Localized and Hertzian Deformations
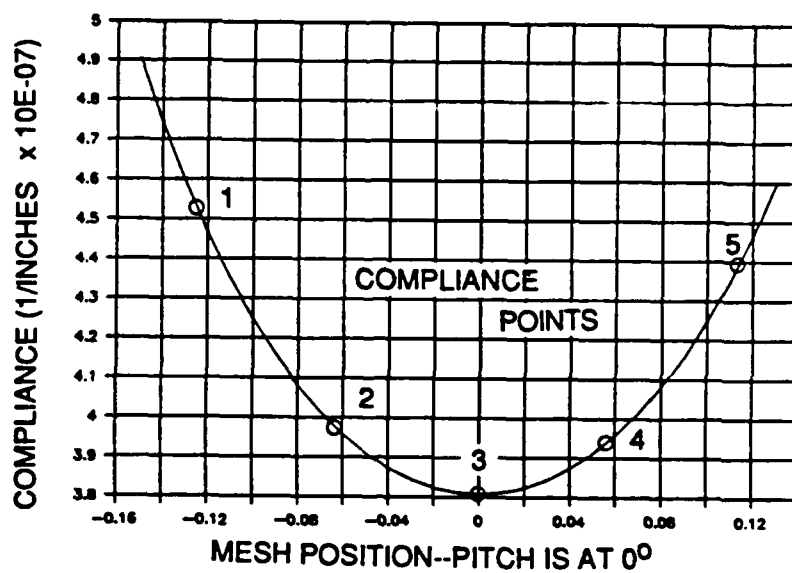
Figure 12: Power Series Compliance Function

Cornell provides an in-depth confirmation of the proposed compliance model, in which calculated deflections are compared to both finite element and experimental data. The conclusion drawn is that the compliance model presented is "probably as accurate as any available" [19].

Chapter 4

NUMERICAL INTEGRATION

4.1. Chapter Overview

The following is a brief overview of the numerical integrator chosen to solve the single-stage equations of motion (Equations 1 through 4), with details of the routine given in Appendix D. All work in this section, unless otherwise noted, is attributed to Katona [20].

For the actual prediction of separation, a numerical solution was chosen over an analytical approximation to permit arbitrary time varying loads and experimental tooth compliance data, along with material or bearing damping functions to be incorporated if desired. Optional inputs such as these would greatly complicate or make impossible an analytical solution, as they may be nonlinear expressions or simply be comprised of raw numerical data.

4.2. The Beta-m Numerical Integration Scheme

The numerical integrator used to solve the gear system's equations of motion is the *beta-m* method. This is a generalized form of the well recognized Newmark scheme [21], and solves

equations of the form:

$$M \ddot{x} + C \dot{x} + K x = f \qquad \text{Equation 24}$$

where **M** is the mass matrix, **C** is the matrix of damping coefficients, **K** is the stiffness matrix, and **f** is a matrix of forcing functions.

The beta-m method is developed by expanding Newmark's integration expressions in a Taylor series, which is then conveniently apportioned for use in an algorithm format. The Taylor series takes on the form:

$$\overset{(k)}{x}_{n+1} = q_k + b_k \overset{(m)}{\Delta x} \qquad \text{Equation 25}$$

where, for $k = 0, 1, ..., m$ (for an mth order approximation with $\beta_m = 1$)

$$q_k = \sum_{j=k}^{m} \overset{(j)}{x}_n h^{j-k}/(j-k)! \qquad \text{Equation 26}$$

$$b_k = \beta_k h^{m-k}/(m-k)! \qquad \text{Equation 27}$$

and x_{n+1} is the displacement at the *next* timestep. The over-scripts (k) and (j) on x take the place of the ususal "dot over-script" notation for time derivative indices, and *m* is the

order of the approximation. In Equations 25 and 26, the q_k term is the Taylor series expansion of x_{n+1} up to the term x_n (and is thus termed a "history vector"), and the last term in Equation 25 may be interpreted as the error in the expansion's approximation of x_{n+1}.

The beta-m method is easily altered through the use of various β values, a sampling of which are provided by Katona. The β's used in Gearsep produce a solution of optimal accuracy with a truncation error order of four. This choice is made in hindsight of the results of the data analysis of Chapter 6. In that analysis, it shall be seen that a beta-m method of increased stability would indeed expand the range of operating conditions under which a stable numerical response (and therefore usable data) results, but it would not expand it into the area of the range where separation is most likely to occur.

Chapter 5

CONFIRMATION OF THE NUMERICAL MODEL
AND SPECIALIZED PROGRAMMING PROCEDURES

5.1. Chapter Overview

This chapter confirms Gearsep's beta-m numerical integration
solution by comparing it with the analytical solution of the
reduced single-stage system presented in Figure 8. This is the
semi-definite (unrestrained) lumped three mass system reduced
from a four mass single-stage system as discussed in Chapter 2. It
should be noted that an actual Gearsep analysis solves the *true*
gear system of Figure 7 (as described by Equations 1 through 4),
not the reduced system (three equations of motion). It should also
be noted that the driving force for the system is the torque applied
to mass 1 (Figure 7): mass 1 represents the motor's internal shafts
and rotating armature.

Also discussed in this chapter is the use of a special case model
for systems with an extreme difference of mass moment of
inertia values between its elements (the J 's of Chapter 2). If in a
particular system the difference between, say, the J value of the
motor and that of the driving gear is too large, round off errors
will occur in the numerical routine and its supporting algorithms.

To characterize the range of relative J values under which this can occur, the top system of Figure 13 will be solved for various motor/load J values with a fixed J value for the gear pair, and the results compared with the solution of the special case model with the same gear pair J. The form of this model is shown at the bottom of Figure 13, which represents a system whose the outer masses are so large in comparison to the gears that they may be assumed to not affect the response, and so, are replaced by fixed supports.
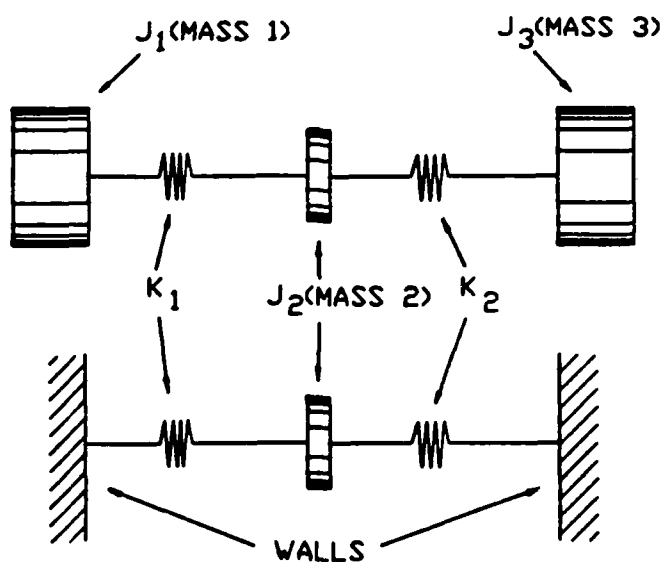
Figure 13: Semi-Definite and Fixed Gear Systems

5.2. Three Mass System Benchmark

5.2.1. Analytical Solution

The benchmark system used to confirm the numerical procedure will be one with symmetric masses and shafts as shown at the top of Figure 13. Note again that this corresponds to the reduced four mass single-stage system of Chapter 2, where R is the radii ratio of the gears at pitch. For the *four* mass system let the arbitrary system parameters be given as follows:

$$J_1 = J_4 = 10 \quad J_2 = J_3 = 5 \quad k_1 = k_4 = 200 \quad R = 1$$

([ft lb]/unit angular acceleration)   ([ft lb]/radian)

This would roughly correspond to a system with outer masses of 2.8 inch thick steel disks with 4 inch radii, inner masses of 4.4 inch thick steel disks with 3 inch radii, and 9 inch long steel shafts with radii of 0.2 inches. For the reduced, three mass system, with subscripts adjusted according to Figure 8:

$$J_1 = J_2 = J_3 = 10 \quad k_1 = k_2 = 200$$

([ft lb]/unit angular acceleration)   ([ftlb]/radian)

The relatively high shaft stiffness values are choosen to make the form of the system response more congruous with that of the full

system analysis presented in Chapter 6.

Following the procedures of Chapter 2 as detailed in Appendix C, this system has the following natural frequencies:

$$\omega_1^2 = 0 \qquad \omega_2^2 = 20.0 \qquad \omega_3^2 = 60.0$$

and an eigenvector matrix of the form

$$[\phi] = \begin{bmatrix} 1 & 1 & 1 \\ 1 & 0 & -2 \\ 1 & -1 & 1 \end{bmatrix} \qquad \text{Equation 28}$$

with arbitrarily choosen initial displacements of:

$$\{q_n(0)\} = [\phi]^{-1}\{\theta(0)\} = [\phi]^{-1}\begin{Bmatrix} 1 \\ 3 \\ 8 \end{Bmatrix} \qquad \text{Equation 29}$$

Note that for a true system with the characteristics described above, such large initial deflections would probably cause plastic deformations: It should be realized that these numbers are not representative of any existing system, but rather, were choosen (in hindsight) because of the simple forms of their results. Equally simple are the system's mode shapes, as depicted in Figure 14.

Using the natural frequencies and the initial displacements to solve the derived displacement relation (Equation 18) is solved, the response of the system's mass 2 is obtained as shown in Figure 15.
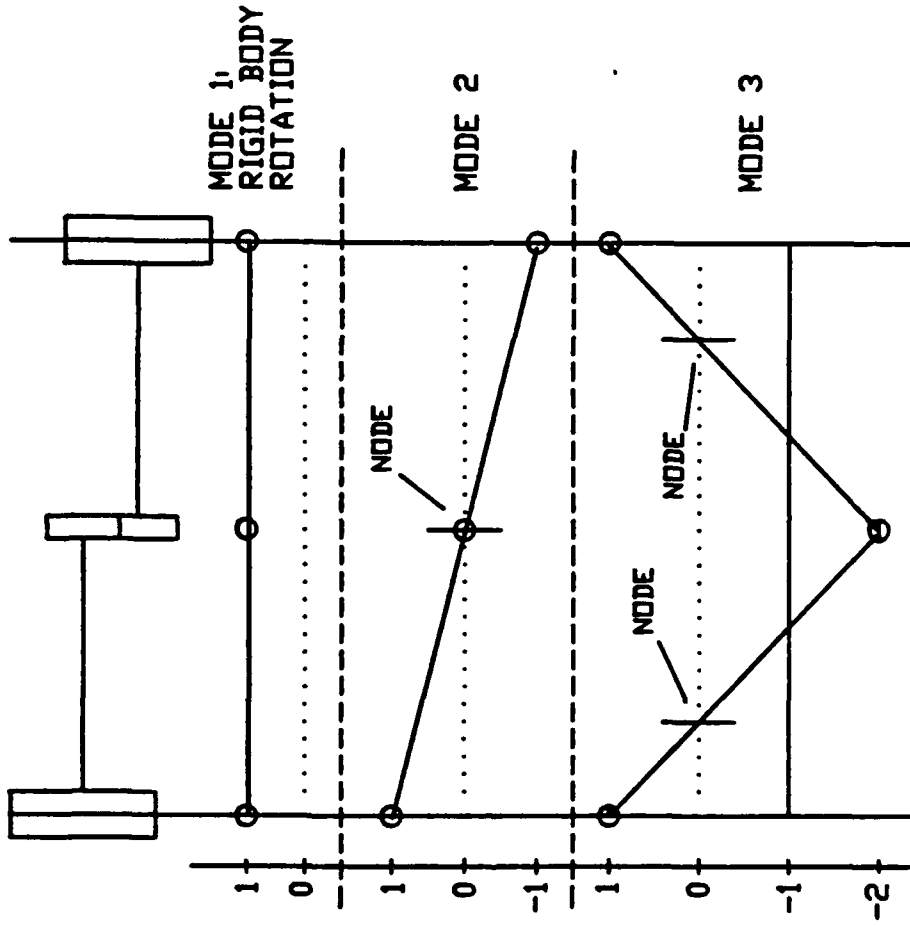
Figure 14: Mode Shapes of Analytical Three-Mass System
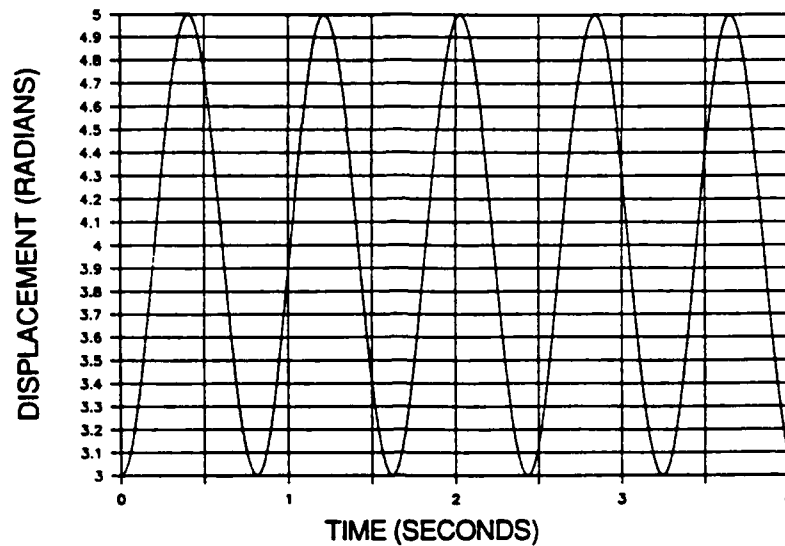
Figure 15: Response of Analytical Three-Mass System

As expected, the system's response is simply a repeating sinusoidal wave, and were it not for the high shaft stiffnesses, the plot would show a superimposed variation in amplitude from the interactions of masses 1 and 3 with mass 2. The phase-plane plot for mass 2 is shown in Figure 16, with a clockwise trace direction. The two-dimensional phase-plane response is in the anticipated form of an ellipse, and shows no signs of instability in either the diaplacement or velocity. This, of course, is indicative of a closed form solution.
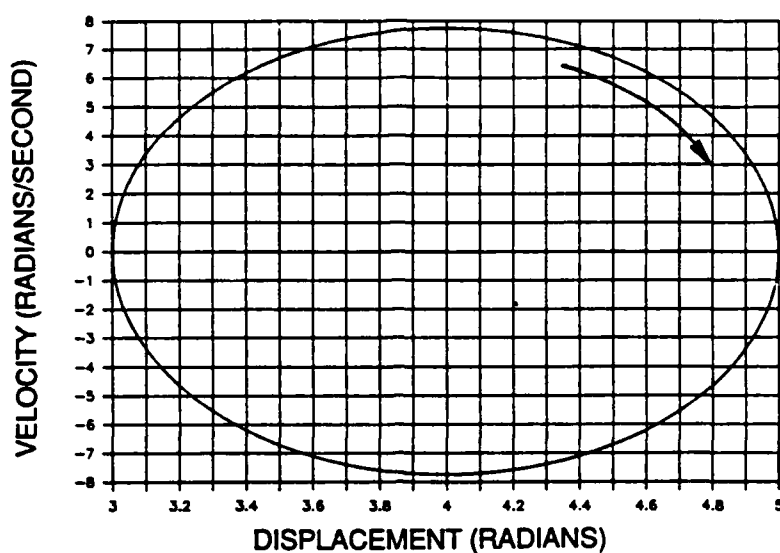
Figure 16:   Phase-Plane Plot of Analytical Three-Mass System

5.2.2.   Numerical Solution

The beta-m method is now used to solve the three mass system
of Figure 8, using the same J's and stiffness values as in Sec. 5.2.1.
The numerical response is taken out to twenty cycles, which in
hindsight is approximately twice the number of cycles needed to
comfortably affirm or disaffirm separation in a true analysis (see
Sec. 6.2.3.). Figure 17 shows a series of numerical responses for
mass 2 plotted against a section of the analytical solution
(originally given in Figure 15) as they approach the end of their
twentieth cycle. Time increments for the numerical plots begin at
0.1 seconds and decrease by a factor of ten for each subsequent
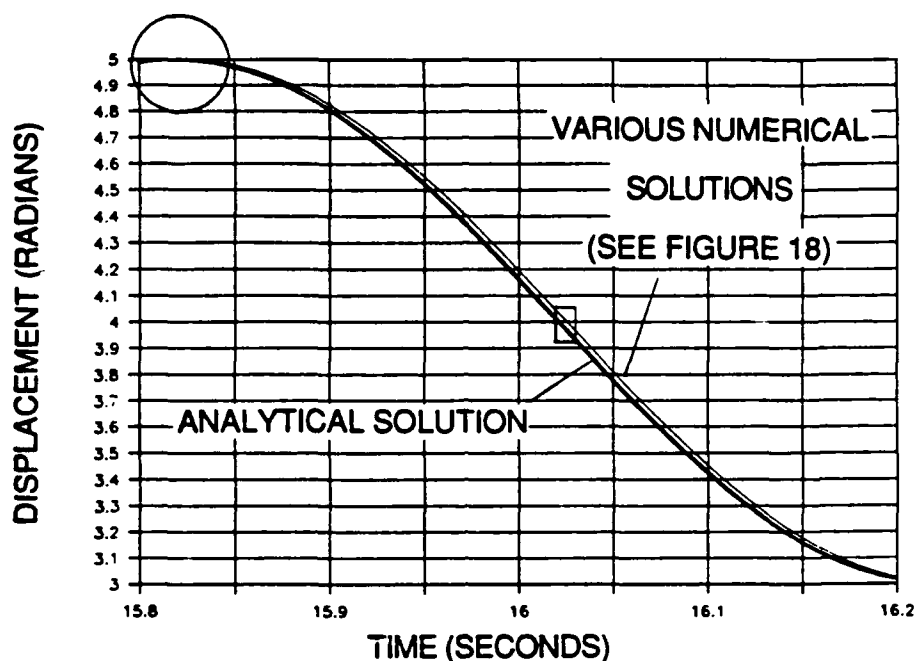
Figure 17: Numerical vs. Analytical Response for Three-Mass System

plot in Figure 17, thus increasing the accuracy of the approximation and forcing the numerical solution to approach the analytical solution. The timestep size was decreased in this manner until the numerical response was within 0.01% of that of the analytical solution, which occurred at a timestep size of 0.001 seconds.

As will be shown later in this section, the largest timestep used in Figure 17 becomes numerically unstable, but still provides an accurate estimate of the response. A timestep size *larger* than this by a factor of ten was attempted, but the result became immediately unstable. It should be noted that each factor of ten stepsize reduction requires an increase in the number of

computations by the same factor.

The nature of beta-m's instabilities can be seen by again examining Figure 17. The peak amplitudes of all responses within the circled area have the same value to within the resolution of the plot, indicating that even for the unstable case, amplitude approximations are qualitatively accurate. The boxed area, however, indicates that a phase shift exists. This is more clearly depicted in Figure 18, which is simply an enlargement of the area in question of Figure 17 (the aspect ratio of the indicated area is altered for clarity). The marked deflections should occur at the same time, but instead, they are increasingly delayed as the timestep size increases, indicating a phase shift.
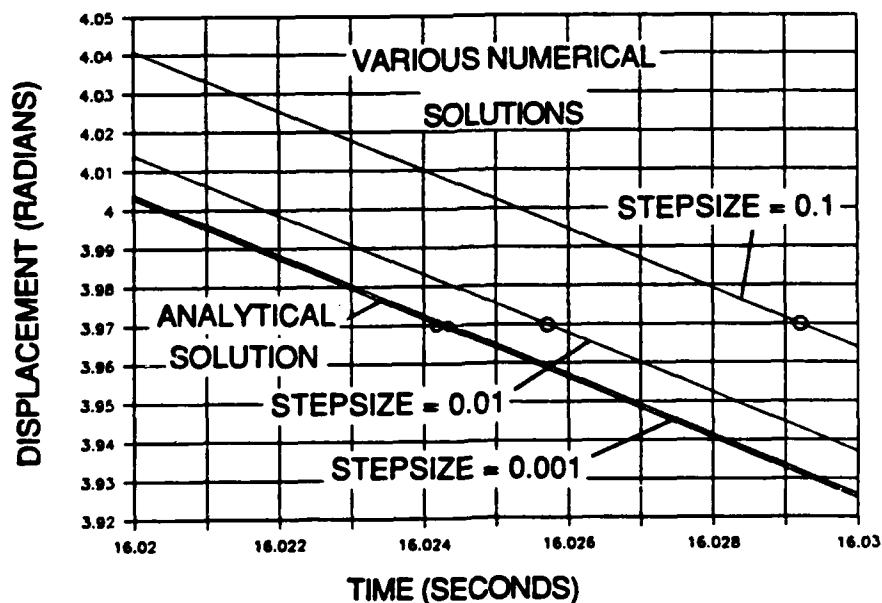
Figure 18: Details of Numerical vs. Analytical Response for Three-Mass System

Figures 19 through 21 show the phase responses for each of the three numerical approximations in Figures 17 and 18. Note again that the numerical routine becomes unstable (visible only in Figure 19). However, as the ultimate goal of Gearsep is to predict relative *displacements*, a phase shift resulting from *velocity* instabilities is not expected to have a significant effect on the accuracy of the analysis.
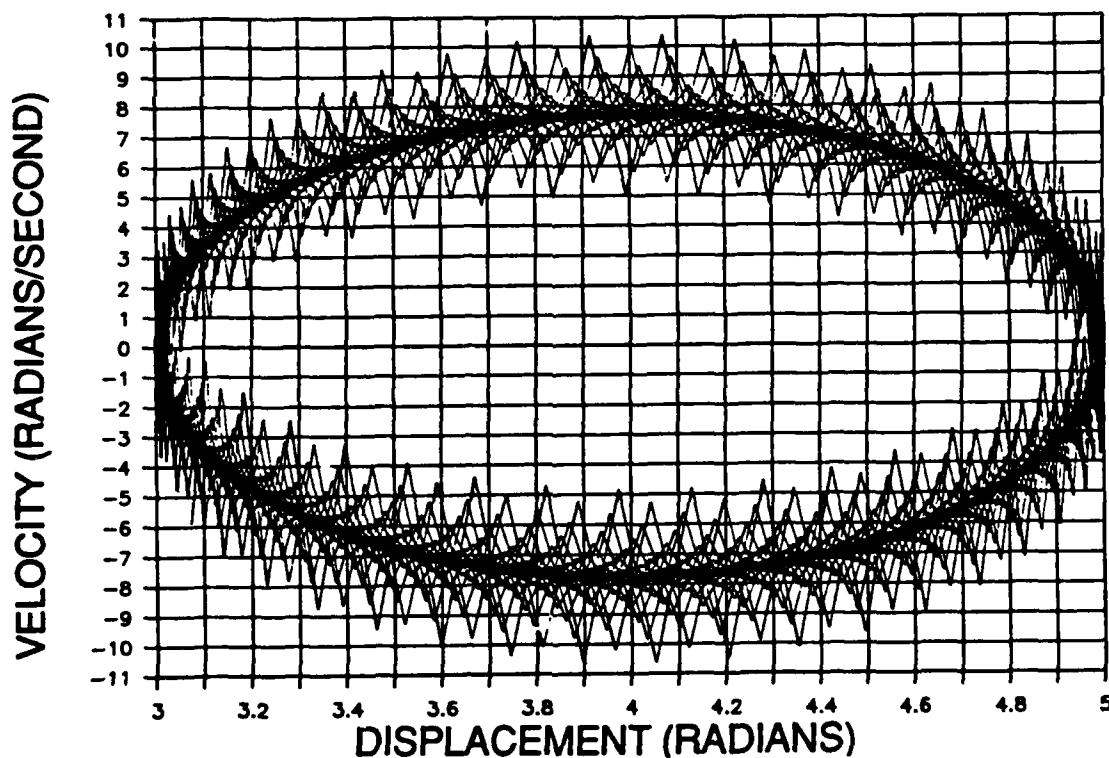
Figure 19: Numerical System Phase-Plane Plot for

Time Step Size = 0.1
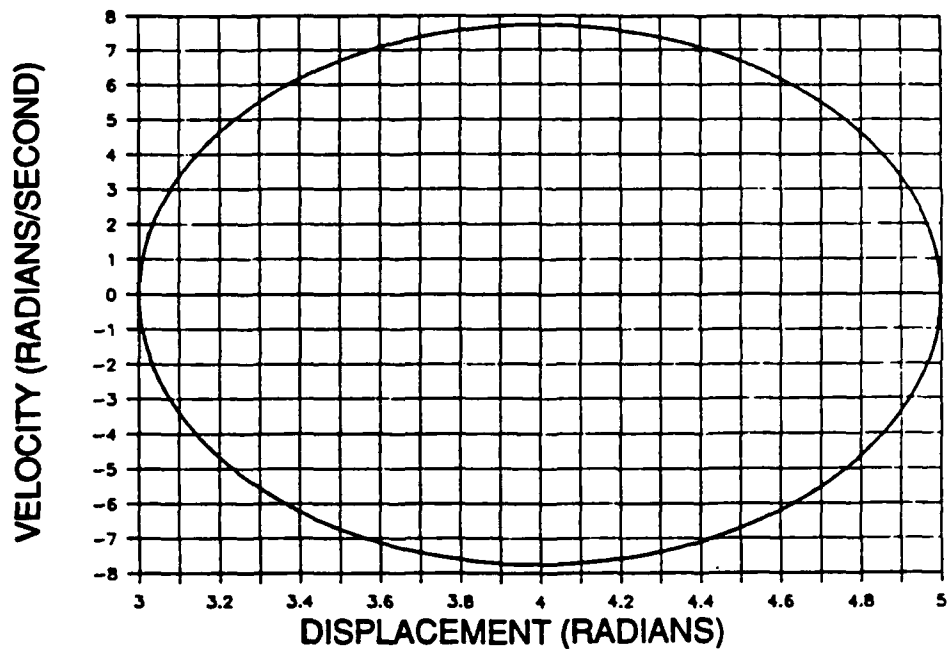
Figure 20: Numerical System Phase-Plane Plot for

Time Step Size = 0.01
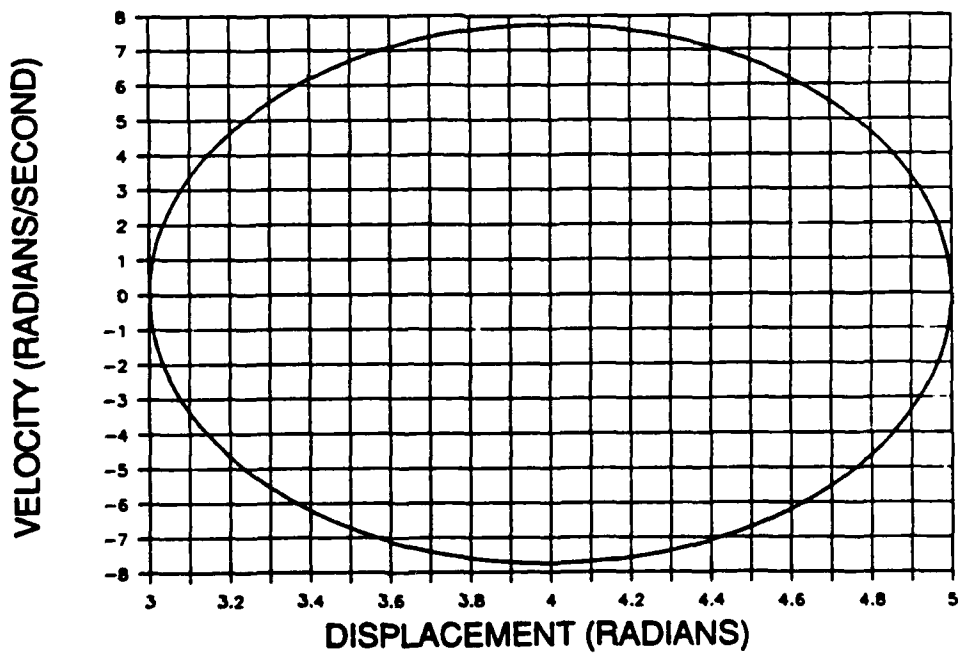
Figure 21: Numerical System Phase-Plane Plot for

Time Step Size = 0.001

5.3. Special Case Modeling Procedures

As discussed in Sec. 5.1., when the moments of inertia of the motor and load masses become very large in comparison with those of the gears, extreme round off errors can occur, destroying the accuracy of the solution. It then becomes necessary for Gearsep to switch from a four mass model to a two fixed-support system. However, it will be seen that as the ratio of the J's increases, the four mass system solution converges toward that of the fixed-support system with considerable accuracy well *before* significant round off error occurs. The one mass solution can therefore be used not only for the extremely high J ratios described, but also down through some range of intermediate values of this ratio. The advantage to using the fixed-support system whenever possible is that Gearsep need only solve *two* equations, as opposed to solving four equations for the entire system.

Because the chosen numerical routine has been shown to accurately represent the analytical response, a tedious analytical solution for the mass moment ratio analysis is avoided by *numerically* solving the fixed-support system as a benchmark. A step size of 0.001 sec will be used in accordance with the results of Sec. 5.2.2., providing a benchmark accurate to within 0.01% of what the analytical solution would be after twenty cycles.

The analysis is similar to that of Sec. 5.2.2., which produced

Figures 17 and 18, except for the use of the numerical routine
benchmark. J values of the gears are the same as those used in the
analysis of Sec. 5.2.1., resulting in a combined mass 2 with J = 10
(see Figure 13). A single fixed-support benchmark solution is
plotted in Figure 22 as it approaches its twentieth cycle, along
with a series of three mass solutions for motor/load J values of
10,000, 100,000, and 1,000,000. For the plot representing a
maximum difference in J values of five orders of magnitude, as
shown in Figure 23, the error is 0.000626 radians, which is within
0.032% of the system's full oscillation range shown in Figure 21.
For mass moment of inertia ratios at or above five orders of
magnitude, then, the fixed-support solution is considered
sufficiently accurate.
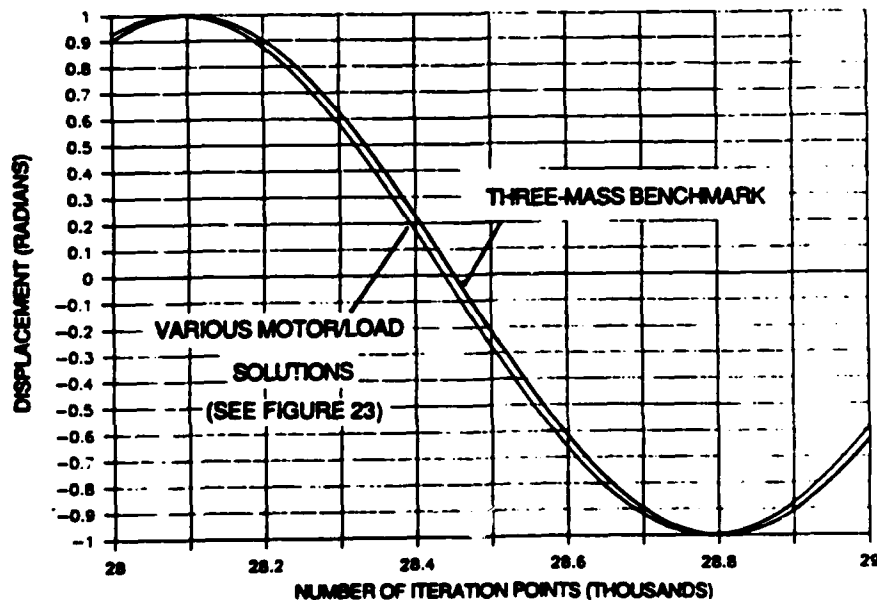
Figure 22:   Numerical vs. Analytical Response for
One-Mass System
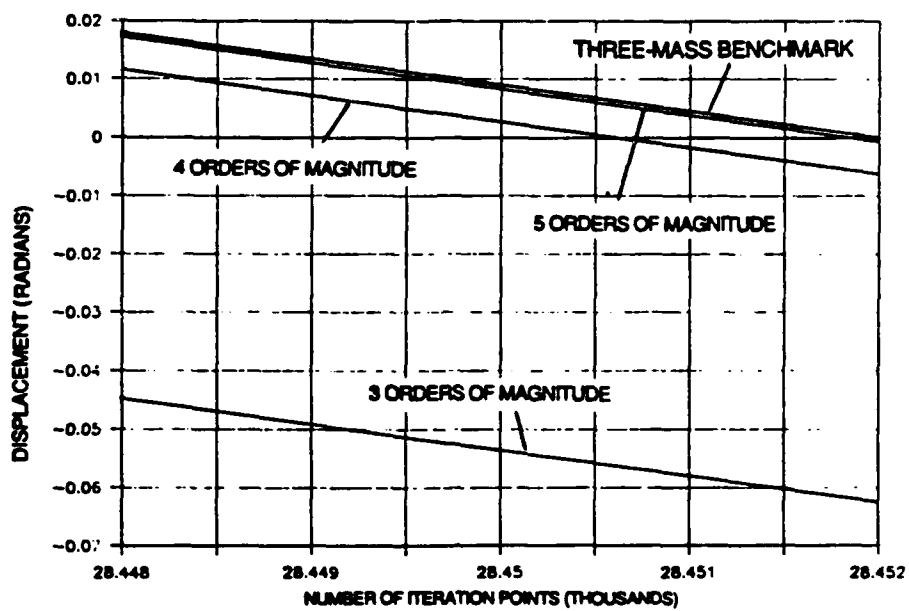
Figure 23:   Details of Numerical vs. Benchmark Numerical

Response for One-Mass System

Chapter 6

SAMPLE GEARSEP APPLICATION AND DATA INTERPRETATION

6.1. Program Overview

As discussed earlier, the Gearsep program is apportioned into
two components: Gearsep1 and Gearsep2. The first calculates the
total compliance of a tooth pair at five selected points along the
line of action, and creates as its output an input file for Gearsep2,
which in turn contains the beta-m numerical integrator and all of
its supporting algorithms. After reading both the input file
produced by Gearsep1 and a third input file containing program
control data, Gearsep2 produces for each iteration of the numerical
integrator an output consisting of the present iteration number,
the corresponding time and tooth pair stiffness, and the relative
displacements, or the *separation* (see Chapter 1, Sec. 1.3.1.), of the
two gears. Details of Gearsep as a whole are given in Appendix B.

The following presents an analysis of a sample gear system
using the Gearsep procedure. Programming features of Gearsep will
also be discussed, along with comments on the program's usage.

6.2. A System Analysis Based on a Four Square Gear Testing Device

The sample gear system is a single-stage component of the four square system proposed in reference [7]. This device, shown in simplified form in Figure 24. allows the testing of individual gear pairs at high shaft loads without expensive high torque motors or elaborate loading devices. This is accomplished through the use of a torque flange which counter twists the shafts to produce the desired load within the four square circuit, as marked in Figure 24. This system, as presented in reference [7], is designed to test spur gears described in Appendix E. Note, however, that shaft stiffnesses and motor/load mass moments of inertia are *not* taken directly from reference [7]. Rather, these values were choosen arbitrarily and were then adjusted so as to produce a spectrum of responses (to be presented shortly) that spans from simple gear motion to the transition to separation as system speed rises. It should be noted, however, that while shaft stiffnesses and motor/load mass moments of inertia are arbitrary, actual gear data (various radii and other dimensions, along with material properties, etc.) are based directly upon reference [7].

The first step in the Gearsep analysis of this or any system is to collect all necessary gear and system specifications. For the case of this particular four square tester, these are, again, listed
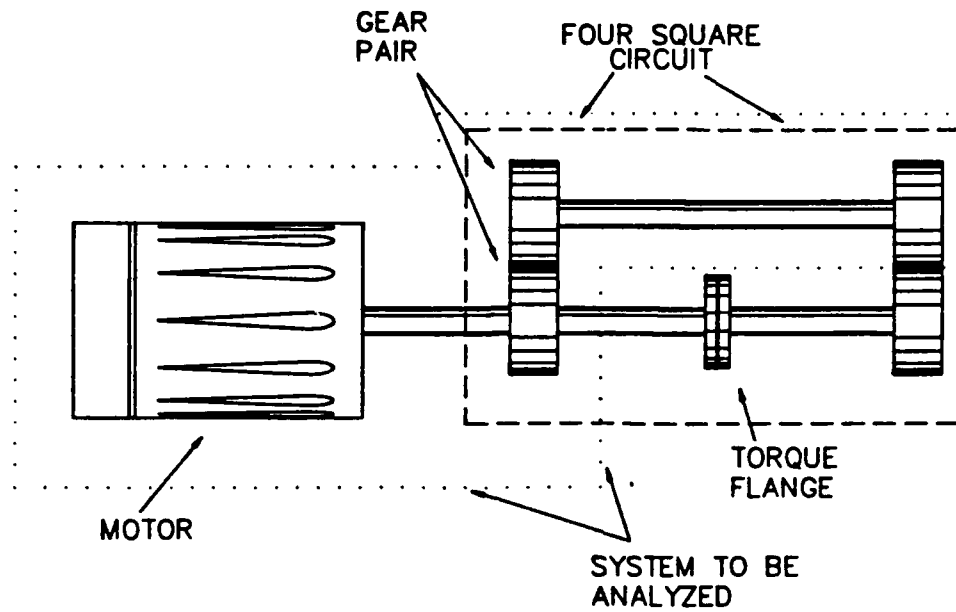
Figure 24: Four Square Gear Tester Layout

in Appendix E. In order to simplify and generalize the analysis, effective inertias (see reference [15]) will *not* be used. Rather, the system will be taken to be that indicated in Figure 24, where the one "leg" of the four square circuit is made symmetric by attaching at the location shown a fictitious load mass equal to that of the motor.

6.2.1. Critical Parameters: Load and Speed

Many common gear systems are designed to operate over a wide range of loads and speeds. Therefore, before an actual analysis takes place, some qualitative ideas should be established as to

where in the ranges of these two parameters the threat of separation is greatest so that it does not become necessary to sample the entire span of loads and speeds in search of separation. To this end, a qualitative investigation is performed based on the linear model first introduced in Figures 1 and 2, and repeated here in Figure 22 with the addition of a time varying load attached to the massless plates.

When the linear model oscillates about its equilibrium position, it is kept within the confines of its datums solely by the action of the applied forces F (see Chapter 1). As F is made smaller, the oscillations of the masses take them closer to their datums, and the system approaches separation: For a rotational system, the applied force F corresponds to the system's torque. From Figure 25, then, as the force F or system torque is made smaller, the block masses or gears are able to rebound closer to their unstressed positions, and thus toward separation. This implies that the lowest operating torque should be chosen to give the greatest possibility for separation.

Returning again to the linear model, if a time varying force of very low frequency is applied to one of the plates (Figure 25) and causes the system to oscillate very slowly, it can be imagined that the system's dynamics would not be greatly disturbed, and that the motion would approximate that of a rigid body: Depending on the spring stiffnesses and the masses involved, the inertias of the

blocks will not come into play if the entire system is displaced

slowly enough. If, however, the frequency of the time varying force

is increased to a great enough extent, the reactions of the masses

will begin to lag behind the motion of the plates. This will in turn

cause greater compression or elongation in each spring, producing a

growing reaction force against the applied force F. If the time

varying forces from the combination of the varying tooth pair

compliance and the alternating single and dual tooth pair contact

are rapid enough, then, again depending on the system's parameters,

the proper conditions may be created for separation. As such, the

system's highest operating speed produces a worst possible case,

and should thus be chosen as a test parameter.
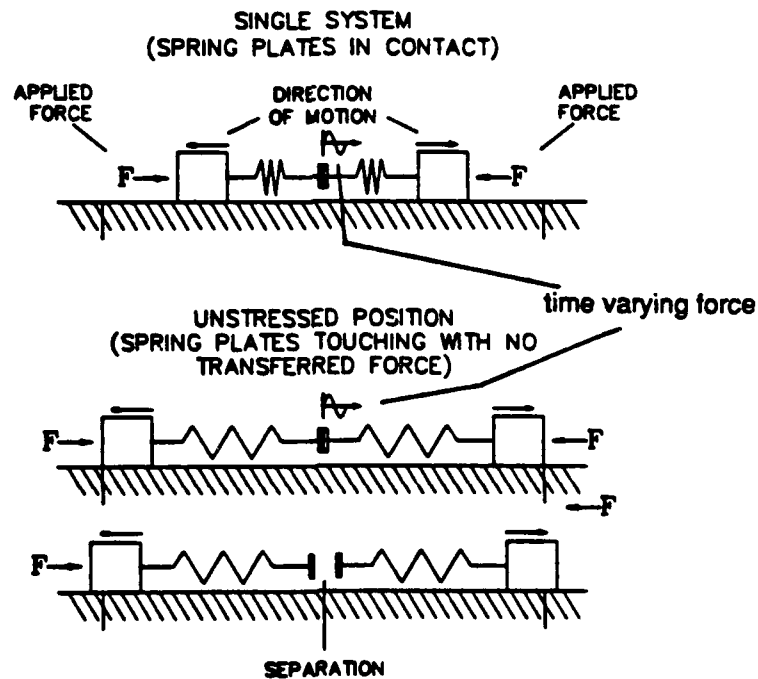
Figure 25: Linear Separation System with Time Varying Force

6.2.2. System Analysis

6.2.2.1. Characterization of Response

As a preliminary to the analysis of the sample system, the system's reaction to specific events within mesh is discussed. (A related discussion may be found in Appendix A, Sec. 3.1., where particular points in mesh are matched to the procedure for calculating tooth pair stiffness.) Figures 26 and 27 show a *representation* of the system's response and its corresponding stiffness profile: Note that these two plots share the same abscissa, and as such, events that take place in the response plot may be directly traced to their cause in the stiffness profile.

When Gearsep2 first invokes the numerical integration routine, it is at a point in mesh where there is only one tooth pair in contact: This will always be the case, and occurs by design as discussed in Appendix B, Section 15. With just this one tooth pair in contact, the total tooth mesh stiffness is in its weakest range, and as such, the contacting teeth are deformed by the greatest amount. In Figure 26, this translates to a series of peak relative gear displacements, each of which is labeled as point 1, and where each of the high frequency displacements (circled and labeled) is a single tooth pair oscillation. Note that these single contact deflection peaks take the system *away* from the point of zero

△—□—extremum of single tooth pair oscillations
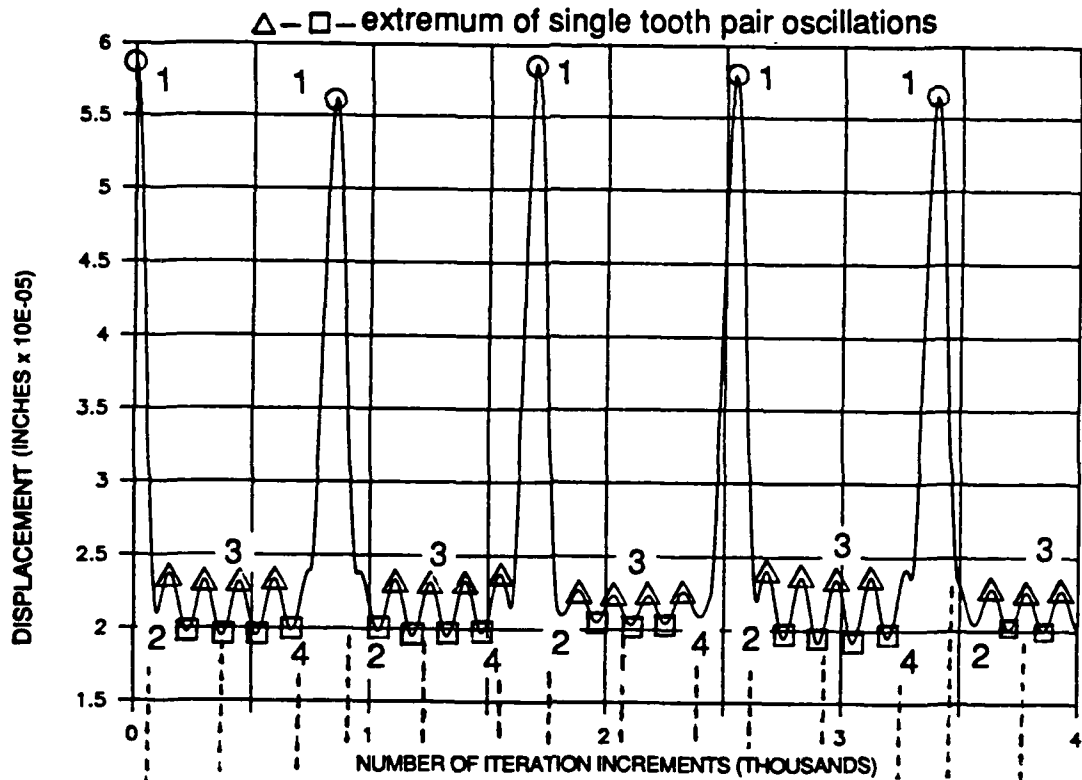
Figure 26: Sample Gear Response
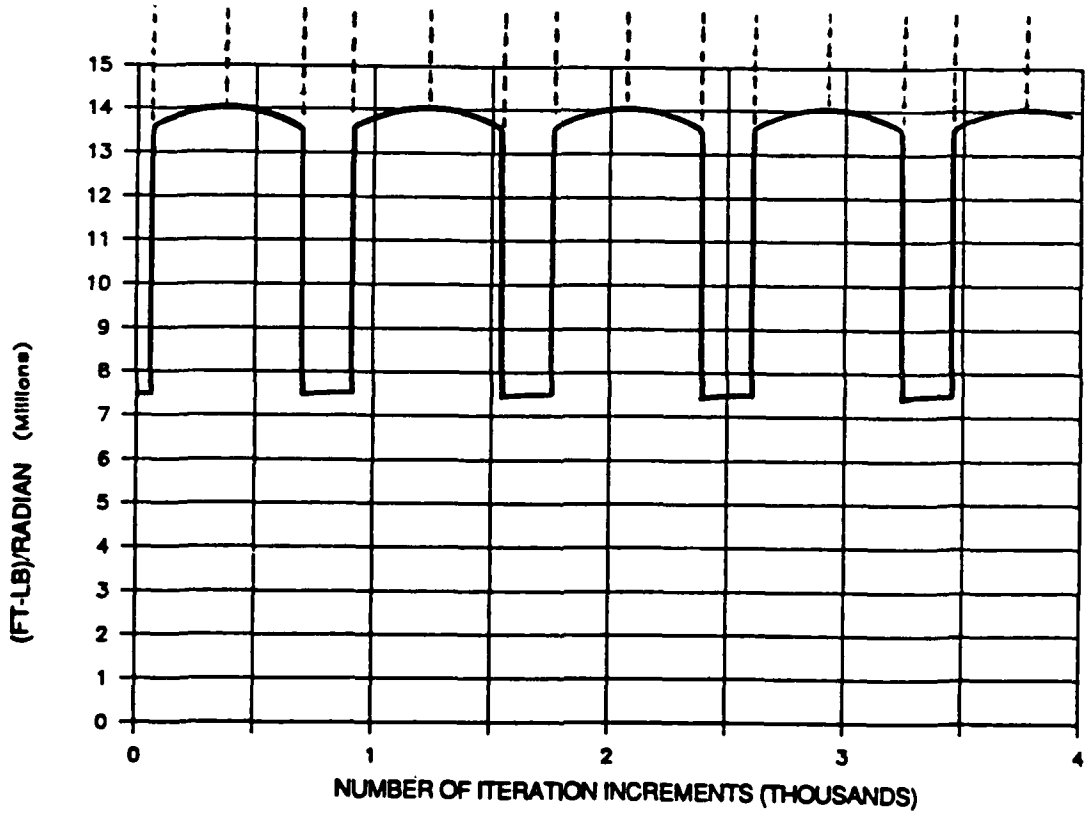
Figure 27: Sample Gear Profile

relative deflection, or, separation.

As the single tooth pair continues through mesh, the pair behind it moves toward its initial contact position at point 2. When both tooth pairs are in full contact, the tooth stiffness is near its maximum value, and as such, the relative gear motion is subdued, as seen at point 3. The original tooth pair then leaves mesh (with the help of another tip relief) at point 4, and the pattern repeats by returning the relative gear motion to its locally highest point. Figure 27 shows this pattern of a series of relatively sedate responses, dipping down and rising back up as the compliance of the tooth pair changes, and regularly interrupted by the spike of single tooth contact. Such a response pattern may be termed the "classic" gear response.

6.2.2.2. Generalized Response Analysis

Gearsep output was collected using the sample system's maximum torque (which is a departure from a proper analysis as discussed in the previous section) over a wide range of operating speeds and timestep sizes. The actual value of the step size is determined within Gearsep2, and is based on the number of iterations, or "points" into which each mesh is divided. This parameter is defined by the user, and is termed the number of *points per mesh*, or *PPM*.

Figures 28 through 39 present a sampling of the total data collected in the effort to characterize the full range of Gearsep responses. Note that the quantity *separation* (described in Chapter 1, Section 1.3.1. as the relative angular displacement of the gear *bodies*) is now plotted against the *number of iterations* performed by the numerical routine, as well as against time. This underscores the fact that *when* particular events occur in mesh is not as important as the magnitude of those events. In addition, plots containing this iteration information can be used to estimate necessary computation for the specific computer in use (the data to follow was generated on a Standard 286 (IBM AT compatable) personal computer located in Penn State's Applied Research Laboratory. Furthermore, in reviewing the definition of separation as it was given in Chapter 1, it may be noted that a separation value of zero corresponds to a zero relative displacement of the gear bodies: This is the "impending separation" discussed in Chapter 1, Section 1.3.1.. As a final note, it should be remembered that the separation represented in the following figures is measured in inches along the line of action, just as were the deflections calculated from the strength of materials equations presented in Chapter 3.
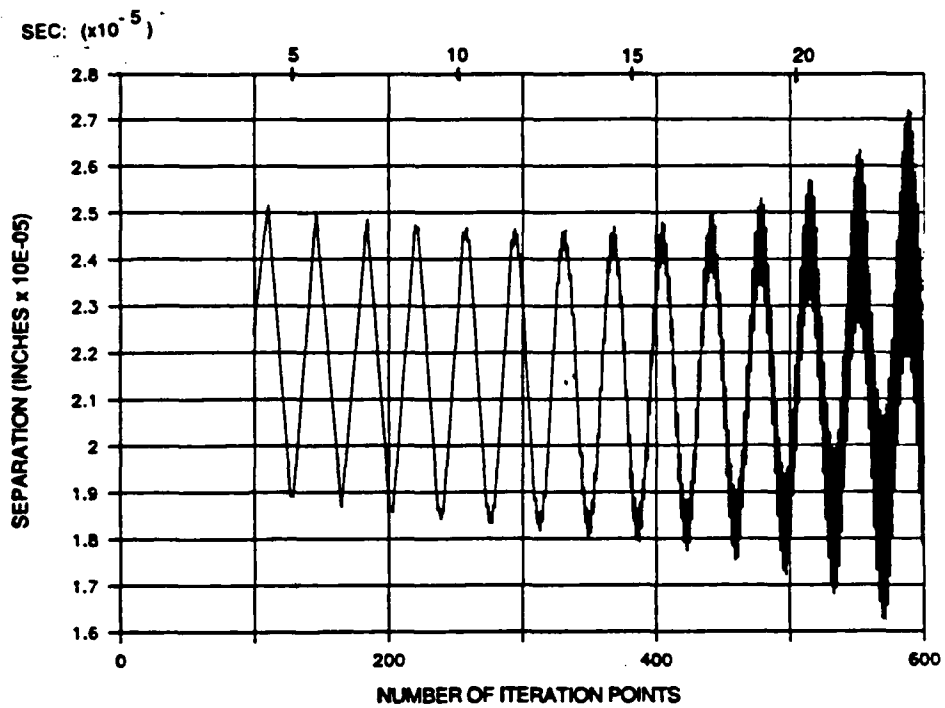
Figure 28: Gearsep Calculated Response
5000 RPM   1500 PPM
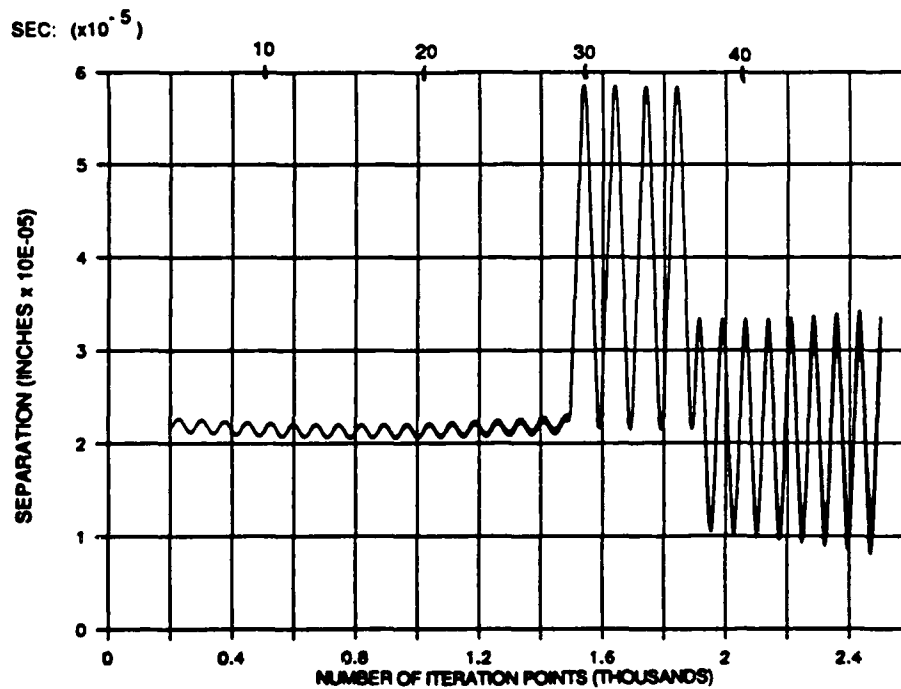
Figure 29: Gearsep Calculated Response
5000 RPM   3000 PPM
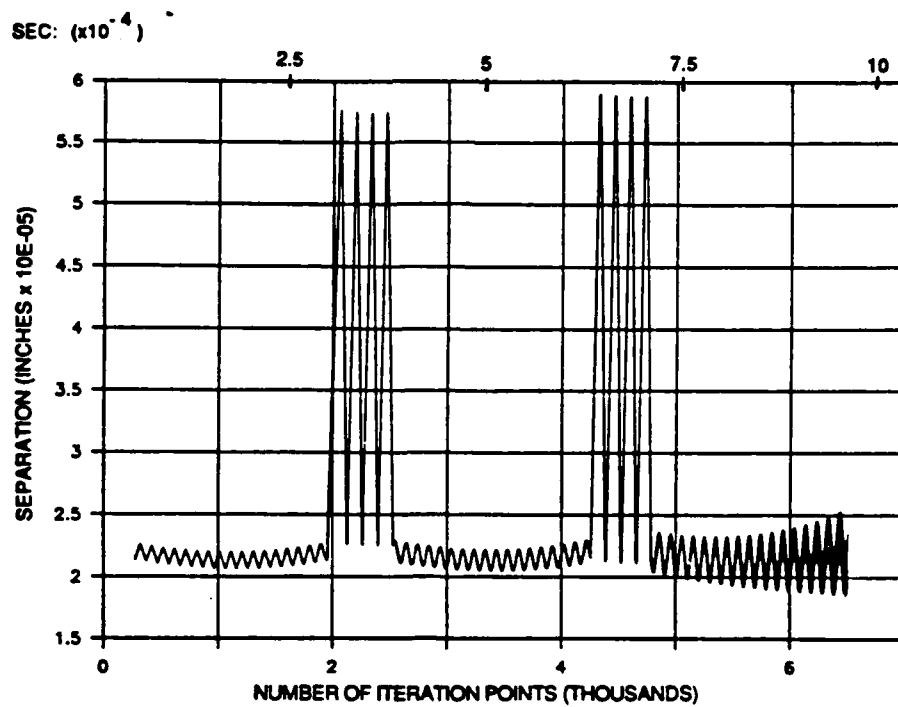
Figure 30:   Gearsep Calculated Response
5000 RPM   4000 PPM
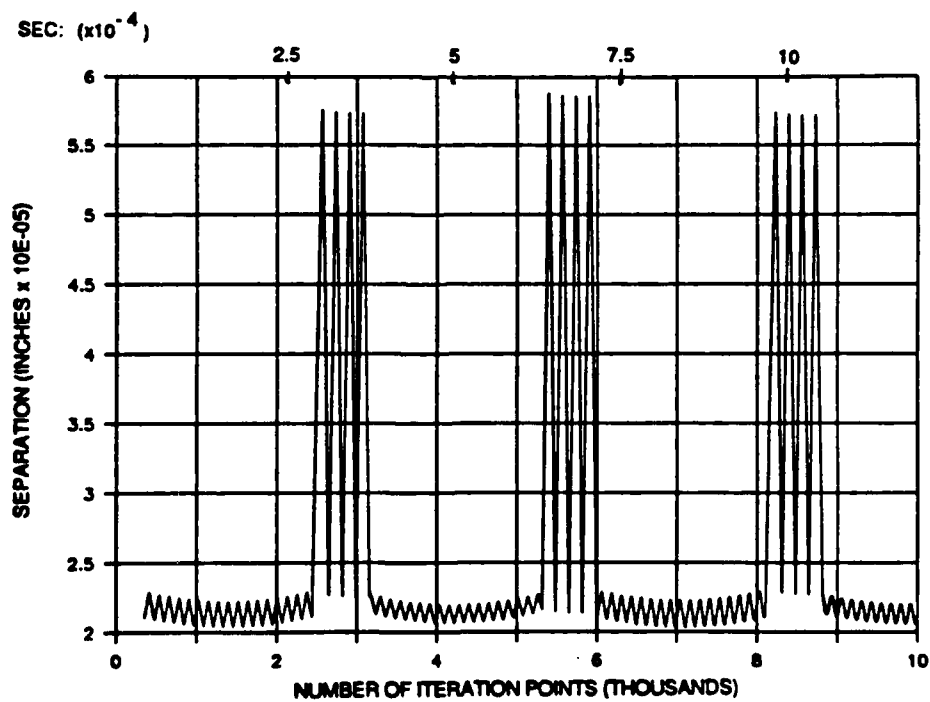
Figure 31:   Gearsep Calculated Response
5000 RPM   5000 PPM
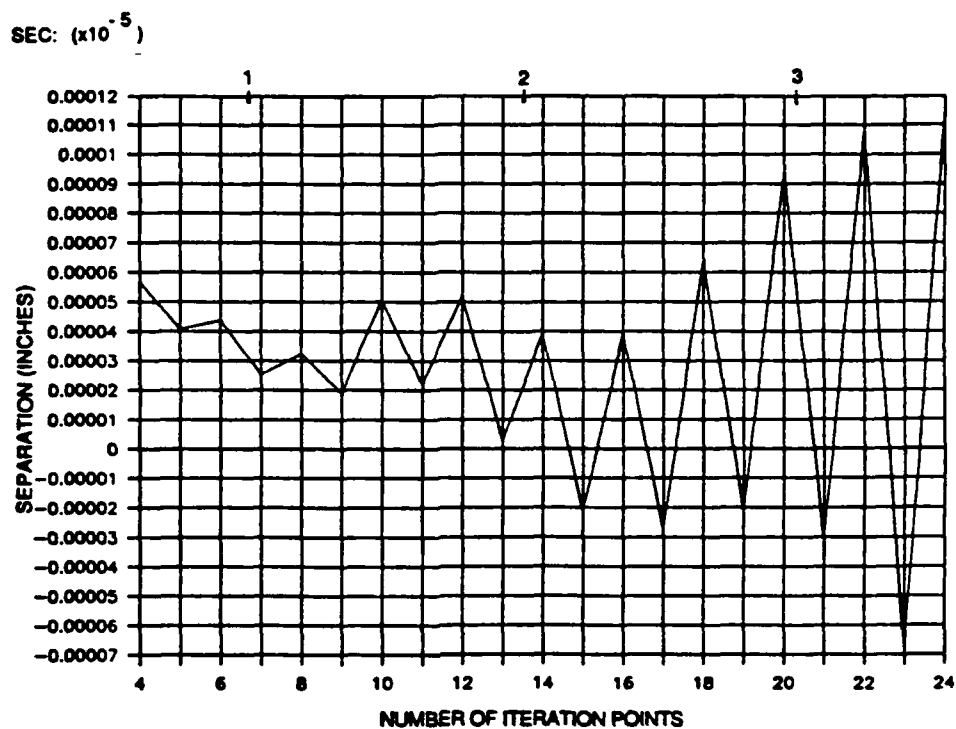
Figure 32: Gearsep Calculated Response
20000 RPM   100 PPM
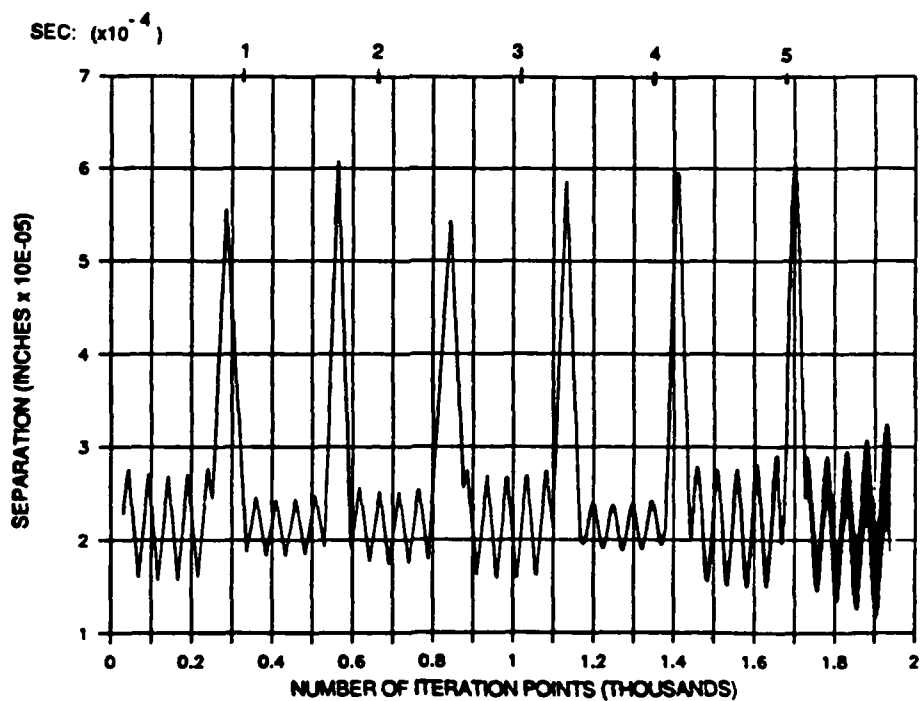
Figure 33: Gearsep Calculated Response
20000 RPM   500 PPM

SEC: (x10^{-4})
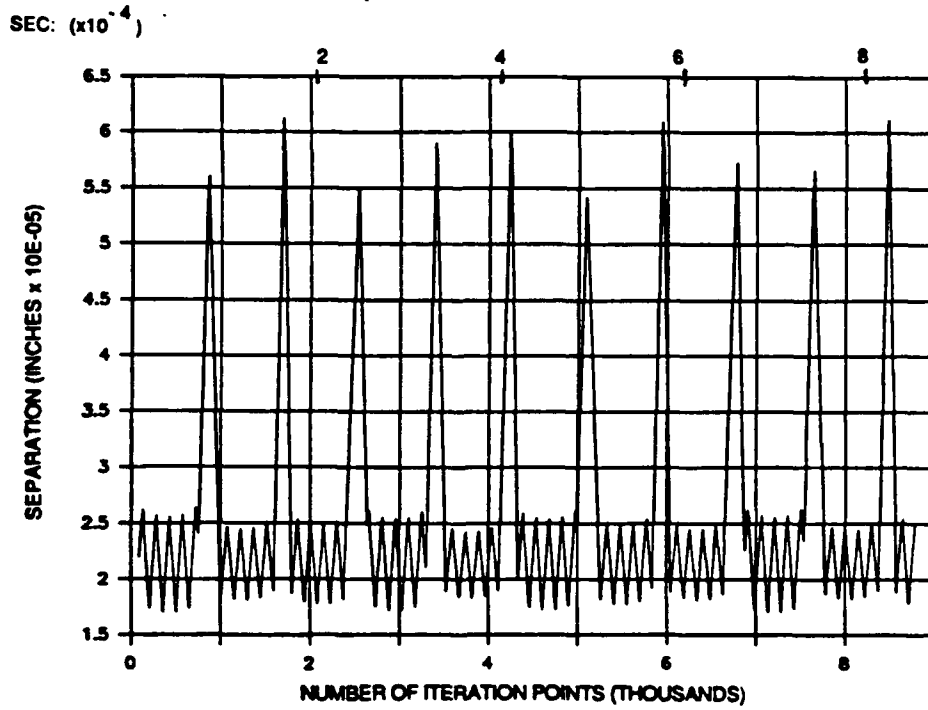
Figure 34: Gearsep Calculated Response
20000 RPM   1500 PPM

SEC: (x10^{-4})
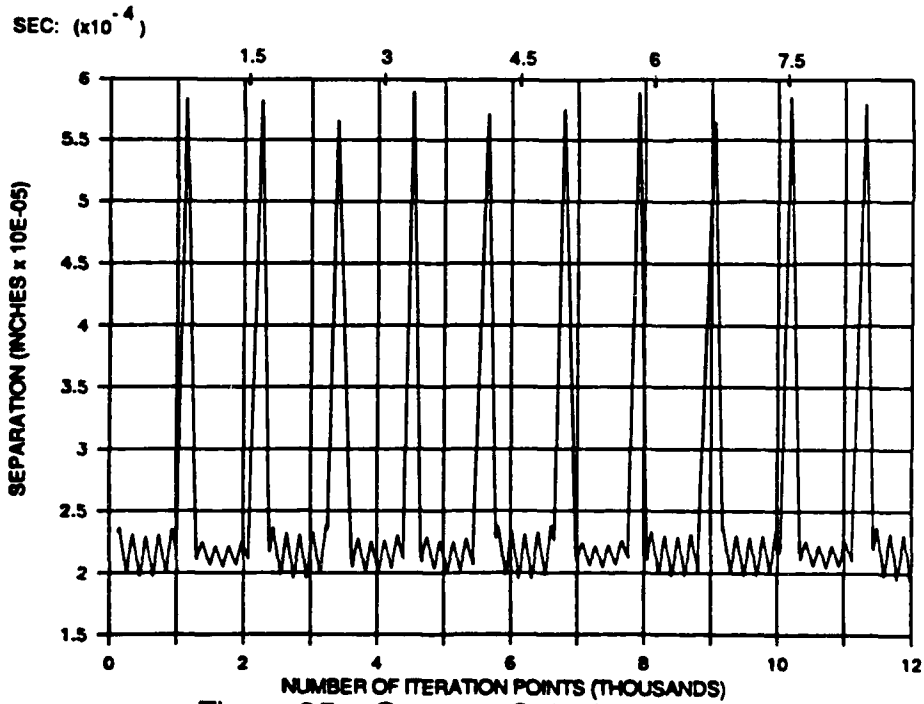
Figure 35: Gearsep Calculated Response
20000 RPM   2000 PPM
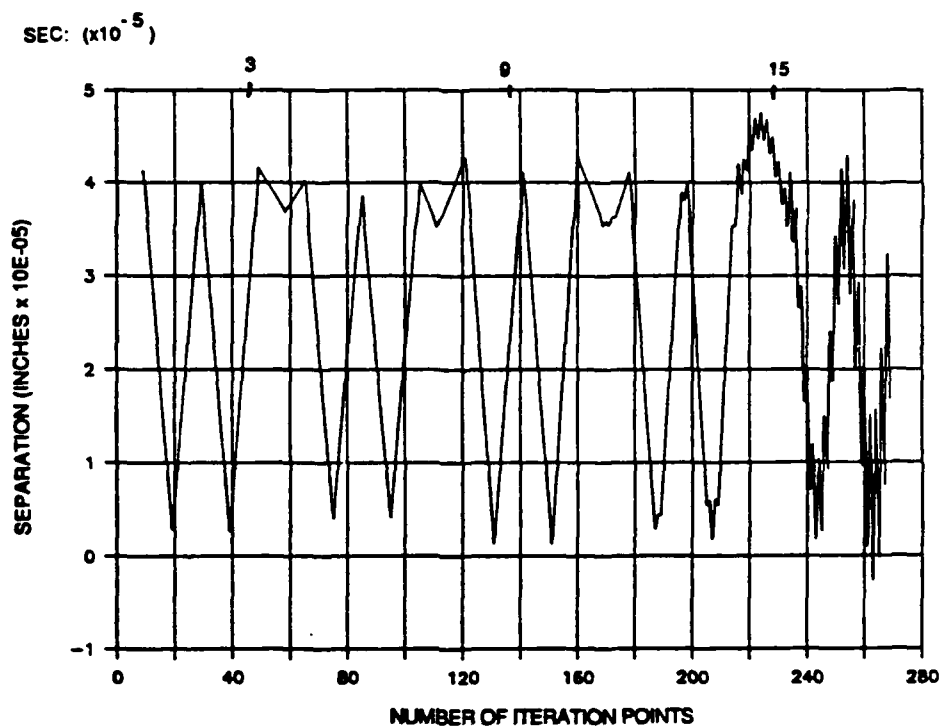
Figure 36:   Gearsep Calculated Response
45000 RPM   100 PPM
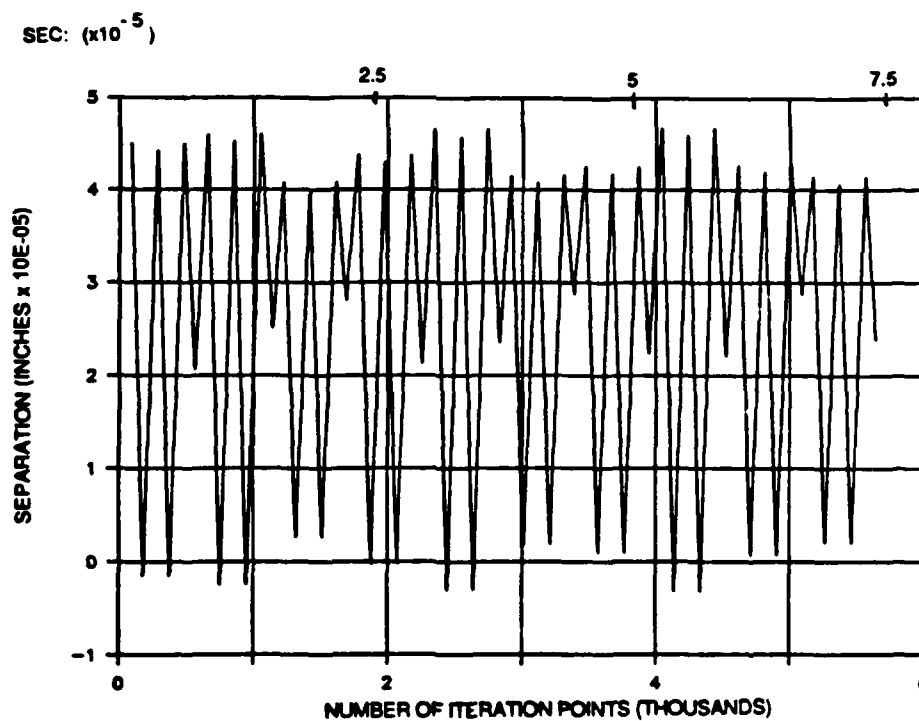
Figure 37:   Gearsep Calculated Response
45000 RPM   500 PPM

SEC: (x10^{-4})
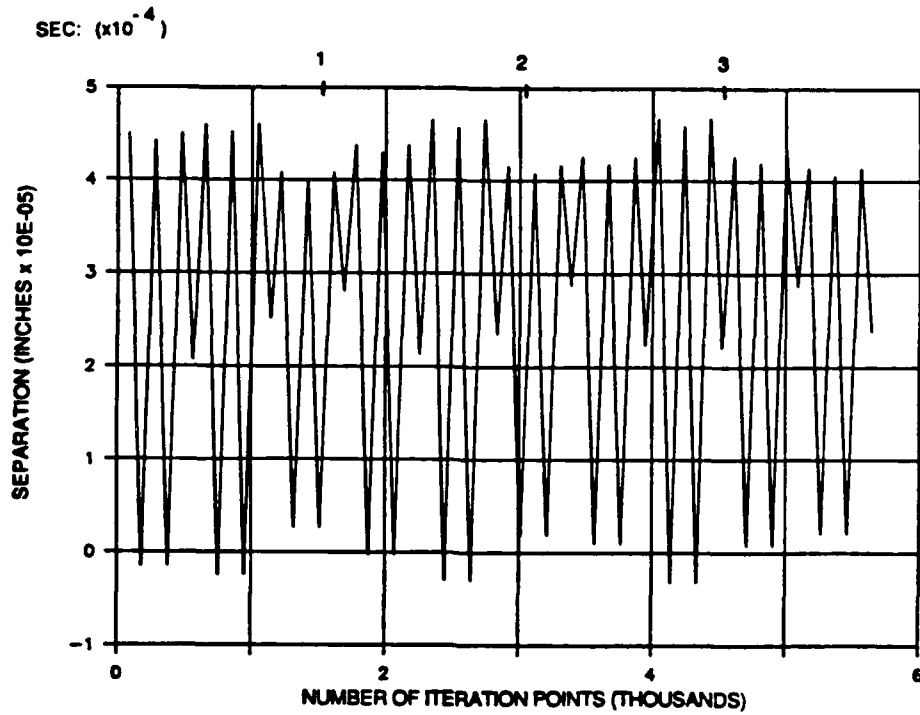
Figure 38: Gearsep Calculated Response
45000 RPM   1000 PPM

SEC: (x10^{-4})
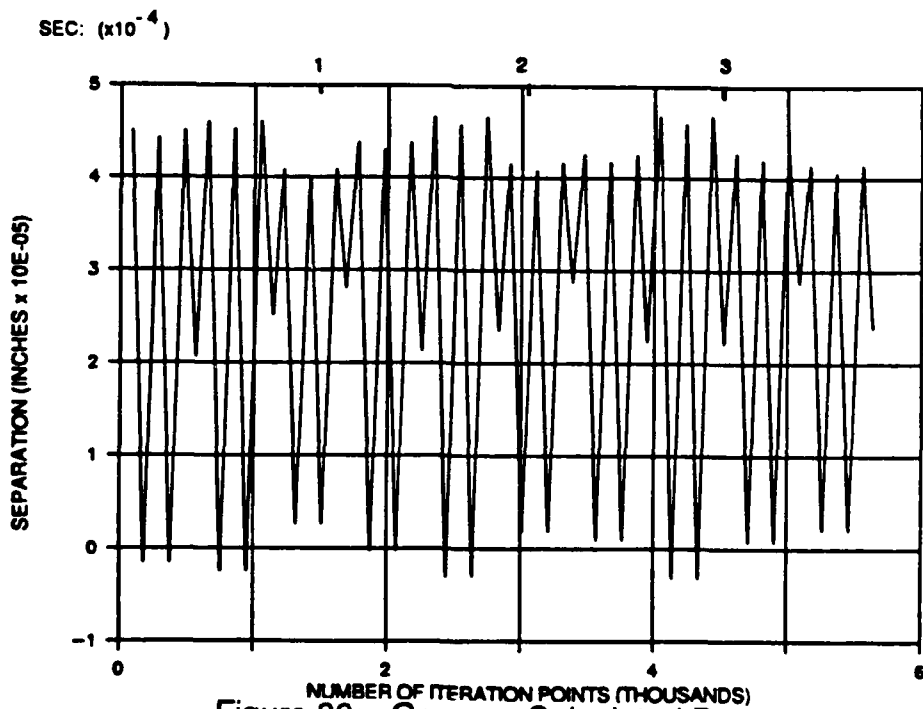
Figure 39: Gearsep Calculated Response
45000 RPM   1500 PPM

6.2.3. Data Analysis

The data set from which the preceding responses were taken began at 5000 RPM and 100 PPM, but this and other cases using small parameters produced immediately unstable responses due to the numerical instabilities discussed in Sec. 5.2.2.. Specifically, attempted runs at 5000 RPM failed at 100, 500, and 1000 PPM, and runs at 10,000 and 15,000 both failed at 100 PPM.

Remnants of the extreme instabilities initially encountered are apparent in responses run at the lower end of the PPM and RPM scales, where the timestep calculated in Gearsep2 is small enough to give a response that is initially stable, but that becomes unstable before a number of meshes takes place that is sufficient to affirm or disaffirm separation. Those responses that did become unstable are plotted up to the point where the instability is apparent but the data are still useful, insofar as the basic trend of the response is still apparent.

In Figure 28, the response at 5000 RPM becomes unstable before a single mesh can be completed, as seen in comparison with Figure 29, whose response survived approximately half way through the second mesh. As timestep size decreases, the true response begins to assemble itself, with each step adding more detail. This process continues through Figure 31, where the limit set on PPM is reached. Although this final plot shows three stable

and very similar meshes that are well away from the zero relative displacement value that indicates separation, it will cannot be concluded that this particular set of parameters (RPM and torque) is a proper one for separation-free system operation. The actual number of stable meshes of the pattern seen in Figure 31 that is necessary to predict the character of the system is at the discretion of the individual investigator, but for this analysis, it is arbitrarily set to a value of *ten*.

Increasing the operating speed to 20,000 RPM decreases the timestep size by a significant amount, but instabilities still occur, as seen in Figure 32. This response was the first obtainable at the lowest attempted PPM value of 100, and is indicative of a response that is all but immediately unstable. At 500 PPM (Figure 33), however, the classic response pattern emerges, but becomes unstable after six meshes. Increasing PPM to 1500 gives the plot in Figure 34, which survives the entire ten meshes stipulated as necessary to confirm that no separation will take place: Note, however, that unlike the system operating at 5000 RPM, the relative gear displacement for this system drops below 2×10^{-5} inches, and as such is closer to separation at this higher speed. Figure 35 was generated with a PPM of 2000, and although it survived well past the required ten meshes, only the first ten are shown. In comparison with Figure 34, it is obvious that Figure 35 also predicts a separation-free case, but it also shows that for a

given RPM, as the step size decreases and numerical accuracy of the solution increases, the response moves *farther away* from separation. Thus if a response at, say, 2000 PPM shows that separation will not occur, the investigator may be confident that a more accurate (and lengthy) analysis will not reveal the opposite.

Upon reexamining Figures 28 through 31, it is seen that the system speed (5000 RPM) is such that approximately four tooth pair oscillations can occur during the space of time that a single tooth pair is in contact, as indicated by the sets of four tall peaks. For an RPM of 20,000, as shown in Figures 29 through 32, meshing has sped up to the point that only one tooth pair oscillation can occur during single contact. It may then be theorized that another large increase in system speed will place the period of single contact below that of tooth pair oscillation. This indeed is the case, as shown in Figures 36 through 39 which show a complete departure from the classic response pattern. Note also the oscillatory variation in the height of the response peaks from interaction with the shaft natural frequency (see Figure 34).

In addition to disrupting the classic response pattern, the aforementioned increase in system speed has also produced signs of tooth separation, as seen in Figures 37 through 39 where the plot becomes negative. This particular case is in what may be termed *separation transition*, characterized by intermittent negative response values that do not grow beyond a small

percentage of the full response range. It should be noted, however, that no matter how small the tooth separation, it still represents a nonlinearity in the response of the *real* system that is not accounted for in the equations of motion (Equations 1 through 4): The ensuing impact is *not* modeled, and nor are the anomalous dynamics that would occur as the system's damping returns it to the original response pattern.

In summary, an increase in PPM and/or RPM decreases the size of the calculated timestep, thus improving beta-m's accuracy. In moving toward the higher numbers of PPM's for a constant RPM, the classic pattern of meshing gear teeth begins to emerge, with its rising and falling from single and dual tooth pair contact. At some point, the increase in RPM pushes the gear pair into a condition of tooth separation.

6.2.4. Gearsep Output and Output Conditioning

Unconditioned Gearsep output consists of an increment number, a time in seconds, a *torsional* gear pair stiffness, and a separation value in inches for every iteration performed. As the number of iterations may easily reach into the tens of thousands, it is advantageous to have Gearsep return only maximum and minimum response values. Because an evaluation of Gearsep data focuses on the magnitude of the response, rather than the details of its twists

and turns, such truncated output provides the same separation information as does the full range of data, but without wasting time and storage space on useless data.

In reconsidering Figure 30, numerical instabilities are seen to be manifested on the response curve as numerous superimposed oscillations. The fact that these instability peaks appear on the plots indicates that Gearsep2 mistakes them for true system oscillation peaks. This discrepancy, however, is used to the program's advantage, and lets it monitor the numerical routine's instabilities by simply counting the number of extremum ("extremum" referring to both maximum and minimum values). Because the majority of the useful/stable response information is described by a relatively small number of data points in the stable area of each plot, an upper limit may be set on the number of extremum allowed, beyond which Gearsep returns an appropriate error message and stops computation. Because this upper limit will change from plot to plot, and would require a trial run to be set properly, it might seem that it would be more straightforward to simply reset the PPM so as to produce a smaller timestep size, and thus a more accurate result. This, of course, is possible at any point in the analysis, but because it is the nature of Gearsep to require a series of "dry runs" simply to determine where the program is stable for any particular system, a great deal of computation effort has probably already been expended by the time

the response in question is examined. For the data in Figures 24 through 36, the upper output limit number was set to a value of 500 as determined emperically. This, again, allows each response to develop to the point where it contains all information necessary to evaluate the case in question without unnecessary and useless data.

Finally, it should be noted that aside from the limitations of the machine on which it is used, there seems to be no limitation to the range of applicability of this model: If numerical instabilities occur because of low system RPM, they can be "adjusted out" with an increase in the numerical "resolution" of the model, accomplished by raising the number of points per mesh (PPM). This is demonstrated in the sequence of plots from Figure 28 to Figure 31 (all at 5000 RPM), from Figure 32 to Figure 35 (all at 20,000 RPM), and from Figure 36 to Figure 39 (all at 45,000 RPM).

CONCLUSIONS

The Gearsep gear tooth separation program has been designed to provide the information necessary to predict separation in a single-stage segment of a spur gear system. Analysis of an arbitrary sample system has produced response curves which have been shown to contain all of the correct signatures of gear mesh for contact ratios between one and two. The response has also been shown to follow the expected trends as system speed is varied.

The program's output may be directly used in the search for system natural frequencies and, with slight alterations to the program's peripheral mathematics, for determining tooth loads from the calculated deflections of individual teeth. Gearsep may also be altered to analyze gears with different material properties in the tooth, fillet, and gear body areas (such as nylon gears with metallic hubs), and gears with a machined narrowing of the tooth cantilever near the tip (crowning). Modeling of gears with contact ratios of two or more is possible, but would require somewhat in-depth alterations of the way Gearsep handles mesh geometry.

There seems to be no limitation to the range of applicability of this model aside from the limitations of the machine on which it is used: If numerical instabilities occur because of low system RPM, they can be "adjusted out" with an increase in the numerical "resolution" of the model, which is accomplished by raising the

number of points per mesh (PPM) as demonstrated in the collection of response plots.

REFERENCES

1. Mark, W. D. "Analysis of Vibratory Excitation of Gear Systems as a Contributor to Aircraft Interior Noise," NASA Technical Memorandum No. 502, Contract No. NAS1-14611, February, 1979.

2. Drago, R. J. Gear System Design for Minimum Noise, unpublished notes.

3. Azar, R. C. and Crossley, F. R. E. "Digital Simulation of Impact Phenomenon in Spur Gear Systems," Transactions of the ASME, August, 1977, pp 792-798.

4. Buckingham, E. Analytical Mechanics of Gears, McGraw-Hill, 1949.

5. Ozguven, H. N. and Houser, D. R. "Mathematical Models Used in Gear Dynamics -- A review," Journal of Sound and Vibration, Vol. 121, No. 3, 1988, pp383-411.

6. Pechersky, M. J. and Chandra, V. "The Measurement of Gear Noise Sources Using Non-Intrusive Laser Technologies," ARL Review, The Pennsylvania State University Applied Research Laboratory, 1987, pp 33-41.

7. Vilanilam, S. V. and Pechersky, M. J. "The Design of a Four Square Gear Tester for Noise and Vibration Measurements," The Pennsylvania State University Applied Research Laboratory Technical Report TR 87-002, December, 1986.

8. Mark, W. D. "Analysis of the Vibratory Excitation of Gear Systems: Basic Theory," The Journal of the Acoustical Society of America, Vol. 63, No. 5, May 1978, pp1409-1430.

9. Nakamura, K. "Tooth Separation and Abnormal Noise on Power-Transmission Gears," Builetin of JSME, Vol. 10, No. 41, 1967, pp 846-854.

10. Tavakoli, M. S. and Houser, D. R. "Optimum Profile Modifications for the Minimization of Static Transmission Errors of Spur Gears," Transactions of the ASME, Vol. 108, March 1986, pp 86-94.

11. Merritt, H. E. Gears, Sir Isaac Pitman & Sons, Ltd., 1955.

12. Dubowsky, S. and Freudenstein, F. "Dynamic Analysis of Mechanical Systems with Clearances," Journal of Engineering for Industry, February, 1971, pp 310-316.

13. Kumar, A. A. and Sanker, T. S. "On Dynamic Tooth Load and Stability of a Spur-Gear System using the Space State Approach," Transactions of the ASME, Vol. 107, March 1985, pp 54-60.

14. Neubert, V. H. Personal Correspondence, 1988, discussion of treatment of Coriolis and gyroscopic gear effects.

15. Wilson, W. K. Practical Solution of Torsional Vibration Problems, Volume One: Frequency Calculations, Chapman & Hall LTD., 1956.

16. Neubert, V. H. "E Mch 401/522 Theory of Vibrations Course Notes," Department of Engineering Science and Mechanics, The Pennsylvania State University, August 10, 1986.

17. Rao, S. S. Mechanical Vibrations, Addison-Wesley, 1986.

18. Mark, W. D. "The Transfer Function Method for Gear System Dynamics Applied to Conventional and Minimum Excitation Gearing Designs," NASA Contractor Report 3626, p 2.

19. Cornell, R. W. "Compliance and Stress Sensitivity of Spur Gear Teeth," Journal of Mechanical Design, Vol. 103, April, 1981, pp 447-459.

20. Katona, M. G. and Zienkiewicz, O. C. "A Unified Set of Single Step Algorithms -- Part 3: The Beta-m Method, a Generalization of the Newmark Scheme," International Journal for Numerical Methods in Engineering, Vol. 21, 1985, pp 1345-1359.

21. Newmark, N. M. "A Method of Computation for Structural Dynamics," Proceedings of the American Society of Civil Engineers, 8, 1959.

22. Cornell, R. W. and Westervelt, W. W. "Dynamic Tooth Loads and Stressing for High Contact Ratio Spur Gears," Journal of Mechanical Design, Vol. 100, January, 1978, pp 69-76.

23. Beer, F. P. and Johnston, E. R. Mechanics of Materials, McGraw-Hill, 1981.

Appendix A

GEARSEP PROGRAM FLOW CHARTS

A.1. Generalized Gearsep Program

The figures that follow represent the entire Gearsep algorithm in flow chart form. Figure 40 is a generalization of Gearsep, with lettered sections corresponding to the flow charts and descriptive text given in subsequent sections.

A.2. Iterating to Find γ_F

As discussed in Sec. 3.3., there is no obvious tooth geometry in Cornell's compliance model to characterize the size of the fillet cantilever (see Figure 10). As such, Cornell has conservatively defined the proper value of γ_F to be that which causes the maximum foundation and fillet deflection (see Equation 19 through 21).

Figure 41 shows the variation of foundation and fillet deflection over a range of γ_F's for all five of the sampled compliance points along the line of action as calculated with Equations 19 and 20 for the sample gear of Appendix E. Note that the plot for each of the contact positions peaks at a different location, corresponding to

Figure 40: Generalized Gearsep Program Algorithm Flow Chart

different optimum values of γ_F. To account for this range of

possible values, Gearsep1 will generate each of these curves and

locate the optimum points using the algorithm shown in Figure 42.
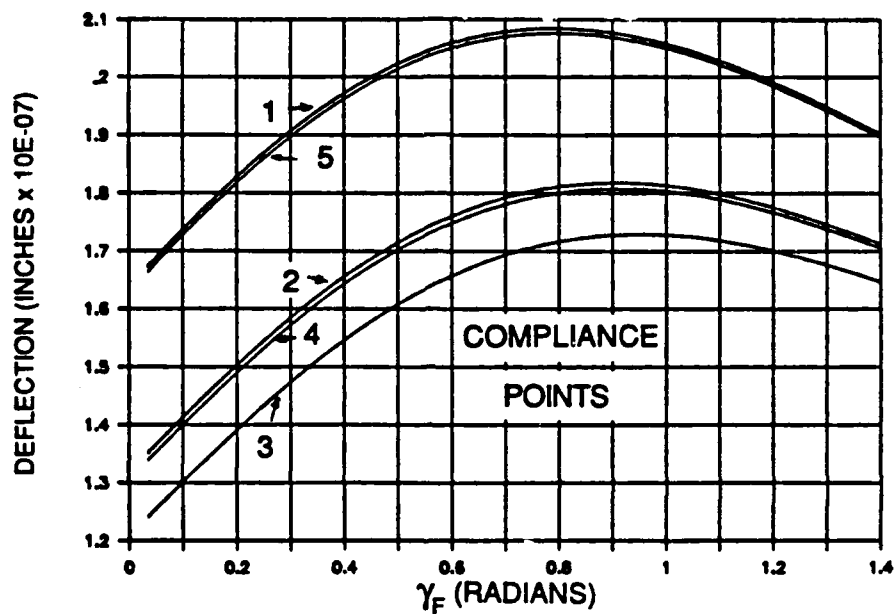
Figure 41: Foundation and Fillet Deflection vs. γ_F

A.3. Calculation of Deflection Due to Bending and Shear

As stated in Chapter 3, the summation term in the equation for

cantilever bending and shear deflection represents an integral over

the length of the cantilever. There is no contingency, however, for

the number of increments into which this summation should be

divided. Figures 43 and 44 show the trends of tooth and fillet

cantilever deflection (respectively) for a range of numbers of
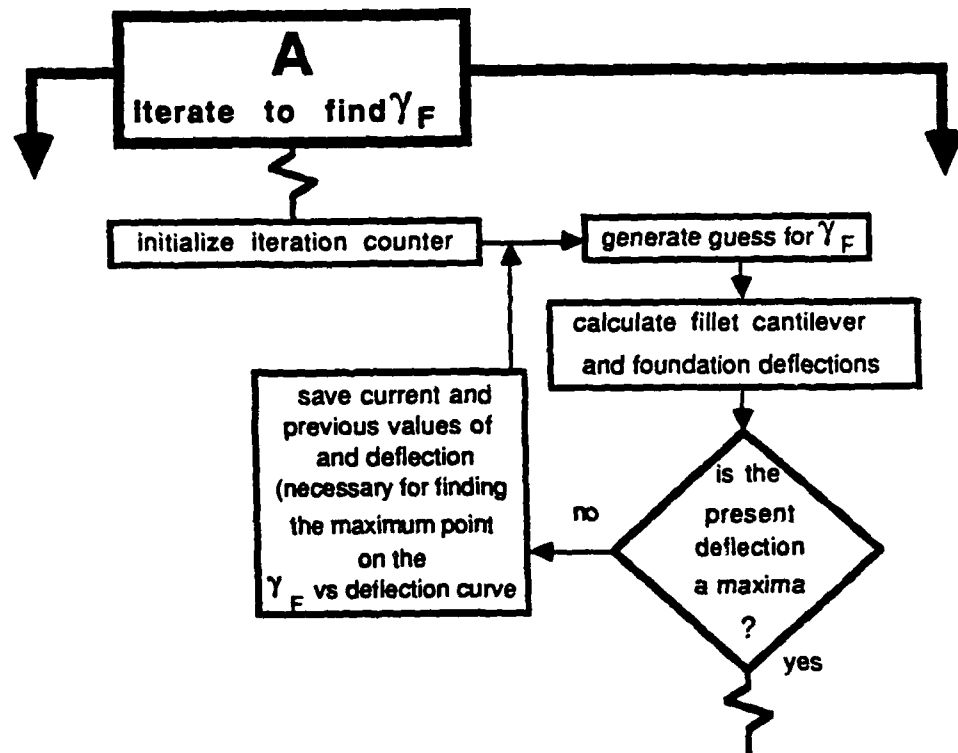
Figure 42: Flow Chart for Finding γ_F
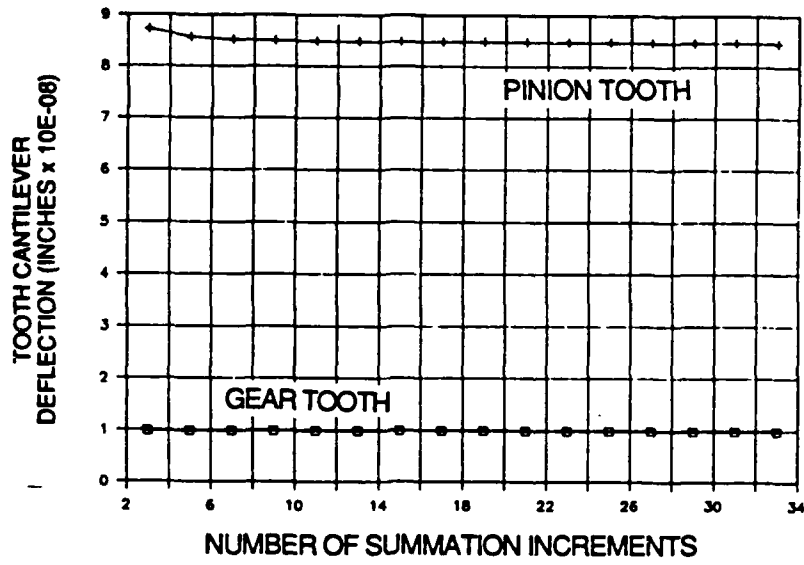
Figure 43: Trends of Tooth Cantilever Deflection
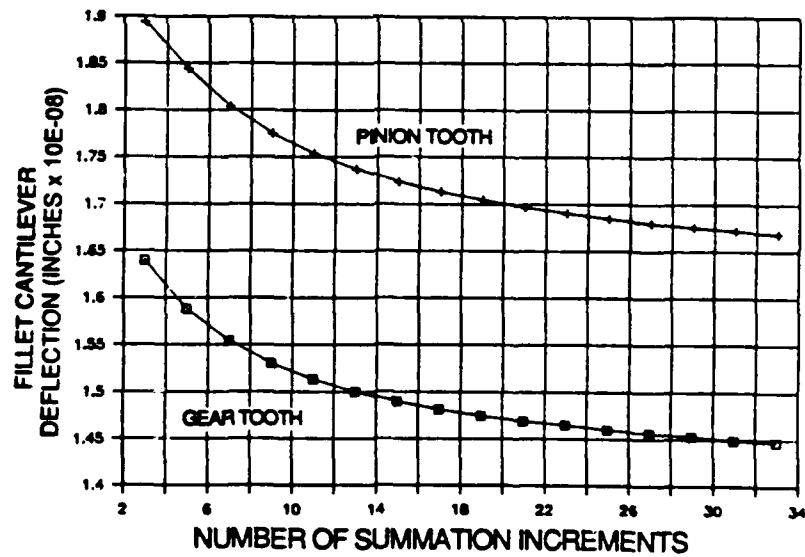
Figure 44: Trends of Fillet Cantilever Deflection

summation increments as calculated by Equation 18. These deflections are calculated at the first compliance point (see Appendix B, Sec. B.1.), where, because of the length of the moment arm through which the tooth load acts, *gear* tooth and fillet deflections are at a maximum, and those of the *pinion* are at a minimum. If the two meshing gears are the same (as they are for the test case), this same analysis applied to compliance point 5 would produce the *exact* results as presented in the following figures, except that the roles of the two teeth would be reversed.

The analysis that produced Figure 44 was actually taken out to fifty summation increments, where it was assumed to have "sufficiently" converged so as to establish "real" values for the deflections. As based on this value, Figure 44 represents values of the separation increment up to the point which produced an error less than a 2%. These values (the last point of each plot) are those used in Gearsep.

It is seen in Figure 43 that tooth deflection does not vary nearly as radically as the range of fillet deflections: Three summation increments yield a deflection value within 1% of the converged "real" value. This is rounded up for use in Gearsep to a value of 10, providing a more conservative and convenient value.

Figure 45 represents the section of Gearsep1 that applies the "strength of materials" equations (Equations 18, 19, and 21) taken from Cornell to either the tooth or fillet cantilever. As stated in
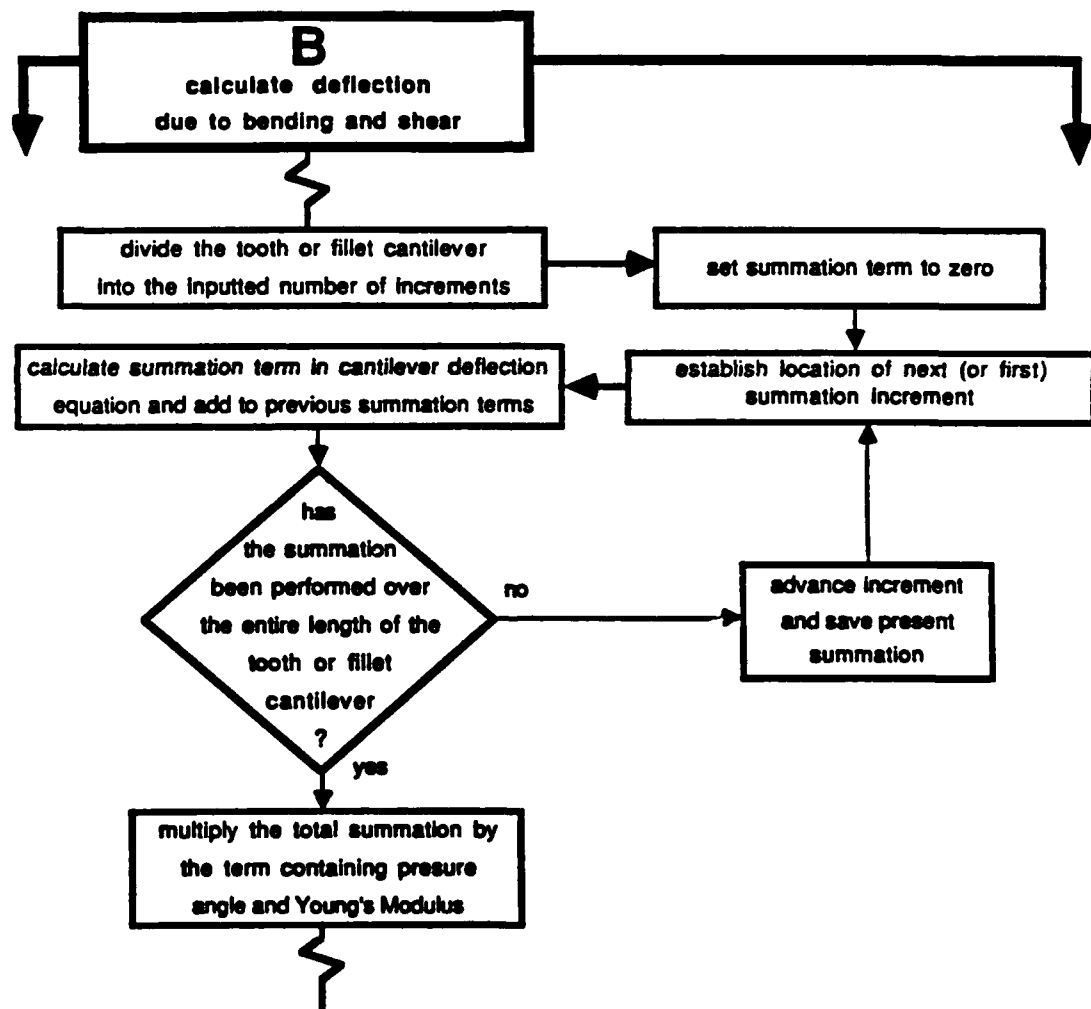
Figure 45:   Bending and Shear Deflection Calculation Algorithm Flow Chart

Chapter 3, this is actually an integration over the length of the cantilever, and is approximated by a summation.

A.4. Stiffness Values at Mesh Iteration Points

A.4.1. Key Mesh Points

As succeeding pairs of teeth roll into and out of contact, a pattern of single and dual tooth pair contact develops. Figures 46a through 46e follow a pair of meshing teeth (tooth pair (1,2)) as they move along their entire range of contact, which defines the full length of the line of action. Within this range of motion lie several points of transition between single and dual contact, where the mesh behavior takes on different characteristics. These will be referred to as *key points*, and may be used as landmarks within the meshing process because they occur at the same location for every tooth pair.

In Figure 46a, tooth pair (1,2) has just entered contact, while the previous tooth pair (3,4) is at some intermediate mesh position just past pitch (the center point of mesh): Note the direction of pinion and gear rotation. Figure 46b shows the transition from the dual contact of Figure 46a to the single contact shown in Figure 46c. As tooth pair (1,2) moves through and away from pitch,
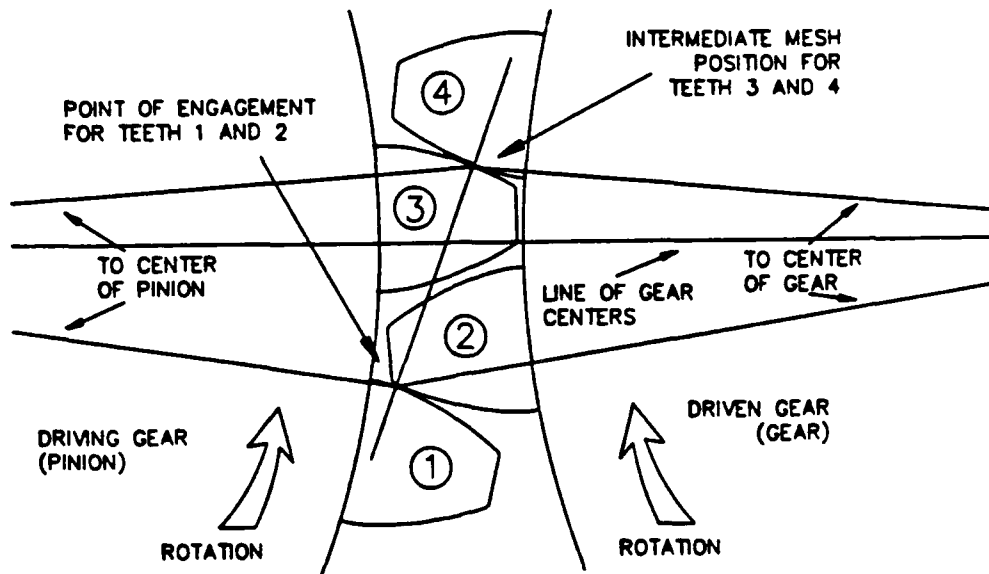
Figure 46a: Key Points in Mesh--Tooth Engagement
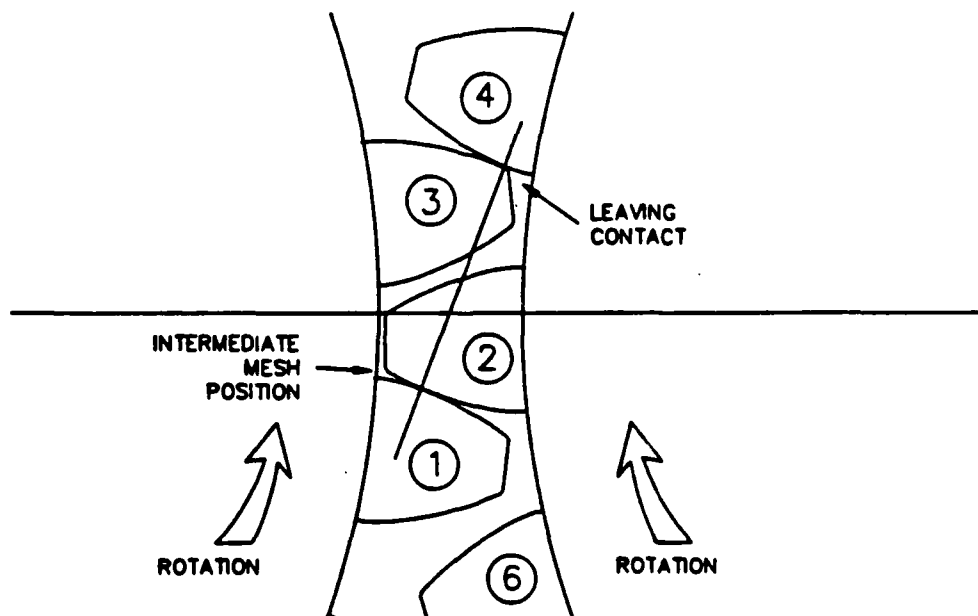
Figure 46b: Key Points in Mesh--First Intermediate Mesh Point
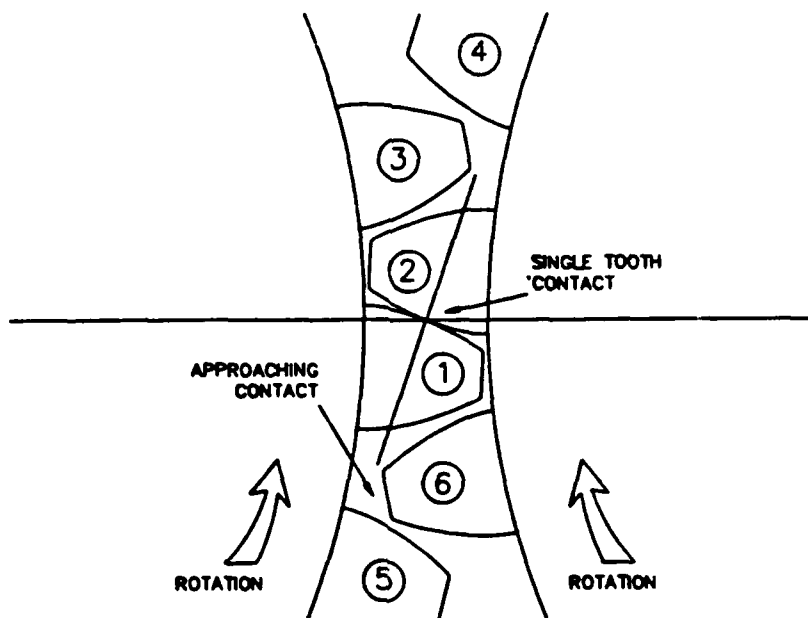
Figure 46c: Key Points in Mesh--Single Tooth Contact
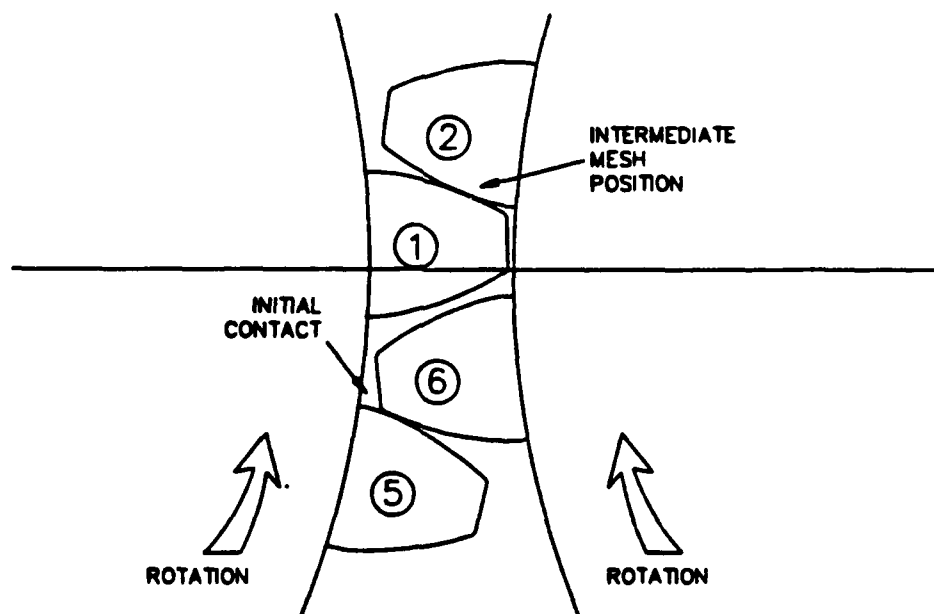
Figure 46d: Key Points in Mesh--Second Intermediate Mesh Point
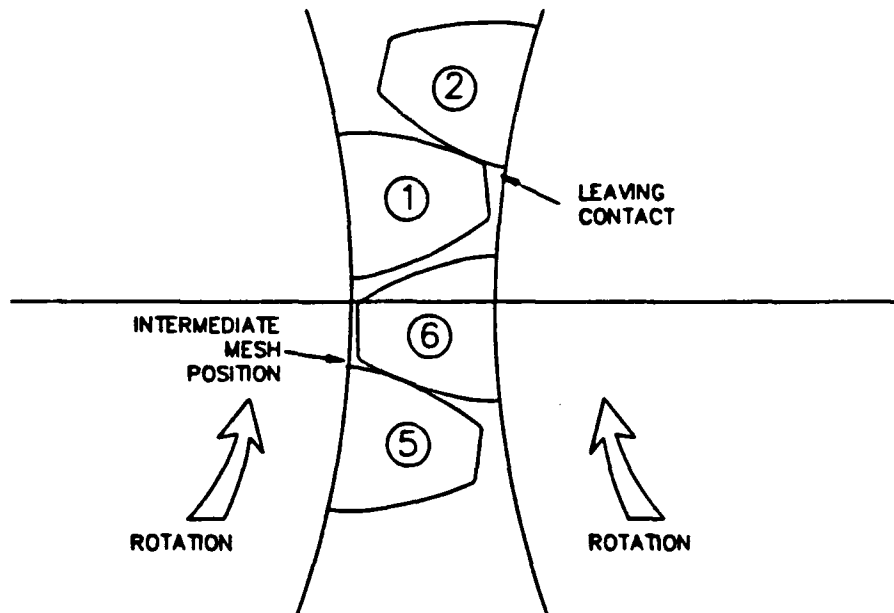
Figure 46e: Key Points in Mesh—Leaving Contact

tooth pair (5,6) comes into contact at the bottom of the line of action, again creating a dual contact condition (see Figure 46d). Finally, Figure 46e shows the second transition from dual to single contact, and also the final contact position of tooth pair (1,2).

A.4.2. Definition of a Mesh Cycle

The repetition of single and dual tooth contacts along with the continuously changing tooth pair compliance, creates the unsteady relative gear motion that drives separation. Figure 47 is a representation of the tooth stiffness profile through the range of motions represented in Figures 46a through 46e, and is labeled in accordance with these figure numbers. A real stiffness profile

consists of a succession of approximated stiffness values taken at each of the hundreds of discrete iteration points into which each mesh is divided, or, *mesh iteration points*. Notice that the actual pattern of repetition does not span the entire length of the line of action. Rather, it begins where one tooth pair enters mesh, and it ends where the *subsequent* pair enters. This range of motion, from the bottom of the line of action (tooth pair (1, 2) in Figure 46a) to the point of initial contact of the next tooth pair (Figure 46c) is defined as one *mesh cycle*. This definition satisfies the obvious requirement that the number of mesh cycles in every rotation of a gear equal the number of teeth on that gear.
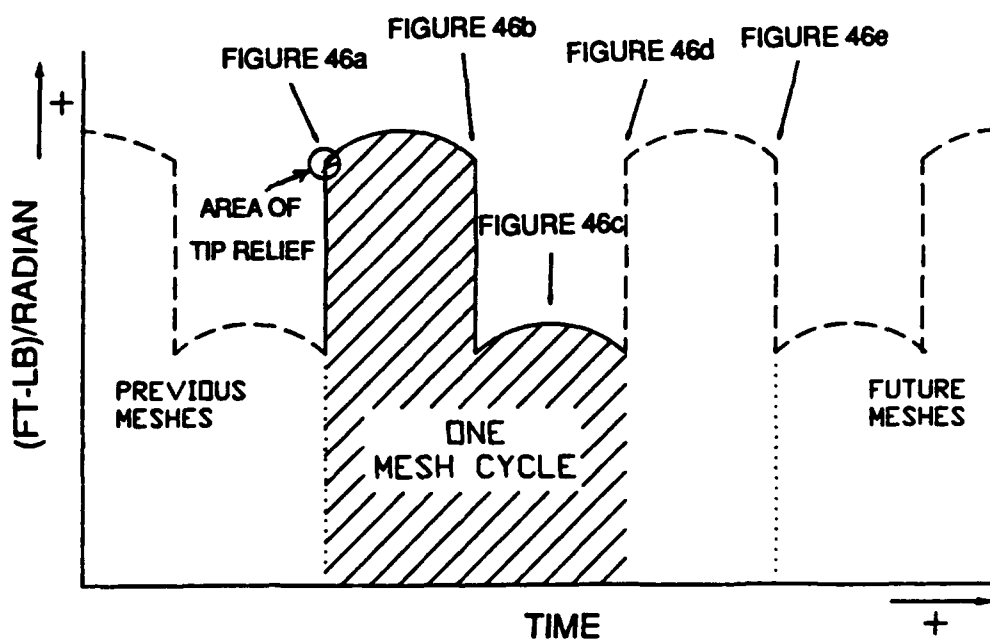
Figure 47: Stiffness Profile Mesh Cycle

It is common in the manufacture of gears to machine away some of the tooth material at the very tip of the involute profile in order to ease initial tooth pair contact (as will be shown in Figure 53). Because this *tip relief* will vary according to gear design and application, its effect on kinematics will not be dealt with directly, but, if desired, it may be easily accounted for in Gearsep1 calculations. Its effect on the tooth pair stiffness would be to remove the sharp corners from the stiffness profile (see circled region of Figure 47), thus producing a gradual transition from no contact to full tooth contact.

A.4.3. Algorithm for Calculating Stiffness Values at Mesh Iteration Points

Figure 48 describes the procedure for using the five term power series created in Gearsep1 in combination with an analytical description of single and dual tooth contact to create and store a complete tooth pair stiffness profile.

A.5. Contact Ratio as a Weighting Term: Application of the Beta-m Routine

Ideally, initial values for the Gearsep dynamic analysis should be determined so as to place the system's reponse directly into

C

calculate and store stiffness
values for all mesh iteration points

initialize tooth iteration counter

calculate compliance at present
tooth iteration point using the five term
analytical compliance equation

is
the tooth
iteration counter less
than the iteration number for the
pre-pitch transition from two tooth
pairs in contact to just
one pair?

yes

calculate the compliance for the
second tooth using the same
analytical equation

no

invert the single compliance
to obtain the "total" stiffness
for the present iteration point

calculate iteration point
stiffness for the present
compliances to obtain a total
sum the inverses of the two

does
the present iteration
point coincide with the post-
pitch transition from one tooth
pairs in contact to
two?

no

yes

Figure 48: Stiffness Calculation and Storage Algorithm Flow Chart

quasi-equilibrium, obviating all transient responses. There are two possible choices for the initial displacements: those corresponding to the stiffness of a single tooth pair in contact, and those corresponding to the stiffness of dual pair contact (see Figure 47). However, using the smaller, single pair stiffness will yield the *precise* quasi-equilibrium condition for a gear pair that has *only* single pair contact. Again, this can only happen for a gear pair with a contact ratio of exactly one, stipulating that exactly one tooth pair is in contact at any given point in mesh. The converse is true for dual pair contact, which is indicative of a gear pair with a contact ratio of exactly *two*. Continuing this argument, it may be theorized that when analyzing a gear pair with a contact ratio lying *between* one and two, the correct initial conditions are those which occur for a stiffness which lies somewhere between that of single tooth contact and dual tooth contact. It would seem then that the weighting term itself would also lie between one and two: A logical candidate is the contact ratio itself.

Following the assumptions stated above, primary estimates of initial conditions are obtained by multiplying the stiffness of a single contacting tooth pair by the gear pair's contact ratio, and applying the beta-m numerical integrator through a single mesh cycle. If these primary estimates are correct, they will be matched by the response calculated for the *end* of this cycle. In the test cases examined, these outputs and inputs were close enough to

tentatively confirm the use of contact ratio as a weighting term, and this technique was subsequently confirmed through reference [22].

As a step towards increasing the accuracy of the initial condition estimates as based on the contact ratio, it is assumed that if these are indeed good estimates, but not *exact* estimates, then the true initial conditions should lie between the input and the newly calculated output values. If this output is then averaged with the input in a bisection scheme and reinserted (for convergence , the result may be assumed to be a better estimate of the true initial values. This averaging and reinserting process is repeated until either the difference between input and output displacements is within some tolerance or an instability occurs in the numerical procedure. It should be noted that the tolerance tests are applied only to the gear *displacements*, while the averaging and reinserting encompass the entire range of derivatives handled by beta-m: displacements and first through third time derivatives.

Figure 49 depicts the procedure described above for finding an accurate estimate for the quasi-equilibrium initial conditions using the contact ratio as a weighting term.

Finally, the beta-m routine is iterated to find the system's response, as depicted in Figure 50. Also included are the various stopping and error check procedures.

D
use contact ratio as a weighting term
and apply beta-m through one mesh cycle

start the mesh cycle at the half way point:
tooth position is at half total number of points per mesh ← **a**

multiply the total stiffness by the system's contact ratio

calculate an initial guess of the system's quasi-equilibrium displacement

does tooth position correspond to that of the post-pitch transition from one tooth in contact to two?

yes → set the present tooth position to "1": stiffness values will now be for two pairs of teeth

no → recall the saved stiffness value for the present point

invoke beta-m and find the system's response

is the new pair of teeth at the starting position of the old pair?

yes → is response at end of cycle within tolerance of response at the beginning or is beta-m unstable?

yes

no → increment the tooth/ teeth to the next position

no → average old initial conditions and new response values and go through another cycle → **a**

Figure 49: Contact Ratio Weighting Term and Beta-m Application Algorithm Flow Chart
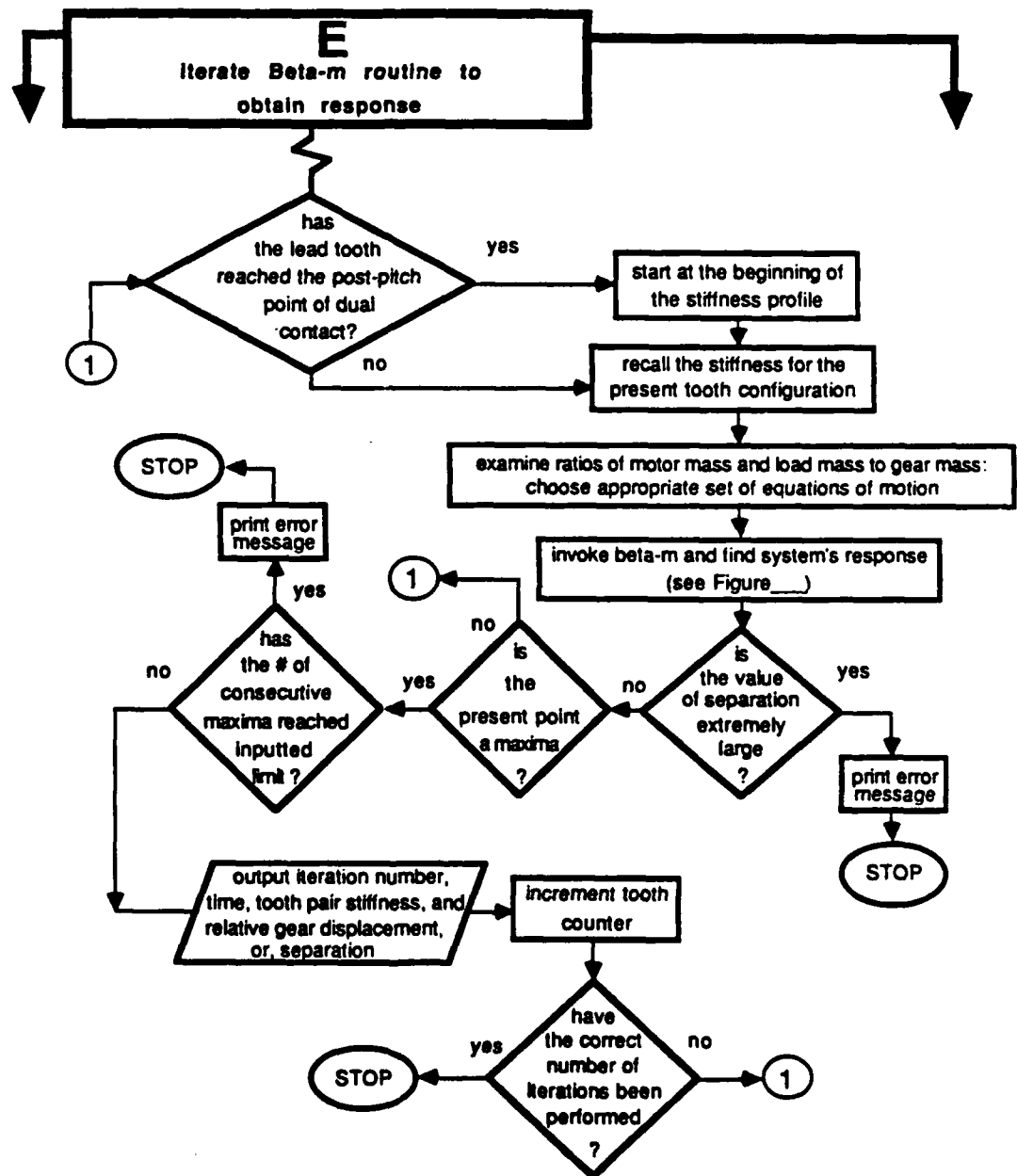
Figure 50: Beta-m Iteration Algorithm

Appendix B

PROGRAM ALGORITHM

B.1.   Sectional Overview

The following is a comprehensive, step by step algorithm
designed to supplement the program flow charts of Appendix A.
This appendix is divided into a series of numbered sections, each of
which contains a series of individual analysis steps, which are
numbered consecutively throughout the chapter. After appropriate
sections, one or more graphical representations of appropriate
variables, expressions, or concepts are presented. Some sections
refer directly to Appendix A, where they are described in detail as
algorithm flow charts. Note that parenthetical variable names are
fortran equivalents of the true variable names, and that they have
been kept to six characters or less, due to the reluctance of
personal computer fortran compilers to recognize the usual eight
character names.

Within the description of each variable, boldfacing will indicate
(if appropriate) lettering in common with the variable name. Note
also that when it is necessary to distinguish between individual
gears within a particular pair, the driving gear will be referred to
as the *pinion*, and the driven gear simply as the *gear*. If, however,

general properties of both are to be discussed, the all-encompassing term *gear* will be used: This convention has already been used throughout Appendix A. It is also helpful to note that the pinion (driving) is usually depicted to the left of the gear (driven), and that variables related to the pinion have a subscript of *1* or *p*, while those related to the gear have a subscript *2* or *g*.

B.2. Gearsep1

B.2.1. Data Input

1) Input the geometries of the pinion and the gear (see Appendix E).

R_o : outer radius

R_p : pitch radius

R_b : base radius

R_r : root radius

R_f : fillet radius

T_p : circular pitch tooth thickness: If this exact value is not available, standard tooth thickness at pitch may be substituted.

N_1 & N_2 : tip relief factors; the percentage for one mesh of involute tooth profile before tip

relief comes into contact. See Appendix A, Section A.3.2..

W_p, W_g : tooth facewidths; also thicknesses of gear.

ϕ_p (phip) : pressure angle

R_{cl} : centerline distance (the constant distance between the two gear centers)

2) Input the material properties of the two gears, and the iteration parameters for the deflection calculations.

$\mu(\mu u)$: Poisson's ratio

E : Young's modulus

nstep : number of increments into which the tooth cantilever will be divided: Again, the cantilever deflection equation must be integrated along the length of the tooth, which, in numerical term, translates into a summation of discrete increments.

nstepf : number of increments into which the fillet area will be divided for its evaluation as a cantilever

B.2.2. Calculations of Geometry Related Varibles

3) **Calculate the varibles related to the base of the tooth cantilever (BOTC) for both the pinion and the gear.** This is defined as that point where the fillet circle blends with the involute tooth profile (see Figure 51).
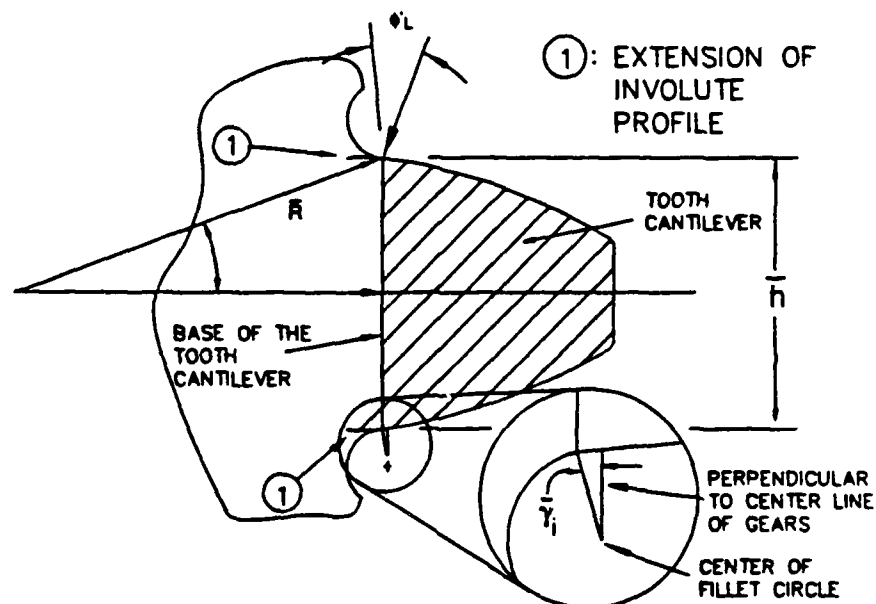
Figure 51: Variables Related to the Base of the Tooth Cantilever

$\overline{R}_i$ (Rbar(i)) :   the radial location defining the BOTC

$\overline{\phi}_i$ (phibar(i)) :   contact pressure angle at the BOTC; This is the system's pressure angle f_p at the contact point in question: In this case, the BOTC.

$$\bar{\phi}_i = (Cos)^{-1}\left(\frac{R_b}{\bar{R}_i}\right) \qquad \text{Equation 30}$$

$\bar{\alpha}_i$ (alfbar(i)) : included tooth angle of the BOTC: This is the angle between the tooth centerline to the radius of the base of the cantilever.

$$\bar{\alpha}_i = \frac{t_p}{2Rp_i} + Tan\phi p_i - \phi p_i - Tan\bar{\phi}p_i + \bar{\phi}p_i \qquad \text{Equation 31}$$

$\bar{x}_i$ (xbar(i)) : the distance along the tooth centerline from gear center (for both pinion and gear) to the BOTC.

$$\bar{x}_i = \bar{R}_i Cos(\bar{\alpha}_i) \qquad \text{Equation 32}$$

$\bar{\gamma}_i$ (gambar(i)) : the angle defining the BOTC with respect to the fillet center

$$\bar{\gamma}_i = \bar{\phi}_i - \bar{\alpha}_i \qquad \text{Equation 33}$$

$\bar{h}_i$ (hbar(i)) : tooth thickness at the BOTC

$$\bar{h}_i = 2\bar{R}_i sin(\bar{\alpha}_i) \qquad \text{Equation 34}$$

$\overline{l_i}$ (lbar(i)) :   distance from the BOTC to the load line

4) Calculate the angles describing the point of initial tooth pair contact and of tooth pair disengagement. These are measured relative to pitch for both gears: *approach* implies pre-pitch (negative values) and *recess* implies post-pitch (positive values).

β_{ap} (BETAap) :   the angle of approach for the pinion

β_{ag} (BETAag) :   the angle of approach for the gear

β_{rp} (BETArp) :   the angle of recess for the pinion

β_{rg} (BETArg) :   the angle of recess for the gear

The equations for these angles are based on the geometry of mesh as depicted in Figure 52, which shows initial and final contact for the *same* tooth pair.

Defining $S_{approach}$ as the engagement point's linear distance along the line of action, applying the Law of Sines and the Law of Cosines:

$$\text{Law of Sines} \qquad \frac{Sin(\theta)}{S_a} = \frac{Sin(90-\phi)}{R} \qquad \text{Equation 35}$$
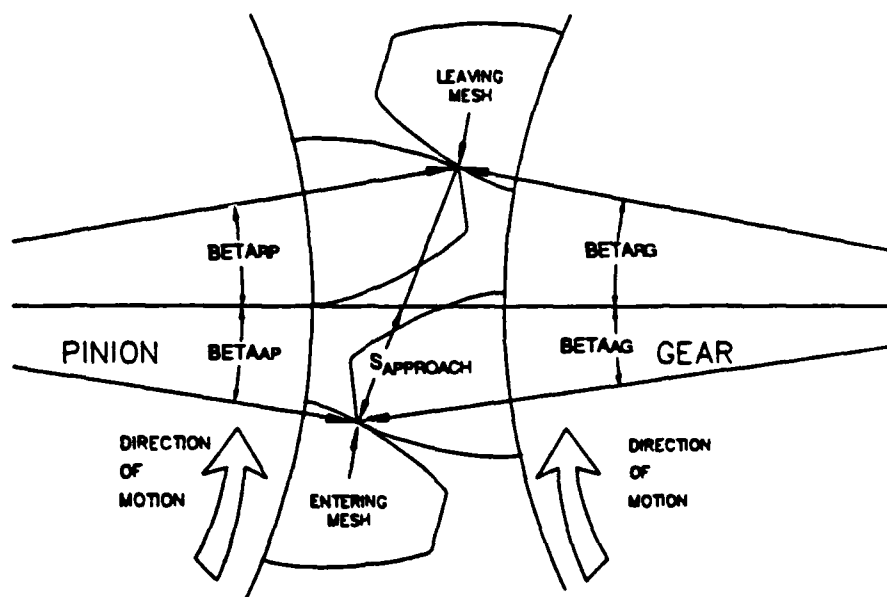
Figure 52: Angles of Approach and Recess

Law of Cosines $\quad R^2 = R_p^2 + S^2 - 2R_pS \, Cos(90-\phi)$ Equation 36

where:

θ : the angular displacement from pitch of an
arbitrary point of tooth contact: For
example, the θ of the initial point of contact
on the pinion is defined as β_{ap}.

ϕ : system pressure angle

R_p : pitch radius

R : radius of mutual contact point

S : distance along line of contact from pitch of
the mutual contact point

Solving the Law of Sines for S_a gives

$$S_a = \frac{R \, Sin\theta}{Cos\phi} \quad \text{with} \quad Sin(90 - \phi) = Cos(\phi) \qquad \text{Equation 37}$$

Substituting into the Law of Cosines gives:

$$R^2 = R_p^2 + \frac{R^2 Sin^2(\theta)}{Cos^2(\phi)} - \frac{2R_p \, R \, Sin(\theta) \, Sin(\phi)}{Cos(\phi)} \qquad \text{Equation 38}$$

where $Sin (90 - \phi) = Cos (\phi)$

After solving this quadratic for R, solve the Law of Cosines for S:

$$S^2 + S(2R_p Sin(\phi)) + R_p^2 - R^2 = 0 \qquad \text{Equation 39}$$

Finally, β_{ap} is found from one last substitution into the Law of Sines:

$$\beta_{ap} = Sin^{-1}\left(\frac{SCos(\phi)}{R}\right) \qquad \text{Equation 40}$$

5) **Generate the angular and radial locations of the five compliance points:** These are analogous in form to the angles and radii depicted in Figure 52. As shown in Figure 53, these angles carry the same pre/post-pitch sign convention as do the

angles of recess and approach (see Section 4). Figure 53 also shows that the first and fifth compliance points are *not* located at the extremes of the line of contact. This is done to account for the aforementioned tip relief (see Appendix A, Section A.3.2.) used to produce a smooth transition into full tooth contact (see expanded portion of Figure 53.) Because in a real gear pair, this tip relief would alter not only the location of full tooth contact, but also the tooth pair stiffness at engagement and disengagement, the first and fifth compliance points are moved "in" by a factor which is input as a percentage of the angles of approach and recess (see Figure 52). For the results given in Chapter 6, a factor of 90% was used.
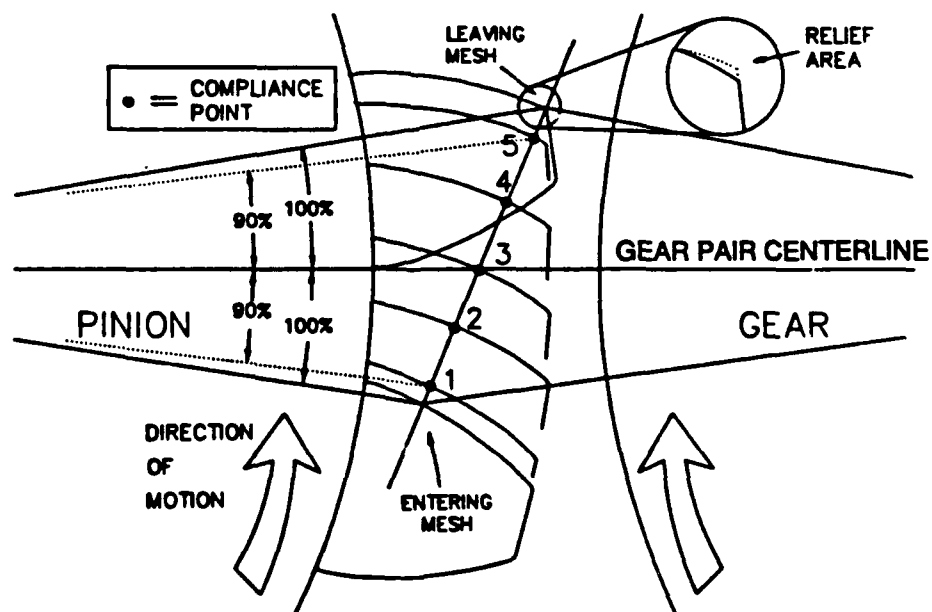
Figure 53: Location of Compliance Points

The angular compliance point locations *with respect to pitch* are:

$\theta p_{1 \text{ thru } 5}$ (thetap(1 thru 5)) :   angular location of compliance

points as measured on the pinion.

$\theta g_{1 \text{ thru } 5}$ (thetag(1 thru 5)) :   angular location of compliance

points as measured on the gear

θ_p's and θ_g's are found as were the angles of approach and recess in Section **4**, except compliance point 3 is now *defined* to lie at pitch. Therefore:

$$\theta p_3 = \theta g_3 = 0 \qquad \text{Equation 41}$$

Rcp_p (Rcp1) :   radial positions of a compliance point as

measured on the pinion

Rcp_g (Rcp2) :   radial positions of a compliance point as

measured on the gear

Calculation of the radial positions of the compliance points relative to the *pinion* utilizes Equation 38. For corresponding radial values on the *gear*, advantage is taken of the symmetry of mesh. As

shown in Figure 52, the two angles β_{ap} and β_{ag} describe two triangles that share a common side. Thus, for any compliance point cp_i, there exists a common distance from pitch, S_i that relates the geometries of the pinion and the gear. From this relation, the equation for compliance point radii as referenced to the gear is obtained:

$$R\,cp_g(\,i\,) = \frac{(R\,cp_p)(Sin(\theta_p))}{(Sin(\theta_g))} \qquad \text{Equation 42}$$

Note that these and all other points on the line of action are described only with respect to the pinion.

6) Calculate the variables related to the compliance points using the same equations as those given in Section 3. All variables are analogous to those related to the BOTC as shown in Figure 51.

ϕ_{ip} (PHIip) :   contact pressure angle for compliance point i as measured on the pinion; This is the system's pressure angle at the point in question

ϕ_{ig} (PHIig) :   contact pressure angle for compliance point i as measured on the gear: As applied to the

pinion:

$$\phi_{ip} = \cos^{-1}\left(\frac{R_b}{R_{cp_p}}\right) \qquad \text{Equation 43}$$

α_{ip} (ALFAip) :   included tooth angle of the compliance point

i as measured on the pinion; This is the

angle from pitch to the radius of point i.

α_{ig} (ALFAig) :   included tooth angle of the compliance point

i as measured on the gear: Again, with

respect to the pinion:

$$\alpha_{ip} = \frac{t_p}{2R_{p_i}} + \tan\phi_p - \phi_p - \tan\phi_{ip} + \phi_{ip} \qquad \text{Equation 44}$$

The previous values are calculated locally in order to find:

ϕ'_{pi} (PHIpm$_p$(i)) :   the compliance point load angularity for the

pinion; This is the system's pressure angle

ϕ_p in localized tooth coordinates.

ϕ'_{gi} (PHIpm$_g$(i)) :   the compliance point load angularity for the

gear

where:

$$\phi'_p = \phi_p - \alpha_{ip} \qquad \text{Equation 45}$$

hcp_{pi} ($Hcp1(i)$) :   compliance point thickness for pinion

hcp_{gi} ($Hcp2(i)$) :   compliance point thickness for gear

The same thickness equation used in **Section 3** is now employed to find the tooth thicknesses at each of the compliance point for both pinion and gear.

$$hcp_{ip} = 2Rcp_{ip} Sin(a_{ip})$$ Equation 46

I; should be noted that while both the load angularity $\phi'_{p\ or\ g}$ and the local pressure angle change continuously along the profile, the system pressure angle $\phi_{ip\ or\ ig}$ does not. The changes in $\phi'_{p\ or\ g}$ and local pressure angle occur because these quantities are the

projections of the line of action (fixed in global coordinates) onto a rotating and translating frame (the tooth) as shown in Figure 54, which may be compared to both Figures 51 and 53.

7)   Iterate to find γ_F as described in Appendix A, Section A.1. This process follows the same steps as those that would be necessary to produce Figure 41: Beginning with an initial guess of 0.45 radians (approximately 26°) and adding to this increments of 0.0175 radians (approximately 1°), calculate fillet and foundation deflection at each point. The process continues up to a value of γ_F = 1.4 radians (just over 80°). The initial guess is chosen to be

15% below the lowest value reported by reference [19], while the
upper iteration boundary is 15% higher than the angle
corresponding to peak deflection at compliance point 3. If these
15% buffers are not sufficient, Gearsep is able to determine
whether the correct γ_F value occurs above or below the indicated
range, and prompt the user for an appropriate adjustment.
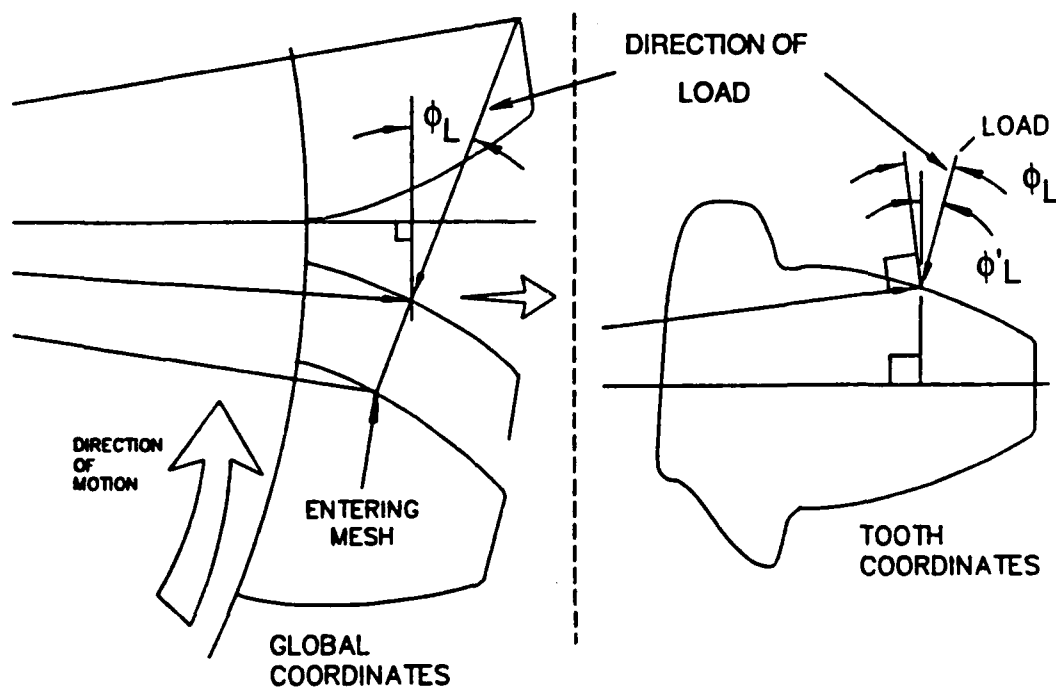
Figure 54: Global and Local Pressure Angles

8) **Calculate the distance from the BOTC to the point**
of intersection of the tooth center line and the line of
action. This point prescribes the *load line*, which is perpendicular
to the tooth centerline and marks the outermost boundary of what
is to be considered the tooth cantilever (see Figure 55).
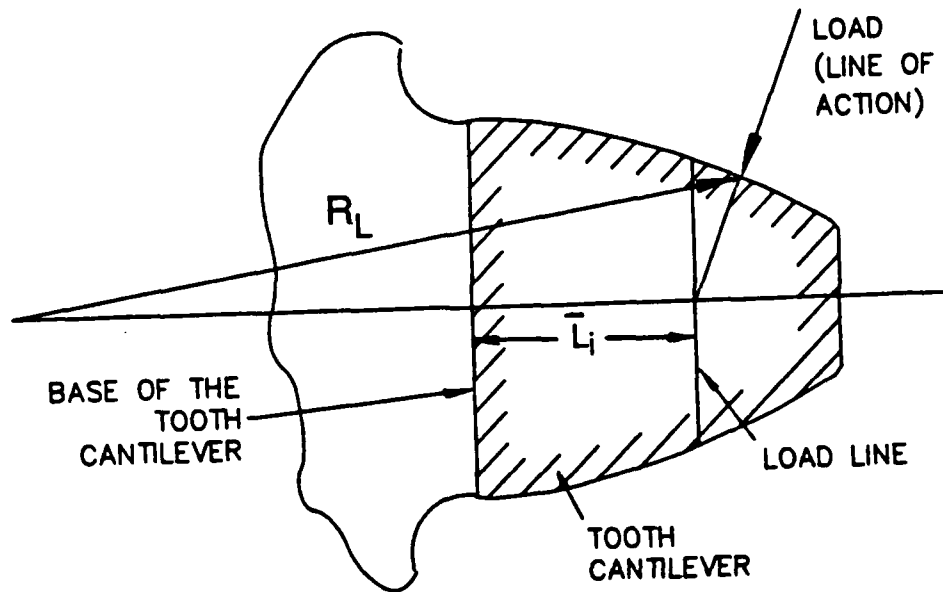
Figure 55: Definition of Load Line

L_{ip} (Lbarp(i)) :   load line distance for pinion

L_{ig} (Lbarg(i)) :   load line distance for gear

B.2.3.   Deformation Calculations

9)   Calculate the deflection of the tooth cantilever at
each compliance point due to bending and shear.

Y_{pi} (Yp(i)) :   cantilever tooth deflection at compliance

point i for the pinion

Y_{gi} (Yg(i)) :   cantilever tooth deflection at compliance

point i for the gear

As given in Chapter 3, Cornell's deflection equation is

$$Y = \frac{L\cos^2\left(\phi_L'\right)}{E} \sum_{i=1}^{n} \delta_i$$

$$\left\{ \frac{I_i^2 - I_i\delta_i + \frac{1}{3}\delta_i^2}{\bar{I}_i} + \frac{\left(2.4(1+\mu) + \tan^2\left(\phi_L'\right)\right)}{\bar{A}_i} \right\} \qquad \text{Equation 47}$$

Descriptions of the variables in this equation are available in Section 3.2..

10) Using the same cantilever deflection scheme, calculate the bending and shear deformation of the fillet cantilever. This follows the same development as the previous step.

11) Calculate the deflection at each compliance point due to foundation flexibility in the direction of loading.

Yff_{pi} (Yffp(i)) :   foundation flexibility deflection of compliance point i for the pinion

Yff_{gi} (Yffg(i)) :   foundation flexibility deflection of compliance point i for the gear

$$Y_{ff} = \frac{L Cos^2\left(\phi_L'\right)}{WE}$$

$$\Omega_1\left[\frac{16.67}{\pi}\left(\frac{l_f}{h_f}\right)^2 + 2(\Omega_2)\left(\frac{l_f}{h_f}\right) + 1.534\left(1 + \frac{Tan^2\left(\phi_L'\right)}{2.4(1+\mu)}\right)\right] \qquad \text{Equation 48}$$

Descriptions of the variables in this equation are available in Section 3.3.

The variables Ω_1 and Ω_2 carry the anticlastic properties of the tooth. If the tooth is determined to be wide enough to require anticlastic analysis from Cornell [9]):

$$\Omega_1 = \left(1 - \mu^2\right), \quad \Omega_2 = \left(\frac{1 - \mu - 2\mu^2}{1 - \mu^2}\right) \qquad \text{Equations 49}$$

Cornell defines a "wide" tooth as having a ratio of its width to its thickness at pitch greater than five [19]. Anticlastic terms take into account the possibility of lateral bending producing a longitudinal bending of opposite sign. If the tooth is sufficiently narrow, non-anticlastic constants may be used:

$$\Omega_1 = 1, \qquad \Omega_2 = 2(1 - \mu) \qquad \text{Equations 50}$$

12) Calculate the localized and Hertzian surface deflections. This requires the local radius of curvature of the involute tooth profile, and a theoretical estimate of the width of the deformed Hertzian contacting surfaces (see Figure 11).

$rloc_p$ (Rlocp) :   local involute radius of curvature for the pinion

$rloc_g$ (Rlocg) :   local involute radius of curvature for the gear

The involute radius of curvature is, conveniently, an intrinsic part of the development of the involute curve. From its geometry, the equation for the involute radius of curvature is obtained:

$$rloc_i = R_b Tan\left(\phi_p\right) \qquad \text{Equation 51}$$

where ϕ_p is the system pressure angle.

b_i (b(i)) :   Hertzian half-contact width for compliance point i

$$b = \left\{ \frac{\frac{4L}{\pi W_i}\left[\left(\frac{1 - \mu_p^2}{E_p}\right) + \left(\frac{1 - \mu_g^2}{E_g}\right)\right]}{\left[\frac{1}{R_{loc_p}} + \frac{1}{R_{loc_g}}\right]} \right\}^{1/2} \qquad \text{Equation 52}$$

Y_{hertz_i} ($Y_{hertz(i)}$) : **Hertz**ian surface deformation of compliance point **i** at the load point and in the direction of loading

$$Y_{hertz_i} = \frac{2L}{\pi W_i}\left[\left(\frac{1 - \mu_p^2}{E_p}\right)\left\{\ln\frac{2\bar{h}_p}{b} - \left(\frac{\mu_p}{2(1 - \mu_p)}\right)\right\} + \left(\frac{1 - \mu_g^2}{E_g}\right)\left\{\ln\frac{2\bar{h}_g}{b} - \left(\frac{\mu_g}{2(1 - \mu_g)}\right)\right\}\right] \qquad \text{Equation 53}$$

13) Sum all of the calculated deflections for each compliance point. Because this analysis is performed for a unit load, each of these total deflections is in fact the tooth pair compliance for the corresponding point.

Y_{tot_i} ($Y_{tot(i)}$) : **total** deflection at the load point and in the direction of loading for a unit load at compliance point **i**

C_i :   total tooth pair compliance at point **i**.

$$C_i = Y_{tot_i} = Y_{b_p} + Y_{b_g} + Y_{f_p} + Y_{f_g} + Y_{ff_p} + Y_{ff_g} + Y_{hertz} \qquad \text{Equation 54}$$

Note again that instantaneous total tooth pair compliace is the sum of all deflections of the point of instantaneous mutual contact and is defined to be in the direction of loading (see Figure 54.)

B.2.4.   Power Series Representation of Compliance

14) Fit a five term power series to the five compliance values. This is the technique used by Cornell [9] (and as such, it was choosen somewhat out of convenience) and its result is a simple analytical expression for tooth pair compliance at any point in mesh. The alternative to this is to repeat the lengthy compliance calculation procedure for each of the hundreds and sometimes thousands of increments into which each mesh will be divided.

The five term (fourth order) power series as given by Cornell takes the form

$$C_i/C_o = \left[1 + A\left(\frac{\theta p_i}{S_d}\right) + B\left(\frac{\theta p_i}{S_d}\right)^2 + C\left(\frac{\theta p_i}{S_d}\right)^3 + D\left(\frac{\theta p_i}{S_d}\right)^4 \right] \qquad \text{Equation 55}$$

In Equation 55:

C_i :   the compliance at compliance point i

θp_i :   the angular position of compliance point i

C_o :   a reference compliance value: compliance at pitch

S_o :   a reference angle: from pitch to point to fifth compliance point (see Figure 53)

θp_o :   an angular reference value

A,B,C, and D :   constant coefficients of the fourth order equation which will determine the function's shape

Notice that the variables from Equation 55 need only be determined with respect to the pinion.

Values for the constants A,B,C and D are determined by applying a standard Gaussian elimination algorithm to the following system of equations:

$$\begin{bmatrix} 1 & \left(\phi_{P_1}/\phi_{P_0}\right) & \left(\phi_{P_1}/\phi_{P_0}\right)^2 & \left(\phi_{P_1}/\phi_{P_0}\right)^3 & \left(\phi_{P_1}/\phi_{P_0}\right)^4 & | & \left(C_1/C_0\right) \\ 1 & \left(\phi_{P_2}/\phi_{P_0}\right) & \left(\phi_{P_2}/\phi_{P_0}\right)^2 & \left(\phi_{P_2}/\phi_{P_0}\right)^3 & \left(\phi_{P_2}/\phi_{P_0}\right)^4 & | & \left(C_2/C_0\right) \\ 1 & \left(\phi_{P_3}/\phi_{P_0}\right) & \left(\phi_{P_3}/\phi_{P_0}\right)^2 & \left(\phi_{P_3}/\phi_{P_0}\right)^3 & \left(\phi_{P_3}/\phi_{P_0}\right)^4 & | & \left(C_3/C_0\right) \\ 1 & \left(\phi_{P_4}/\phi_{P_0}\right) & \left(\phi_{P_4}/\phi_{P_0}\right)^2 & \left(\phi_{P_4}/\phi_{P_0}\right)^3 & \left(\phi_{P_4}/\phi_{P_0}\right)^4 & | & \left(C_4/C_0\right) \end{bmatrix}$$

Equation 56

B.3.   Gearsep2

B.3.1.   Data Input

15) Input the system's specifications.

$J_{1 \text{ thru } 4}$:   the mass moments of inertia of:

1 :   motor

2 :   pinion

3 :   gear

4 :   load mass

$k_{1 \text{ or } 2}$:   shaft stiffnesses

1 :   shaft between motor and pinion

2 : shaft between gear and load

C : a generalized damping (may include bearing and/or shaft and gear material's damping properties)

PPM : the number of iteration points into which each mesh is divided

RPM : system speed in revolutions per minute

Torque : applied system torque in foot-pounds

num : total number of iterations

DR : ratio of the pinion base diameter to the gear base diameter

e : profile errors in angular coordinates (optional) [Kumar]

This final variable, e, gives the Gearsep user the ability to analyze the effect on system performance if there exists a machining errors in the tooth or if a particle of some sort becomes attached to the tooth surface. It should be noted, however, that in its present form, Gearsep contains only the necessary framework for such an analysis, and does not deal with it directly.

B.3.2. Supporting Calculations

16) **Calculate the locations of the mesh transition points: from one pair of teeth in contact to two, and similarly, from two teeth to one.**

> Dulpt1 : the *post*-pitch initiation of dual tooth pair contact
>
> Dulpt2 : the *pre*-pitch initiation of single tooth pair contact

The two dual points are listed in this order (post *before* pre)because the initial mesh iteration position is set at $^{PPM}/_2$, which is very close to pitch (compliance point 3) in Figure 53. As such, meshing begins with one tooth pair in contact, and the first transition encountered is that at which mesh switches from one pair of teeth in contact to two, namely, Dualpt1 (see Figure 46d).

17) **Calculate and store stiffness values for all mesh iteration points.** This is performed before any application of the numerical integration is made, and the stiffness values retrieved according to the position of the teeth in mesh.

Note that when the "gear tooth deflection" is calculated using Equation 54, that deflection is *linear.* It is the linear deflection of the point of mutual tooth contact in the direction of the applied

force. Because of this, any spring constant calculated directly from these deflections will also be linear. However, the system's equations of motion (Equations 1b - 4b) require *torsional* spring constants, and so, the linear constants must be converted using Equation 57:

$$K_{linear}\left(\frac{lb}{in}\right) R^2\left(in^2\right) = K_{torsional}(in\ lb) \qquad \text{Equation 57}$$

In Equation 57:

K_{linear} : linear stiffness (spring constant)

$K_{torsional}$: torsional stiffness

R : base radius of pinion

This is based on the gear geometry in Figure 56, where the line of action is shown extending in both directions, and, at the points indicated, becomes tangent to the base circle of each gear. Because the deflections from Equation 54 are defined along the direction of this line, the calculated *linear* spring stiffnesses will act along the same line. As such, the base radius is the moment arm of the spring force in Equation 57, and $K_{torsional}$ is $K_{TOOTH\ PAIR}$ as used in Chapter 2 to derive the reduced equations of motion. (The variable $K_{TOOTH\ PAIR}$ as used in the program GEARSEP and in the remaining of

this appendix will be known simply as K_{total}, implying the total stiffness of two meshing teeth.)
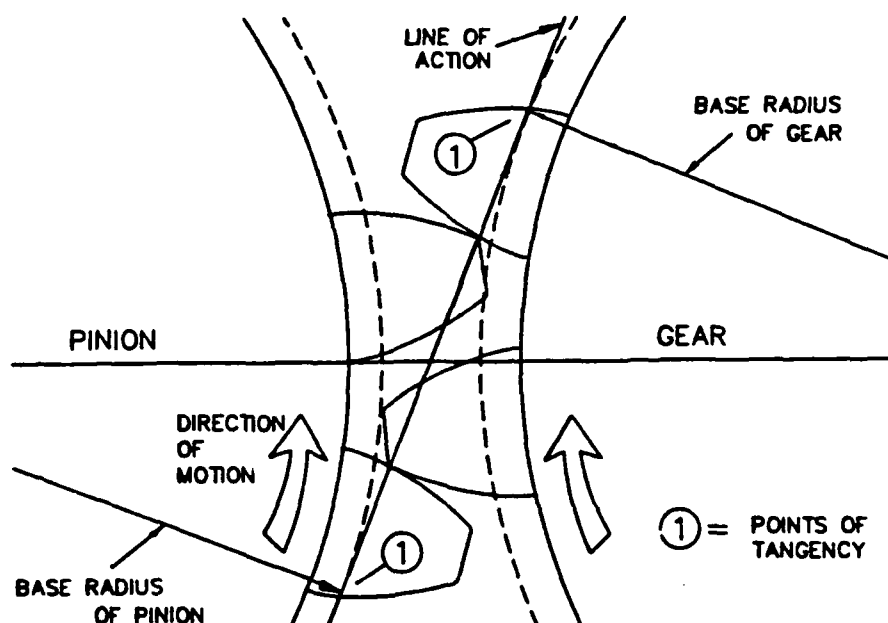
Figure 56: Gear Geometry and the Line of Action

18) **Determine the primary guess for the initial conditions of the dynamic analysis using the contact ratio as a weighting term**, as discussed in Appendix A, Section A.4. These initial displacements are given as follows:

$$\theta_1 = (T/2)\left(\frac{1}{K_2} + \frac{1}{(CR)(K_{total})} + \frac{1}{K_1}\right) \quad \text{Equation 58}$$

$$\theta_3 = (T/2)\left(\frac{1}{K_2} + \frac{1}{(CR)(K_{total})} - \frac{1}{K_1}\right) \quad \text{Equation 59}$$

$$\theta_3 = (T/2)\left(\frac{1}{K_2} - \frac{1}{(CR)(K_{total})} - \frac{1}{K_1}\right) \qquad \text{Equation 60}$$

$$\theta_4 = -\theta_1 \qquad \text{Equation 61}$$

This primary guess of initial conditions is run through a single mesh cycle, after which gear displacement output (θ_2) is compared with the input (Equation 59). if the relative error between input and output is within a given tolerance, the primary estimates are taken as the true initial conditions: The tolerance used by Gearsep in the sample analysis (Chapter 6) is a relative error of 1×10^{-5}, which is a full three orders of accuracy above the computer's approximate order of accuracy of 1×10^{-8}, and a full order of accuracy above the number of significant digits of the gear input data from reference [7] as listed in Appendix E. If, however, the error is not within tolerance, the estimates and output are repeatedly adjusted and reinserted into the numerical integrator until tolerance is met or until the integrator becomes unstable (see Appendix A, Section A.2.).

B.3.3.   Numerical Integration

19)   **Perform the dynamic analysis on the single-stage system using the numerical integrator:** This begins with the

initial conditions just calculated. Iteration variables are controlled by incrementing a tooth counter, which keeps a running track of the positions of the meshing gear teeth. As this counter advances through the various key points shown in Figures 46a through 46e, corresponding stiffness values (see Figure 47) are fed to the beta-m integration routine, which generates separation data by solving the following equations of motion, given in Chapter 2 (see Appendix D for numerical solution details):

$$J_1\ddot{\theta}_1 + k_1(\theta_1 - \frac{r_3}{r_2}\theta_2) = 0 \qquad \text{Equation 62}$$

$$\left[J_3 + \left(\frac{r_3}{r_2}\right)^2 J_2\right]\ddot{\theta}_3 - \frac{r_3}{r_2}k_1\theta_1 + \left[\left(\frac{r_3}{r_2}\right)^2 k_1 + k_2\right]\theta_3 - k_2\theta_4 = 0 \qquad \text{Equation 63}$$

$$J_4\ddot{\theta}_4 + k_2(\theta_4 - \theta_3) = 0 \qquad \text{Equation 64}$$

The output from the numerical integrator is as described in Chapter 6, Section 6.1., and may be plotted directly from the output file to yield the system's response.

Appendix C

ANALYTICAL MODELING PROCEDURE

The modeling procedure used to solve the single-stage system in

Chapter 3 is now reviewed in detail, and all figure and equation

references herein are made directly to that chapter. Furthermore,

all of the following work, unless otherwise noted, is attributed to

Neubert [19].

C.1. System Elements and Homogeneous Solution

For the analytical solution, the gears are assumed to be perfect

rotational elements. In addition, damping is assumed to be

negligible, masses are arbitrary, and shaft inertias are ignored.

The solution will be found for a set of arbitrary initial

displacements of the lumped three-mass system shown in Figure 8.

The equations of motion are:

$$J_1 \ddot{\theta}_1 + k_1 \left(\theta_1 - \frac{r_3}{r_2} \theta_2 \right) = 0 \qquad \text{Equation 65}$$

$$\left[J_3 + \left(\frac{r_3}{r_2}\right)^2 J_2 \right] \ddot{\theta}_3 - \frac{r_3}{r_2} k_1 \theta_1 + \left[\left(\frac{r_3}{r_2}\right)^2 k_1 + k_2 \right] \theta_3 - k_2 \theta_4 = 0 \qquad \text{Equation 66}$$

$$J_4 \ddot{\theta}_4 + k_2(\theta_4 - \theta_3) = 0 \qquad \text{Equation 67}$$

These may be written in matrix form as:

$$
\begin{bmatrix}
J_1 & 0 & 0 \\
0 & J_3 + \left(\frac{r_3}{r_2}\right)^2 J_2 & 0 \\
0 & 0 & J_4
\end{bmatrix}
\begin{Bmatrix} \ddot{\theta}_1 \\ \ddot{\theta}_2 \\ \ddot{\theta}_3 \end{Bmatrix}
+
\begin{bmatrix}
k_1 & -\frac{r_3}{r_2}k_1 & 0 \\
-\frac{r_3}{r_2}k_1 & \left(\frac{r_3}{r_2}\right)^2 k_1 + k_2 & -k_2 \\
0 & -k_2 & k_2
\end{bmatrix}
\begin{Bmatrix} \theta_1 \\ \theta_2 \\ \theta_3 \end{Bmatrix}
=
\begin{Bmatrix} 0 \\ 0 \\ 0 \end{Bmatrix}
$$

$$\text{Equation 68}$$

Assuming a solution of the form:

$$\{\theta_n\} = \{A\}\text{SIN}(\omega t - \psi) \qquad \text{Equation 69}$$

and substituting into Equation 68 results in the following system of equations:

$$\left[\begin{bmatrix} -\omega^2 J_1 & 0 & 0 \\ 0 & -\omega^2 J_3 - \omega^2\left(\frac{r_3}{r_2}\right)^2 J_2 & 0 \\ 0 & 0 & -\omega^2 J_4 \end{bmatrix} + \begin{bmatrix} k_1 & -\frac{r_3}{r_2}k_1 & 0 \\ -\frac{r_3}{r_2}k_1 & \left(\frac{r_3}{r_2}\right)^2 k_1 + k_2 & -k_2 \\ 0 & -k_2 & k_2 \end{bmatrix}\right] \begin{Bmatrix} A_1 \\ A_2 \\ A_3 \end{Bmatrix} = \begin{Bmatrix} 0 \\ 0 \\ 0 \end{Bmatrix}$$

<div align="right">Equation 70</div>

Because the solution $A_1 = A_2 = A_3 = 0$ produces the trivial case, the determinant of the coefficient matrix must equal zero:

$$\begin{vmatrix} -\omega^2 J_1 + k_1 & -\frac{r_3}{r_2}k_1 & 0 \\ -\frac{r_3}{r_2}k_1 & -\omega^2\left[J_3 + \left(\frac{r_3}{r_2}\right)^2 J_2\right] + \left(\frac{r_3}{r_2}\right)^2 k_1 + k_2 & -k_2 \\ 0 & -k_2 & -\omega^2 J_4 + k_2 \end{vmatrix} = 0$$

<div align="right">Equation 71</div>

The result is the following quadratic relation:

$$\omega^2 = \frac{-b \pm \sqrt{b^2 - 4ac}}{2a} \qquad \text{Equation 72}$$

with:

$$a = J_1 J_4\left(J_3 + J_2 R^2\right) \qquad \text{Equation 73}$$

$$b = -R^2\left[J_1 J_2 k_2 + k_1 J_4 (J_1 + J_2)\right] - k_2 J_1(J_3 + J_4) - J_3 J_4 k_1 \qquad \text{Equation 74}$$

$$c = k_1 k_2 \left[R^2 (J_1 + J_2) + J_3 + J_4\right] \qquad \text{Equation 75}$$

It should be noted that given the form of the determinant in Equation 71, the resulting equation is cubic in ω^2. However, in the subsequent algebra, a root is lost, showing that the system is indeed *semi-definite*: The lost root corresponds to the trivial mode of rigid body motion of the system as a whole (simple rolling with no shaft deflections).

Returning to the matrix equations of motion:

$$\begin{bmatrix} -\omega^2 J_1 + k_1 & -R k_1 & 0 \\ -R k_1 & -\omega^2\left[J_3 + (R)^2 J_2\right] + (R)^2 k_1 + k_2 & -k_2 \\ 0 & +k_2 & -\omega^2 J_4 + k_2 \end{bmatrix} \begin{Bmatrix} A_1 \\ A_2 \\ A_3 \end{Bmatrix} = \begin{Bmatrix} 0 \\ 0 \\ 0 \end{Bmatrix}$$

$$\text{Equation 76}$$

The following equations give the system's amplitude ratios, which are the relative displacements of the masses during natural motion:

$$A_{2n} = \frac{k_1 - \omega_n^2 J_1}{R k_1} \qquad \text{Equation 77}$$

$$A_{3n} = -R\left(\frac{k_1}{k_2}\right) + \left\{-\omega_n^2\left(J_3 + R^2 J_2\right) + R^2 k_1 + k_2\right\}\frac{A_{2n}}{k_2}$$ Equation 78

$$n = 1, 2, 3$$

These values make up the *eigenvector* or *modal matrix*, which is normalized with respect to the displacement of the first mass, as seen by the unit entries populating row one. All other elements are functions of the system's inertias, natural frequencies, shaft stiffnesses, and the gear radii ratio r_3/r_2, as contained in the set of variables $A_{i,j}$, where the subscripts are row and column positions. For the system under consideration:

$$[\phi] \equiv \begin{bmatrix} 1 & 1 & 1 \\ 1 & A_{22} & A_{23} \\ 1 & A_{32} & A_{33} \end{bmatrix}$$ Equation 79

Notice that the first column also shows unit displacements as a complete mode shape. This is indicative of a semi-definite system, where the first displacement mode is a simple rigid body rotation [17], and the first natural frequency is zero.

C.2. Particular Solution:

The equations of motion are solved using generalized

coordinates so as to produce uncoupled equations of motion. Let

$$\{\theta(t)\} = [\phi]\{q(t)\} \qquad \text{Equation 80}$$

$$\{\ddot{\theta}(t)\} = [\phi]\{\ddot{q}(t)\} \qquad \text{Equation 81}$$

Substituting these expressions into the equations of motion and premultiplying by $[\phi]^T$ gives an elementary form of the *modal equations of motion*:

$$[\phi]^T[m][\phi]\{\ddot{q}(t)\} + [\phi]^T[k][\phi]\{q(t)\} = \{0\} \qquad \text{Equation 82}$$

defining the *modal mass matrix* as

$$[M_n] = [\phi]^T[m][\phi] \qquad \text{Equation 83}$$

with

$$[m] = \begin{bmatrix} J_1 & 0 & 0 \\ 0 & J_3 + R^2 J_2 & 0 \\ 0 & 0 & J_3 \end{bmatrix} \qquad \text{Equation 84}$$

Also define the *modal stiffness matrix* as:

$$[K_n] = [\phi]^T[k][\phi] \qquad \text{Equation 85}$$

However, because of orthogonality between modes:

$$[K_n] = [\phi]^T [k] [\phi] \equiv [M_n \omega_n^2] \qquad \text{Equation 86}$$

This gives the *modal equation of motion*:

$$[M_n]\{\ddot{q}(t)\} + [M_n \omega_n^2]\{q(t)\} = \{0\} \qquad \text{Equation 87}$$

Assume a solution of the form

$$\{q_n(t)\} = \{E_n \sin\omega_n t + G_n \cos\omega_n t\} \qquad \text{Equation 88}$$

and the modal equatons become:

$$M_n \ddot{q}_n + M_n \omega_n^2 q_n = 0 \qquad \text{Equation 89}$$

$$n = 1, 2, 3$$

Choosing a set of arbitrary initial conditions:

displacements: let $\quad \{q_n(0)\} = [\phi]^{-1}\{\theta(0)\} = [\phi]^{-1}\begin{Bmatrix} 1 \\ 3 \\ 8 \end{Bmatrix}$ $\qquad$ Equation 90

velocities: let $\quad \{\dot{q}_n(0)\} = [\phi]^{-1}\{\dot{\theta}(0)\} = [\phi]^{-1}\begin{Bmatrix} 0 \\ 0 \\ 0 \end{Bmatrix}$ $\qquad$ Equation 91

where the displacements are in radians and the velocities are in radians/seconds.

Evaluating the assumed solution at time t = 0, and then differentiating to evaluate initial velocities:

$$\{q_n(0)\} = \{G_n\} \qquad \text{Equation 92a}$$

$$\{\dot{q}_n(0)\} = \{E_n\} \qquad \text{Equation 92b}$$

This yields:

$$G_1 = 4.0 \qquad E_1 = 0$$

$$G_2 = -3.5 \qquad E_2 = 0$$

$$G_3 = 0.5 \qquad E_3 = 0$$

(radians)

Substituting back into the assumed solution and definition of generalized coordinates (Equation 81) results in the solution of the single-stage system. The displacement equations are:

$$\theta_1(t) = A_{11}q_1(t) + A_{12}q_2(t) + A_{13}q_3(t)$$
$$= (1)(4)\cos\omega_1 t + (1)(-3.5)\cos\omega_2 t + (1)(0.5)\cos\omega_3 t$$

Equation 93

In a similar fashion to that of Equation 93:

$$\theta_2(t) = (1)(4)\cos\omega_1 t + (0)(-3.5)\cos\omega_2 t + (-2)(0.5)\cos\omega_3 t$$

Equation 94

$$\theta_3(t) = (1)(4)\cos\omega_1 t + (-1)(-3.5)\cos\omega_2 t + (1)(0.5)\cos\omega_3 t$$

Equation 95

Appendix D

THE BETA-m NUMERICAL INTEGRATION SCHEME

The numerical integration routine used to solve the gear

system's equations of motion is the *beta-m* method, a generalized

form of the well recognized Newmark scheme. Beta-m is proposed

by Katona [20], the source of all work to follow unless otherwise

noted.

D.1. Background

The beta-m method solves equations of the form:

$$M\ddot{x} + C\dot{x} + Kx = f \qquad \text{Equation 96}$$

where M, C and K are the system's masses, damping coefficients,
and stiffnesses, respectively.

The true Newmark method relates displacement and velocity at
time t_{n+1} to known values at time t_n with the following
expressions:

$$x_{n+1} = x_n + h x_n^{(1)} + h^2((1-2\beta_N)x_n^{(2)} + 2\beta_N x^{(2)})/2 \qquad \text{Equation 97}$$

$$x_{n+1}^{(1)} = x_n^{(1)} + h x_n + h^2((1-2\beta_N)x_n^{(2)} + 2\beta_N x_{n+1}^{(2)})/2 \qquad \text{Equation 98}$$

where the timestep $h = t_{n+1} - t_n$, and γ_n and β_n are Newmark's integration parameters.

D.2.   Method Derivation

Katona develops the beta-m method by writing the Newmark expressions in a Taylor series expansion:

$$x_{n+1}^{(k)} = \sum_{j=k}^{2} x_n^{(j)} h^{j-k}/(j-k)! + \beta_k(h^{2-k}/(2-k)!)\Delta x^{(2)} \qquad \text{Equation 99}$$

where Equations 97 and 98 are written with $k = 0$ and $k = 1$, respectively, and Δ is the forward difference operator:

$$\Delta x^{(k)} = x_{n+1}^{(k)} - x_n^{(k)} \qquad \text{Equation 100}$$

It can be seen that Equation 99 has the standard form of a Taylor series expansion. By definition, then, it is exact to the term x_n with a term approximating x_n. The approximating term may be placed in its usual Taylor expansion form by letting $\beta_0 = 1/3$ and

β_1=1/2. However, as Katona points out, "there is nothing sacred about [the choices made for] β_0 and β_1 because x_N is not exact but, rather, approximated by a forward difference." This implies that the method itself is adjustable through various β values.

Noting that the *method order m* also gives the highest order of the time derivative utilized in the method (m = 2 is Newmark; Gearsep2 uses m = 4), Katona defines the beta-m method in the following compact form:

$$\overset{(k)}{x_{n+1}} = q_k + b_k \overset{(m)}{\Delta x} \qquad \text{Equation 101}$$

with

$$q_k = \sum_{j=k}^{m} \overset{(j)}{x_n} h^{j-k}/(j-k)! \qquad \text{Equation 102}$$

and

$$b_k = \beta_k h^{m-k} \Big/ (m-k)! \qquad \text{Equation 103}$$

where the over-script (k) is the time derivative index.

In Equations 101 through 103, the q_k term is the Taylor series expansion of x_{n+1} up to the term x_n, and is thus known as a "history vector", and the last term in Equation 101 may be interpreted as an

approximation to the next Taylor series term, and contains an "unknown increment" Δx for which we will solve. By comparing Equations 101 through 103 with Equation 99, it is seen that Katona has simply given a convenient name to each of the various parts of Newmark's Taylor series expansion, and called them the "beta-m family of methods."

Implementation of the beta-m method requires that the unknowns x_{n+1}, $\dot{x}_{n+1}$, and $\ddot{x}_{n+1}$ be approximated in terms of the increment Δx. Doing so, the original equation of motion (written at time t_{n+1}):

$$M\ddot{x}_{n+1} + C\dot{x}_{n+1} + Kx_{n+1} = f_{n+1} \qquad \text{Equation 104}$$

can be written as

$$[b_2 M + b_1 C + b_0 K]\overset{(m)}{\Delta x} = f_{n+1} - \{Mq_2 + Cq_1 + Kq_0\} \qquad \text{Equation 105}$$

where the b's and q's come from Equations 102 and 103. Solving Equation 105 for Δx, the remaining unknowns are updated from Equation 101.

The following algorithm is adapted from Katona:

1. Given x_n, $\dot{x}_n$,...., $\ddot{x}_n$ at time t_n, we seek a solution at t_{n+1}.

2. Form the right-hand-side vector of Equation 105:

$$R = f_{n+1} - Mq_2 - Cq_1 - Kq_0$$

3. Solve for the primary unknown, Δx

$$[b_2 M + b_1 C + b_0 K] \overset{(m)}{\Delta x} = R$$

4. Update the solution vectors (i.e. Equation 101)

$$\overset{(k)}{x}_{n+1} = q_k + b_k \overset{(m)}{\Delta x}$$

5. Advance timestep, and return to Step 2.

Katona performs stability and accuracy analyses on the beta-m method in general, and similar quantitative analyses are performed on actual separation predictions in Chapter 6.

139

Appendix E

GEAR DATA

E.1. Required Data

The following data is taken from reference [7] except where noted.

W : gear facewidth
W = 1.333 in

C_1 : standard distance between gear centers
C_1 = 3.6471 in

R_o : outer radius
R_o = 1.9415

R_p : pitch circle radius
R_p = 1.8235 in

R_b : base circle radius
R_b = 1.69075 in

E : Young's Modulus of steel
$E = 30 \times 10^6$ psi

N : number of teeth
N = 31

n : gear speed
n = 9000 RPM (max)

T_p :   circular pitch tooth thickness (at pitch)
$T_p = 0.1831$

ϕ :   pressure angle
$\phi = 22$ degrees

r :   fillet radius
$r = 0.0570$

Not given in reference [7]:

μ :   Poisson's ratio for steel
$\mu = 0.3$ (from reference [23])

E.2. Calculated Data

As noted in Chapter 6, Sec. 6.6., the values of mass moment of inertia and shaft stiffness used in the sample analysis a₁e *not* representative of those in reference [7], but rather, it is the detailed *gear geometry* that is extracted from this source. To facilitate the presentation of the analysis results, the true system dimensions and masses were replaced by a set of qualitatively chosen values: It was decided to increase the moments of inertia of the *motor and load* mass and decrease that of the gears so as to obtain a system response that focuses mainly on the response of the gear pair itself, and that is not visually clouded by the coupling between the masses. By simply editing the Gearsep data input

files, however, any or all of these quantities may be altered to exactly describe any single-stage system, including the four square system in question. However, it is not the object of this report to affirm or disaffirm any particular gear system, but rather, to confirm a generalized procedure.

With this approach in mind, the system is described beginning with the equation for mass (in slugs) of any of its elements (gears or shafts):

$$\text{mass } m = \frac{\left[\pi \rho r^2 \, l\right]}{g} \qquad \text{Equation 106}$$

where:

ρ :   density of steel

      $r = 0.286 \text{ lbm/in}^2$ (reference [23])

r :   radius of system element

l :   length of system element

g :   gravitational acceleration

      $g = 32.2 \text{ ft/sec}^2$

and:

$$\text{mass moment of inertia } J = \frac{1}{2}mr^2 \qquad \text{Equation 107}$$

([ft lb]/unit angular acceleration)

1) Model the electric motor as a solid steel cylinder, representing windings and armature. Again, the dimensions chosen for this model are *not* those of reference [7]. With the aforementioned goal of a visually clear response, focusing on the gear pair rather that the system as a whole, both the motor and load mass moments of inertia were arbitrarily set to 250 ft lb/(unit angular acceleration): This arbitrary value indeed proved to provide a response of the desired form. To give a measure of physical reality to this moment of inertia value, consider that it may be represented by a solid steel disk of the following dimensions:

$$r_{motor/load} = 6.5 \text{ in}$$
$$l_{motor/load} = 10 \text{ in}$$

The gear moment of inertia is chosen based on that calculated above:

$$J_{gear} = 0.002 \text{ ft lb/(unit angular acceleration)}$$

This places just over five orders of magnitude between J_{gear} and

$J_{motor/load}$. The "half" order of magnitude is based on an assumption
made very early in the investigation that exactly incremental J's
would perhaps create system resonances which would interfere
with the attempt to characterize the model's common behavior.

A gear with the J value given above might have the dimensions:

$$r_{gear} = 0.75 \text{ in}$$

$$l_{gear} = 0.45 \text{ in}$$

Although these dimensions are impossible given outer gear radii,
etc. as given in **Section E.1.**, they provide a sufficient difference
in J values to provide the aforementioned uncoupled response.

2) The shaft stiffnesses were chosen in a similar arbitrary
manner as the J's: K values are artificially high so as to appear
clearly in the analysis of Chapter 6, yet not interfere with the gear
response (see Chapter 6, Sec. 6.2.3.).

$$K_{shaft} = 2000.0 \text{ ft lb/radian}$$

A shaft with this spring constant might have the following
dimensions:

$$r_{shaft} = 0.2 \text{ in}$$

$$l_{shaft} = 18 \text{ in}$$